Mon. Not. R. Astron. Soc. **271**, 257–299 (1994)

Elemental abundances for a sample of southern galactic planetary nebulae

Robin L. Kingsburgh[1,2] and M. J. Barlow[1]

[1] *Department of Physics and Astronomy, University College London, Gower Street, London WC1E 6BT*
[2] *Instituto de Astronomía, Universidad Nacional Autónoma de México, PO Box 439027, San Diego, CA 92143–9027, USA*

Accepted 1994 May 18. Received 1994 May 18; in original form 1993 December 30

ABSTRACT

We present spectrophotometric observations of a sample of 80 southern galactic planetary nebulae (PN), and derive elemental abundances for 68 objects, supplementing the optical observations with UV data in 25 cases. We define Type I PN as those objects that have experienced envelope-burning conversion to nitrogen of dredged-up primary carbon. Such nebulae are recognised by their having nitrogen abundances that exceed the total C + N abundance of H II regions in the same galaxy. In our own galaxy, this criterion corresponds to N/O > 0.8. In the current sample, 11 nebulae having N/O > 0.8 are thereby classified as Type I. For these Type I PN, no evidence is found for oxygen depletion, compared with non-Type I PN. No trend is found between the N/O and O/H ratios for the entire sample, and the mean O/H ratios for the non-Type I and Type I PN are the same within the errors; $O/H = (4.93 \pm 2.22) \times 10^{-4}$ by number for 42 non-Type I PN and $O/H = (4.42 \pm 1.44) \times 10^{-4}$ for 11 Type I PN. Also, no difference is found between the oxygen abundances in the PN in this sample and the oxygen abundances in galactic H II regions. Hence we find no evidence for the ON cycle (which is predicted to operate during the second dredge-up) to have significantly altered the surface abundances of the progenitor stars, even for the Type I PN.

The helium abundances derived for the non-Type I PN are in accord with those predicted by Becker & Iben for the first and third dredge-up phases. A comparison between the nitrogen abundances in the PN and the carbon + nitrogen abundances in galactic H II regions indicates that roughly 36 per cent of the initial carbon is converted into nitrogen in the case of the non-Type I PN, consistent with predictions for the first dredge-up by Becker & Iben. In order to explain the high nitrogen abundances derived for the Type I PN, however, envelope-burning of dredged-up carbon into nitrogen, following the third dredge-up, is definitely required. Total C + N + O abundances are found to be correlated with C/H for the combined non-Type I and Type I sample; the carbon has been enhanced by He-burning processed material brought up by the third dredge-up.

Key words: stars: abundances – planetary nebulae: general.

1 INTRODUCTION

The abundances in planetary nebulae (PN) trace both the abundances of the interstellar medium (ISM), from which the progenitor stars formed, and the surface abundances of the progenitor asymptotic giant branch (AGB) stars, which were enriched by material from interior nucleosynthesis zones dredged up to their surfaces. Thus, by studying the abundances in PN, we are able to trace the history of galactic chemical evolution, *and* help constrain stellar evolutionary models. Nitrogen, carbon and helium are produced by stellar nucleosynthesis, whereas oxygen, neon, argon and sulphur trace the metallicity of the region in which the star formed.

There have been a few studies of the abundances for large samples of PN. Abundances derived from optical observations alone have been presented by Torres-Peimbert & Peimbert (1977, hereafter TPP77) and Barker (1978, hereafter Ba78) for northern hemisphere objects. An extensive

number of southern PN (~400) have been observed by Acker et al. (1989) and abundances for a subset of this sample have been presented by Köppen, Acker & Stenholm (1991). Recent optical observations of southern PN have also been presented by de Freitas Pacheco et al. (1991) and de Freitas Pacheco, Maciel & Costa (1992).

In the derivation of abundances using spectra that cover only optical wavelengths, not all stages of ionization are seen for all elements, and hence the derived abundances can be somewhat uncertain. The combination of UV spectra with optical spectra enables important stages of ionization of nitrogen and oxygen to be used in the abundance analysis, as well as three stages of ionization of carbon. The derivation of carbon abundances is important in order to determine the nature of carbon production in the progenitor AGB stars.

Aller & Czyzak (1983, hereafter AC83) and Aller & Keyes (1987, hereafter AK87) performed an abundance analysis for 92 northern hemisphere PN, combining optical and UV spectra (when UV observations were available). AC83 and AK87 combined the traditional empirical approach with a general modelling of the PN. The models fitted the general excitation of each nebula and duplicated certain excitation-sensitive line ratios as well as possible. The ionization correction factors found in the models were then applied to ionic abundances derived from the observed line fluxes and an empirical set of abundances derived. Extensive modelling using UV, optical and IR line fluxes has been performed for only a small number of PN, for example NGC 7662 (Harrington et al. 1982) and NGC 3918 (Clegg et al. 1987).

This abundance study combines extensive optical observations of 74 planetary nebulae, covering the wavelength range of 3150–7400 Å, with *IUE* observations for approximately half of this sample. The derivation of abundances includes the use of a new ionization correction factor (ICF) scheme, which is based on detailed photoionization models of 10 PN (Walton et al., in preparation, hereafter WBCM). This scheme allows more accurately for unobserved high-ionization stages, which can be particularly important for Type I PN (see Section 7.1). It also approximates for effects like the efficiency of charge-exchange reactions, which the more simplified IFC schemes cannot take into account.

2 UV AND OPTICAL OBSERVATIONS AND DATA ANALYSIS

2.1 *IUE* observations

Low-resolution, large-aperture spectra obtained with the SWP, LWR and LWP cameras of the *IUE* satellite were accessed via the *IUE* Uniform Low-Dispersion Archive (ULDA, Talavera 1988) using the ULDA Software Support Package (USSP). The spectra were extracted to ensure that saturated areas were excluded. In order to compensate for the decline in sensitivity with time of the *IUE* cameras, the correction factors of Bohlin & Grillmair (1988), Clavel, Gilmozzi & Preito (1986) and Teays & Garhart (1990) were applied to the SWP, LWR and LWP spectra, respectively. When many spectra for one object were available, they were merged, weighted according to exposure time. In the cases of NGC 2440, 2371-2 and 5189, the nebula is larger than the *IUE* aperture (10×23 arsec^2), and ionization stratification between different observed areas of the nebula is evident; the spectral line intensities differ from spectrum to spectrum. For these objects, the highest signal-to-noise ratio (S/N) spectrum was adopted for the subsequent analysis.

In addition, new *IUE* spectra of Fg 1, M 3-1 and M 1-13 were obtained by us in 1991 April using the SWP camera.

2.2 Optical observations

59 objects were observed with the 3.9-m AAT at Siding Spring Observatory during 1978 February, March, August and October. The 250B grating was used in the RGO Spectrograph with the 25-cm camera at the *f*/8 focus, with the IPCS as detector. The resolution was 5.5 Å, as judged by the FWHM of comparison arc lines. The wavelength coverage was 3150–7400 Å. Eight spatial increments each covered 2.3 arcsec, yielding a total slit length of 18.4 arcsec. Each nebula was observed with the slit centred on the nebular centre (usually on the central star, if visible), at a position angle (east of north) that is listed in the penultimate column of Table 1. Both wide-slit (typically 10 arcsec) and narrow-slit (typically 1 arcsec) observations were made of most objects, for absolute spectrophotometry and maximum resolving power, respectively. Generally, multiple exposures were made for each object, with a variety of neutral density (ND) filters, in order to obtain both unsaturated strong lines and high S/N on faint lines. Lines with a peak count rate of $\lesssim 3$ Hz were used in the analysis, in order to ensure linearity of the IPCS detector.[1]

Medium-resolution data also obtained at the AAT are included in this analysis. The spectra were obtained during runs in 1979 July, 1980 July, 1981 July, 1986 November and 1987 December. Full details of these observations are given in section 2.1 of Kingsburgh & Barlow (1992).

In 1978 April, 30 objects were observed using the Boller & Chivens Spectrograph and Image Dissector Scanner (IDS, Robinson & Wampler 1972) at the *f*/15 focus on the AAT. A 1200 g mm^{-1} grating was used, covering 3400–5200 Å at a resolution of ~8 Å. The slit length was 2.1 arcsec, the slit width was 1.8 arcsec, and the separation between the object and sky slots was 40 arcsec.

J 900 and K 3-67 were observed with the 1-m JKT at La Palma Observatory in 1989 December. A 300 line mm^{-1} grating was used in the Richardson–Brealey Spectrograph with a UV-coated GEC CCD as detector. The wavelength coverage was 3600–5500 Å at a resolution of ~9 Å. The slit lenth was 6 arcmin. On-chip binning of four pixels along the spatial direction was performed upon readout. The spectra of J 900 were trailed during the exposure and hence trace the mean emission across the nebula.

Finally, fluxes longward of 5200 Å for M 3-6 and NGC 2793 were measured from spectra kindly provided by Dr Jeremy Walsh, obtained using the SAAO 1.9-m telescope in 1980, with the RPCS as detector.

Table 1 presents a log of all UV and optical observations, giving the object discovery name in order of increasing Right Ascension, and the PK catalogue number (Perek &

[1]The format of the IPCS (8×2048) permitted non-saturated peak count rates up to ~7 Hz for the narrow-slit spectra and ~6 Hz for the wide-slit spectra.

Table 1. Observing log.

Object(PK No.)	IUE OBSERVATIONS			OPTICAL OBSERVATIONS								Diam.
	Cam. No.	Date	Exp. (sec)	Date	Tel./Det.	Rsn. (Å)	λ Range (Å)	Sl.Wi. (″)	ND (dex)	Exp (sec)	PA (°)	(arcsec)
IC 2003 (161–14.1)	SWP7261	29 11 79	5400	26 08 78	AAT/IPCS	5.5	3150-7400	0.9	0.34	200	45	10.5
	SWP7260	29 11 79	1800	26 08 78	AAT/IPCS	5.5	3150-7400	1.3	2.1	350	45	(CJA87)
	LWR6255	29 11 79	2700	26 08 78	AAT/IPCS	12	3150-7400	6.5	1.2	200	45	
K 3-67 (165–09.1)				11 12 89	JKT/CCD	9	3600-5500	1.0	–	1200	90	2.2(AK90)
J 900 (194+02.1)	SWP8677	06 04 80	3000	11 12 89	JKT/CCD	9	3600-5500	1.0	–	1500	90	6
	SWP7965	16 02 80	2000									(AK90)
	LWR7429	06 04 80	4500									
	LWR6937	29 11 78	3000									
M 1-8 (210+01.1)				28 03 78	AAT/IPCS	5.5	3150-7400	1.0	–	340	60	18.4
				10 11 86	AAT/IPCS	1.2	3550-4500	1.2	–	700	180	(PK67)
PB 1 (226–03.1)				28 03 78	AAT/IPCS	5.5	3150-7400	1.0	–	1883	60	10.0
				28 03 78	AAT/IPCS	15	3150-7400	10.2	1.46	150	60	(A92)
				28 03 78	AAT/IPCS	15	3150-7400	10.2	0.88	350	60	
M 3-1 (242–11.1)	SWP41323	30 04 91	3600	28 03 78	AAT/IPCS	5.5	3150-7400	1.0	0.34	750	60	11
				28 03 78	AAT/IPCS	15	3150-7400	14.8	1.78	70	60	(ZPB89)
				28 03 78	AAT/IPCS	15	3150-7400	14.8	1.2	150	60	
				28 03 78	AAT/IPCS	15	3150-7400	10.0	0.88	450	60	
				10 11 86	AAT/IPCS	1.2	3550-4500	1.2	–	250	250	
M 1-11 (232–04.1)	LWP5896	03 05 85	1800	31 12 87	AAT/IPCS	1.2	3250-4250	0.7	–	300	90	2.2
	LWP5897	03 05 85	9300	10 10 78	AAT/IPCS	5.5	3150-7400	1.0	0.34	300	90	(AK90)
	SWP25846	03 05 85	1800	10 10 78	AAT/IPCS	8	3150-7400	6.7	0.88	700	90	
SkWl 3-2 (258–15.1)				18 02 78	AAT/IPCS	5.5	3150-7400	1.0	–	1500		100×67
				18 02 78	AAT/IPCS	15	3150-7400	10.0	0.62	500		
M 1-12 (235–03.1)				10 10 78	AAT/IPCS	5.5	3150-7400	1.0				1.8(AK90)
M 1-13 (232–01.1)	SWP41324	09 04 91	10200	19 02 78	AAT/IPCS	5.5	3150-7400	1.0	–	550	90	15
				19 02 78	AAT/IPCS	15	3150-7400	13.3	1.78	150	90	(A73)
				19 02 78	AAT/IPCS	15	3150-7400	13.3	1.2	200	90	
				31 12 87	AAT/IPCS	1.2	3250-4250	1.7	–	250		
NGC 2371-2 (189+19.1)	SWP38260	27 02 90	3600	28 03 78	AAT/IPCS	5.5	3150-7400	1.0	0.34	800	60	57.2
	LWP17428	27 02 90	12420	28 03 78	AAT/IPCS	15	3150-7400	10.0	0.62	300	60	(CJA87)
	SWP38258	26 02 90	12000									
	LWP17435	28 02 90	3600									
M 3-3 (221+05.1)				28 03 78	AAT/IPCS	5.5	3150-7400	1.0	–	270	60	12.3
				28 03 78	AAT/IPCS	15	3150-7400	10.0	–	450	60	(PK67)
				31 12 87	AAT/IPCS	1.2	3250-4250	1.5	–	80		
NGC 2440 (234+02.1)	SWP32722	14 01 88	900	18 02 78	AAT/IPCS	5.5	3150-7400	1.0	1.2	300	90	74x42
	LWP12489	14 01 88	4800									(CJA87)
NGC 2438 (231+04.2)	SWP15501	15 10 81	10800	19 02 78	AAT/IPCS	5.5	3150-7400	1.0	0.62	200	90	80
				19 02 78	AAT/IPCS	5.5	3150-7400	1.0	–	1800	90	(ZPB89)
				19 02 78	AAT/IPCS	15	3150-7400	10.0	1.2	150	90	
NGC 2452 (243–01.1)	SWP13946	09 05 81	12000	28 03 78	AAT/IPCS	5.5	3150-7400	1.0	–	600	60	18.8
	SWP11246	06 02 81	9000	28 03 78	AAT/IPCS	15	3150-7400	10.0	0.34	380	60	(PK67)
	LWR12325	11 01 82	10800	31 12 87	AAT/IPCS	1.2	3250-4250	1.3	–	105		
M 3-4 (241+02.1)				19 02 78	AAT/IPCS	5.5	3150-7400	1.0	–	1500	90	14
				19 02 78	AAT/IPCS	15	3150-7400	16	1.46	100	90	(ZPB89)
				19 02 78	AAT/IPCS	15	3150-7400	16	1.2	100	90	
				19 02 78	AAT/IPCS	15	3150-7400	16	–	300	90	
M 3-5 (245+01.1)				19 02 78	AAT/IPCS	5.5	3150-7400	1.0	–	300	90	7
				19 02 78	AAT/IPCS	15	3150-7400	10.0	1.76	100	90	(ZPB89)
				19 02 78	AAT/IPCS	15	3150-7400	10.0	0.62	300	90	
M 3-6 (254+05.1)				27 04 78	AAT/IDS	8.0	3400-5200	1.8	–	720		11
				31 12 87	AAT/IPCS	1.2	3250-4250	1.5	–	80		(ZPB89)
A 30 (208+33.1)	LWR7170	13 03 80	3900	28 03 78	AAT/IPCS	5.5	3150-7400	1.0	–	1030	60	126
	SWP8217	13 03 80	1200	28 03 78	AAT/IPCS	15	3150-7400	10.0	–	900	60	(J79)
He 2-15 (261+02.1)				28 03 78	AAT/IPCS	5.5	3150-7400	1.0	–	600	60	20.0
				28 03 78	AAT/IPCS	15	3150-7400	10.0	–	300	60	(MA82)
K 1-2 (253+10.1)				18 02 78	AAT/IPCS	5.5	3150-7400	1.0	–	600	90	65
				18 02 78	AAT/IPCS	15	3150-7400	10.0	0.62	134	90	(PK67)
IC 2448 (285–14.1)	LWR2756	30 10 78	1800	26 04 78	AAT/IDS	8	3400-5200	1.8	–	480		19.4
	SWP17474	24 07 82	600									(11.3 inner)
	LWR8733	07 08 80	2600									(LMPM87)
	SWP10033	07 08 80	900									
NGC 2792 (265+04.1)	SWP16018	01 11 82	5400	26 04 78	AAT/IDS	8	3400-5200	1.8	–	960		13
	LWR12326	01 11 82	6840									(CJA87)
	SWP16032	01 12 82	10020									
PB 4 (275–04.1)				26 04 78	AAT/IDS	8	3400-5200	1.8	–	960		10.1(MA75)
NGC 2867 (278–05.1)	LWR4518	14 05 79	1800	28 03 78	AAT/IPCS	5.5	3150-7400	1.0	–	800	60	56
	SWP5215	12 05 79	3000	28 03 78	AAT/IPCS	15	3150-7400	10.0	–	200	60	(CJA87)
	SWP5234	14 05 79	300	28 03 78	AAT/IPCS	12	3150-7400	6.0	–	550	60	
	LWR4510	12 05 79	3600	26 04 78	AAT/IDS	8	3400-5200	1.8	–	960	60	
He 2-28 (275–02.1)				26 04 78	AAT/IDS	8	3400-5200	1.8	–	720		10.0(MA75)
He 2-29 (275–02.2)				28 03 78	AAT/IPCS	5.5	3150-7400	1.0	–	400	60	14.0(MA75)

Table 1 – *continued*

Object(PK No.)	IUE OBSERVATIONS			OPTICAL OBSERVATIONS								Diam.
	Cam. No.	Date	Exp. (sec)	Date	Tel./Det.	Rsn. (Å)	λ Range (Å)	Sl.Wi. (″)	ND (dex)	Exp (sec)	PA (°)	(arcsec)
NGC 2899 (277–03.1)				26 04 78	AAT/IDS	8	3400-5200	1.8	–	480		EAST
				26 04 78	AAT/IDS	8	3400-5200			480		WEST
				19 02 78	AAT/IPCS	5.5	3150-7400	1.0	0.62	1500	90	56(CJA87)
He 2-37 (274+03.1)				19 02 78	AAT/IPCS	5.5	3150-7400	1.0	–	1000	90	30.0(MA82)
Lo 4 (274+09.1)				18 02 78	AAT/IPCS	5.5	3150-7400	1.0	–	1500	90	48
				18 02 78	AAT/IPCS	12	3150-7400	6.1	–	400	90	(Lo77)
NGC 3195 (296–20.1)	SWP17465	23 07 82	1800	18 02 78	AAT/IPCS	5.5	3150-7400	1.0	–	1800	90	44
	LWR13754	23 07 82	1980	18 02 78	AAT/IPCS	12	3150-7400	5.8	0.34	300	90	(PK67)
He 2-48 (282+03.1)				19 02 78	AAT/IPCS	5.5	3150-7400	1.0	–	1800	90	30(PK67)
He 2-51 (288–05.1)				28 03 78	AAT/IPCS	5.5	3150-7400	1.0	–	850	60	12.4
				28 03 78	AAT/IPCS	15	3150-7400	10.0	–	450	60	(MA82)
Pe 2-7 (285+02.1)				28 03 78	AAT/IPCS	5.5	3150-7400	1.0	–	750	60	st
				28 03 78	AAT/IPCS	12	3150-7400	6.7	–	450	60	(A92)
Pe 1-3 (288–02.1)				25 04 78	AAT/IDS	8	3400-5200	1.8	–	660		8.0(MA82)
He 2-55 (286+02.1)				18 02 78	AAT/IPCS	5.5	3150-7400	1.0	–	1200	90	18
				18 02 78	AAT/IPCS	15	3150-7400	10.0	–	300	90	(WH)
He 2-57 (289+01.1)				18 02 78	AAT/IPCS	5.5	3150-7400	1.0	–	500	90	27×15
				18 02 78	AAT/IPCS	15	3150-7400	10.0	–	200	90	(WH)
IC 2621 (291–04.1)				25 04 78	AAT/IDS	8	3400-5200	1.8	–	840	90	5(CJA87)
ESO 216-02 (288+08.1)				18 02 78	AAT/IPCS	5.5	3150-7400	1.0	–	800	90	36
				18 02 78	AAT/IPCS	5.5	3150-7400	2.0	0.62	300	90	(We77)
K 1-22 (283+25.1)	SWP16969	15 05 82	4200	18 02 78	AAT/IPCS	5.5	3150-7400	1.0	0.34	800	90	181(ZPB89)
Fg 1 (290+07.1)	SWP41325	19 04 91		18 02 78	AAT/IPCS	5.5	3150-7400	1.0	0.34	800	90	27.2
				18 02 78	AAT/IPCS	15	3150-7400	10.0	0.88	150	90	(MA75)
PB 8 (292+04.1)				25 04 78	AAT/IDS	8	3400-5200	1.8	–	720		5(A82)
He 2-76 (298–01.2)				28 03 78	AAT/IPCS	5.5	3150-7400	1.0	–	900	60	16×12(WH)
He 2-77 (298–00.1)				28 03 78	AAT/IPCS	5.5	3150-7400	1.0	–	750	60	26×18(WH)
Th 2-A (306–00.1)				25 04 78	AAT/IDS	8	3400-5200	1.8	–	960		24.4
				26 08 78	AAT/IPCS	5.5	3150-7400	0.9	–	900	80	(MA82)
				26 08 78	AAT/IPCS	15	3150-7400	10	0.34	500	80	
				26 08 78	AAT/IPCS	15	3150-7400	10	–	70	80	
NGC 5189 (307–03.1)	SWP25364	05 03 85	3600	28 03 78	AAT/IPCS	5.5	3150-7400	1.0	0.88	60	60	140
	LWP5456	05 03 85	3600	28 03 78	AAT/IPCS	5.5	3150-7400	1.0	1.2	260	60	(PK67)
	SWP8219	13 03 80	4500	28 03 78	AAT/IPCS	5.5	3150-7400	1.0	0.34	550	60	
	LWR7171	13 03 80	4500	28 03 78	AAT/IPCS	12	3150-7400	6.7	1.46	150	60	
				28 03 78	AAT/IPCS	12	3150-7400	6.7	1.28	450	60	
				07 07 79	AAT/IPCS	1.2	3060-4030	0.9	–	300	180	
				06 07 79	AAT/IPCS	0.5	3660-3980	1.5	–	100	180	
MyCn 18 (307–04.1)				25 04 78	AAT/IDS	8	3400-5200	1.8	–	720		12.6
				26 08 78	AAT/IPCS	5.5	3150-7400	0.9	0.62	250	80	(MA75)
				26 08 78	AAT/IPCS	15	3150-7400	14	2.1	200	80	
				26 08 78	AAT/IPCS	12	3150-7400	6.5	1.46	300	80	
				08 07 79	AAT/IPCS	0.8	4150-4640	1.7	–	1000		
He 2-97 (307–09.1)				25 04 78	AAT/IDS	8	3400-5200	1.8	–	720		<3
				26 08 78	AAT/IPCS	5.5	3150-7400	0.9	0.34	100	80	(MA82)
				26 08 78	AAT/IPCS	15	3150-7400	10.0	2.1	100	80	
				26 08 78	AAT/IPCS	15	3150-7400	10.0	1.46	500	80	
				07 07 79	AAT/IPCS	0.5	3660-3970	0.9	–	335		
NGC 5307 (312+10.1)	SWP28436	05 06 86	1800	26 08 78	AAT/IPCS	5.5	3150-7400	0.9	0.62	150	80	13
	SWP30149	24 01 87	3600	26 08 78	AAT/IPCS	12	3150-7400	6.5	1.2	300	80	(M82)
				07 07 79	AAT/IPCS	0.5	3060-4030	0.9	–	500	180	
				06 07 79	AAT/IPCS	1.2	3660-3980	1.5	–	60	180	
				25 04 78	AAT/IDS	8	3400-5200	1.8	–	720		
He 2-99 (309–04.1)	SWP28463	09 06 86	2400	26 08 78	AAT/IPCS	5.5	3150-7400	0.9	0.88	300	80	30
	SWP30371	24 02 87	2700	26 08 78	AAT/IPCS	12	3150-7400	6.5	1.2	300	80	(KSFL89)
	LWP10186	24 02 87	1200	25 04 78	AAT/IDS	8	3400-5200	1.8	–	720		
NGC 5315 (309–04.2)	SWP4324	21 02 79	41620	25 04 78	AAT/IDS	8	3400-5200	1.8	–	720		13
	LWR3819	21 02 79	1500									(MA82)
	LWR2755	30 10 78	1800									
	SWP3193	30 10 78	1800									
	LWR1779	04 07 78	2100									
	SWP1915	04 07 78	1800									
	SWP8000	20 02 80	1800									
	LWR6963	20 02 80	1800									
IC 972 (326+42.1)				26 04 78	AAT/IDS	8	3400-5200	1.8	–	960		44(MA82)
He 2-105 (308–12.1)				18 02 78	AAT/IPCS	5.5	3150-7400	1.0	–	150	90	35
				18 02 78	AAT/IPCS	12	3150-7400	4.6	0.62	150	90	(MA82)
He 2-107 (312–01.1)				26 04 78	AAT/IDS	8	3400-5200	1.8	–			10.0
				26 08 78	AAT/IPCS	5.5	3150-7400	0.9	–	170	80	(MA82)
				26 08 78	AAT/IPCS	5.5	3150-7400	0.9	0.34	50	80	
				26 08 78	AAT/IPCS	15	3150-7400	14.0	0.88	100	80	
				26 08 78	AAT/IPCS	12	3150-7400	6.5	0.62	300	80	

Table 1 – *continued*

Object(PK No.)	IUE OBSERVATIONS			OPTICAL OBSERVATIONS								Diam.
	Cam. No.	Date	Exp. (sec)	Date	Tel./Det.	Rsn. (Å)	λ Range (Å)	Sl.Wi. (″)	ND (dex)	Exp (sec)	PA (°)	(arcsec)
He 2-111 (315–00.1)	LWP15489	10 05 89	9000	28 03 78	AAT/IPCS	5.5	3150-7400	1.0	–	458	60	31.4
	SWP36236	10 05 89	3600	06 88	AAT/IPCS	1.2		1.0	–	140		(PK67)
	LWP15326	08 04 89	3000									
	SWP35964	08 04 89	3720									
He 2-112 (319+06.1)				28 03 78	AAT/IPCS	5.5	3150-7400	1.0	–	60	60	14.6
				06 88	AAT/IPCS	1.2		1.0	–	60		(MA85)
ESO 223-10 (324+09.1)				26 04 78	AAT/IDS	8	3400-5200	1.8	–	960		18(We77)
He 2-119 (317–05.1)				18 02 78	AAT/IPCS	5.5	3150-7400	1.0	–	1200	90	50
				18 02 78	AAT/IPCS	15	3150-7400	10.0	0.62	100	90	(MA82)
				18 02 78	AAT/IPCS	15	3150-7400	10.0	–	400	90	
NGC 5873 (331+16.1)	SWP30150	24 01 87	1800	07 07 79	AAT/IPCS	1.2	3060-4030	0.9	–	250	60	7
	SWP30148	24 01 87	3600	06 07 79	AAT/IPCS	0.5	3660-3980	1.5	–	30		(M82)
				26 04 78	AAT/IDS	8	3400-5200	1.8	–	480		
NGC 5882 (327+10.1)	SWP16349	16 02 82	1800	07 07 79	AAT/IPCS	1.2	3060-4030	0.9	–	300	60	14.3
	SWP12599	16 02 82	3860	25 04 78	AAT/IDS	8	3400-5200	1.8	–	720		(M81)
Me 2-1 (342+27.1)	LWR77374	12 05 80	2400	26 04 78	AAT/IDS	8	3400-5200	1.8	–	960		7
	SWP5352	14 05 79	5400									(AK90)
	SWP5233	14 05 79	540									
	LWR4517	14 05 79	1800									
NGC 5979 (322–05.1)	SWP35644	01 03 89	6000	26 04 78	AAT/ IDS	8	3400-5200	1.8	–	720		8
	LWP15119	01 03 89	3600									(A82)
He 2-138 (320-09.1)	SWP6720	02 10 79	240	08 10 78	AAT/IPCS	5.5	3150-7400	1.0	1.2	200	90	7
	LWR5735	02 10 79	180	08 10 78	AAT/IPCS	8	3150-7400	10.0	1.78	300	90	(A92)
He 2-141 (325–04.1)				26 04 78	AAT/IDS	8	3400-5200	1.8	–	570		14(A82)
He 2-142 (327–02.1)				26 04 78	AAT/IDS	8	3400-5200	1.8	–	480		3.0(A82)
NGC 6026 (341+13.1)				26 08 78	AAT/IPCS	5.5	3150-7400	0.9	0.88	250	60	42
				26 08 78	AAT/IPCS	12	3150-7400	6.5	1.2	250	60	(ZPB89)
				08 07 79	AAT/IPCS	0.8	4150-4640	1.7	–	250	210	
				25 04 78	AAT/IDS	8	3400-5200	1.8	–	720		
Mz 2 (329–02.2)				28 03 78	AAT/IPCS	5.5	3150-7400	1.0	–	600	90	23(A92)
NGC 6153 (341+05.1)	LWP4476	01 10 84	7200	09 10 78	AAT/IPCS	12	3150-7400	6.7	0.34	600	90	28.0
	LWP7715	24 02 86	6660	26 04 78	AAT/IDS	8	3400-5200	1.8	–	480		(PK67)
	SWP27779	24 02 86	12600									
PC 14 (336–06.1)				26 08 78	AAT/IPCS	5.5	3150-7400	0.53	0.34	500	60	7.0
				26 08 78	AAT/IPCS	15	3150-7400	14.1	2.1	150	60	(MA82)
H 2-1 (350+ 04.1)				08 10 78	AAT/IPCS	5.5	3150-7400	0.9	0.34	200	90	2.2
				08 10 78	AAT/IPCS	8	3150-7400	6.7	0.88	400	90	(ZPB89)
IC 4642 (334–09.1)				25 04 78	AAT/IDS	8	3400-5200	1.8	–	960		16.4(CJA87)
Tc 1 (345–08.1)	SWP13412	06 03 81	1200	10 10 78	AAT/IPCS	5.5	3150-7400	0.9	1.2	700	90	9.6
	SWP13413	06 03 81	240	10 10 78	AAT/IPCS	8	3150-7400	6.7	1.78	100	90	(PK67)
	LWR10078	06 03 81	450									
M 1-26 (358–00.2)	SWP5563	18 06 79	2700	10 10 78	AAT/IPCS	5.5	3150-7400	0.9	1.2	300	90	4.2
	LWR4803	18 06 79	3600	10 10 78	AAT/IPCS	8	3150-7400	6.7	1.46	750	90	(A92)
IC 4673 (003–02.3)				08 10 78	AAT/IPCS	5.5	3150-7400	0.9	–	889	90	15
				08 10 78	AAT/IPCS	12	3150-7400	6.7	–	600	90	(CJA87)
				08 10 78	AAT/IPCS	15	3150-7400	15.7	–	300	90	
NGC 6751 (029–05.1)				08 10 78	AAT/IPCS	5.5	3150-7400	0.9	–	1000	90	20
				08 10 78	AAT/IPCS	5.5	3150-7400	0.9	1.2	150	90	(CJA87)
				08 10 78	AAT/IPCS	12	3150-7400	6.7	1.78	150	90	
				08 10 78	AAT/IPCS	12	3150-7400	6.7	0.34	450	90	
				08 10 78	AAT/IPCS	12	3150-7400	6.7	0.88	100	90	
				08 11 86	AAT/IPCS	1.2	3550-4500	1.0	–	400		
				26 04 78	AAT/IDS	8	3400-5200	1.8	–	3700		
He 2-434 (320-28.1)	SWP28231	27 04 86	900	09 10 78	AAT/IPCS	5.5	3150-7400	0.9	0.34	1000	90	<10
	LWP8112	27 04 86	900	09 10 78	AAT/IPCS	5.5	3150-7400	0.9	1.78	200	90	(A82)
				09 10 78	AAT/IPCS	12	3150-7400	6.8	1.2	500	90	
				08 11 86	AAT/IPCS	1.2	3550-4500	1.2	–	450		
A 65 (017–21.1)				09 10 78	AAT/IPCS	5.5	3150-7400	0.9	–	1500	90	104
				09 10 78	AAT/IPCS	12	3150-7400	4.1	–	600	90	(ZPB89)
NGC 6905 (061–09.1)				09 10 78	AAT/IPCS	5.5	3150-7400	0.9	–	1000	90	39
				09 10 78	AAT/IPCS	5.5	3150-7400	0.9	1.2	120	90	(CJA87)
				09 10 78	AAT/IPCS	5.5	3150-7400	0.9	0.88	200	90	
				09 10 78	AAT/IPCS	12	3150-7400	6.7	0.62	600	90	
				09 10 78	AAT/IPCS	12	3150-7400	6.7	1.2	200	90	
				26 04 78	AAT/IDS	8	3400-5200	1.8	–	480		
				08 07 79	AAT/IPCS	1.2	3060-4030	0.9	–	300		

Table 1 – *continued*

Object(PK No.)	IUE OBSERVATIONS Cam. No.	Date	Exp. (sec)	OPTICAL OBSERVATIONS Date	Tel./Det.	Rsn. (Å)	λ Range (Å)	Sl.Wi. (″)	ND (dex)	Exp (sec)	PA (°)	Diam. (arcsec)
NGC 7009 (037-34.1)	SWP8579	23 03 80	180	10 10 78	AAT/IPCS	12	3150-7400	4.1	1.76	1000	90	29.3
	SWP23382	02 07 84	360	08 07 79	AAT/IPCS	0.34	3060-4030	0.9	–	1500	240	(CJA87)
	LWR1611	03 06 78	1200									
	SWP9262	12 06 80	300									
	SWP1709	03 06 78	600									
	SWP8679	06 04 80	240									
	SWP9387	27 06 80	420									
	SWP1707	03 06 78	120									
IC 5148-50 (002-52.1)				26 08 78	AAT/IPCS	15	3150-7400	12.7	–	500	80	135
				26 08 78	AAT/IPCS	5.5	3150-7400	0.9	–	1560	80	(CJA87)
				08 11 86	AAT/IPCS	1.2	3550-4500	1.0	–	350		

References to Table 1: A73 – Allen (1973); A82 – Acker et al. (1982); A92 – Acker et al. (1992); AK90 – Aaquist & Kwok (1990); CJA87 – Chu, Jacoby & Arendt (1987); J79 – Jacoby (1979); KSFL89 – Kaler et al. (1989); Lo77 – Longmore (1977); LMPM87 – Louise et al. (1987); M82 – Milne (1982); MA75 – Milne & Aller (1975); MA82 – Milne & Aller (1982); PK67 – Perek & Kohoutek (1967); We77 – Weinberger (1977); WH – Westerlund & Henize (1967); ZPB89 – Zijlstra, Pottasch & Bignell (1989).

Kohoutek 1967). For the UV observations, the *IUE* camera number, the date and the exposure time are given. For the optical observations, the date, the telescope, the detector, the resolution, the wavelength range, the slit width, the ND filter, the exposure time and the position angle of the slit are given. Nebular angular diameters and references for the diameter are also given in Table 1.

2.3 Data reduction

The IPCS spectra were reduced with the SDRSYS package (Straede 1980). If the diameter of the nebula was less than the slit length, the outer sky increments were summed, scaled, and subtracted from the nebular increments. If, however, the nebula was larger than the slit length, all eight spatial increments were added and no sky subtraction could be performed. Wavelength calibration was done with fifth-order polynomial fits to 30–40 CuAr arc lines. The effect of atmospheric extinction was removed by correcting the spectra using mean Siding Spring extinction coefficients. If the objects were observed through ND filters (which have a slight wavelength dependence), they were divided by the appropriate filter response function. Absolute flux calibration was then performed for nebulae whose diameters were less than the entrance aperture by means of observations of standard stars from the list of Oke (1974). For nebulae with diameters larger than the entrance aperture, only relative flux calibration could be done. Because the fluxes of the Oke (1974) standard stars were usually only listed for wavelengths $\gtrsim 3400$ Å, it was necessary to extrapolate the calibration for wavelengths shortward of 3400 Å for the IPCS data. Several bright isolated PN central star spectra were used to do this. As these objects are extremely hot, their dereddened flux distribution at optical wavelengths originates from the Rayleigh–Jeans tail of their overall flux distribution, and can be easily extrapolated to shorter wavelengths. A straight line was fitted to the spectra longward of 3400 Å in log (absolute flux) versus log (wavelength) space, and extrapolated to $\lambda = 3150$ Å. A mean of several such fits then provided the calibration for the IPCS spectra shortward of 3400 Å, for a given night.

The IDS spectra were reduced in a similar manner to that used for the IPCS spectra, also with the SDRSYS package. The object spectra were summed and the sky spectra, which were observed simultaneously, were subtracted. No filters were used during these observations.

The JKT spectra were reduced using the FIGARO package (Shortridge 1989). The spectral images were initially bias-subtracted, then divided by a normalized flat-field and cleaned of cosmic rays. Wavelength and flux calibrations were performed as above.

2.4 Data analysis

Fluxes from the UV and optical spectra were measured with the DIPSO package (Howarth & Murray 1988) at the University College London STARLINK node. For some lines, the emission-line fitting routine (ELF) written by P. J. Storey was used to fit Gaussians to the lines via least-squares. Gaussian fitting was used when adjacent lines were somewhat blended, or when the line was of poor S/N and its width could be constrained to be the same as a nearby strong line, or when the errors on the fluxes of a line were important for subsequently derived nebular quantities.

With the low-resolution UV spectra, there is a possibility that some of the lines originate from the wind of the central star, rather than the surrounding nebula (e.g. N v 1240 Å). The FWHM of an emission line was used in order to ascertain whether a line was stellar or nebular in origin. The resolution of the *IUE* low-resolution spectra is ~6–7 Å. If the FWHM of a line was $\gtrsim 8$–9 Å, the line was judged likely to be stellar. Also, the presence of central star emission lines in the optical spectra served as a guide for determining whether wide lines in UV spectra were stellar or nebular in origin. If the speed of the wind of the central star were $\lesssim 1400$ km s^{-1}, however, the lines would be unresolved by the SWP spectra. In this case, one would need to examine the line profiles in high-resolution *IUE* data.

For the IPCS data, multiple exposures have been taken with a variety of ND filters, in order to obtain fluxes of both strong and weak lines. In order to merge the line fluxes from several spectra, scaling was done through an unsaturated Balmer line. In some extreme cases, only the wide-slit spectra were usable for the fluxes of the strongest lines; however, as the resolution is degraded in the wide-slit spectra, the scaling was sometimes less straightforward. For example, if Hβ, Hα

and [N II] 6584 Å were saturated in all narrow-slit spectra, and the latter were blended in a wide-slit spectrum together with [N II] 6584-Å, the narrow-slit [N II] 6548/Hγ ratio would be used to estimate the [N II] 6548-Å flux, the [N II] 6548-Å flux would be set to $2.94 \times F(6548)$ (because both transitions originate from the same upper level they have a fixed intensity ratio), and the remaining flux in the wide-slit blend would be attributed to Hα. Errors in this kind of de-convolution would propagate as errors in the derived reddening parameter and errors in the dereddened line intensities. In such cases, however, we generally find good internal consistency in deriving the reddening parameter (two exceptions are described below), and good consistency with previously published fluxes.

Other than occasional problems in dealing with saturated lines in the IPCS data, line-fitting and flux measurement were generally straightforward. Some IDS data, on the other hand, provided new problems. Very strong lines in the IDS spectra have Gaussian cores with Lorentzian wings. The strength of the wings varies with the strength of the line. If the lines were isolated, their total fluxes could be measured straightforwardly with DIPSO. However, if other lines were present nearby, both narrow and broad Gaussian profiles were fitted to the core and wings of the strong line,[2] and a single Gaussian was fitted to nearby weaker lines. In order to estimate the width of the broad component, first a fit to the core and wings of a single line of comparable strength was made, where the central wavelengths of both Gaussians were constrained to be equal. The resulting FWHM of the broad component was then adopted for the FWHM of the broad component of a line present in a blend. Such blending presented most problems with the Hγ, [O III] 4363-Å blend when Hγ was strong, as [O III] 4363 Å was blended with the red wing of Hγ. Hence the [O III] 4363-Å flux and T_e(O III) are more uncertain for the IDS data than for the IPCS data. The [O III] 4363-Å flux was only adopted from IDS data when no other measurements were available.

In order to obtain final adopted fluxes for each line from several spectra, the IPCS low- and medium-resolution and the IDS relative fluxes were averaged for each line, and weighted according to exposure time and S/N considerations.

[2]Although the wings have a Lorentzian profile, it was found that a Gaussian profile provided an adequate fit to the wings.

3 RESULTS

3.1 Absolute Hβ fluxes

For the PN where absolute flux calibration of the wide-slit spectra was possible, absolute Hβ fluxes were measured. These are presented, together with absolute He II 4686-Å fluxes in Table 2. Table 2 also presents Hβ fluxes from the literature, for comparison purposes. Fluxes from O'Dell (1963) and Webster (1969) are adjusted by -0.02 dex, following the recommendations of Shaw & Kaler (1989).

Table 2. Absolute Hβ and He II 4686-Å fluxes.

Object	Diam. (arcsec)	Sl. Wi. (arcsec)	-log(F(Hβ))	-log(F(4686))	-log(F(Hβ))$_{literature}$
PB 1	9	10.2	12.10[a]	12.73	12.02(CSC83)
M 3-1	11	14.8	11.36	-	11.32(SK89), 11.27(CSC83), 11.29(GMC85)
M 1-13	15	13.3	11.75	-	11.86(Ka83), 11.67(CSC83)
M 3-3	12.3	15	12.66	13.17	12.32(SK89)
M 3-4	14	16	11.95	12.91[c]	-
M 3-5	7	10	12.09[b]	12.78[b]	12.20(SK89)
He 2-51	12.4	10	12.42	13.08	12.38(SK89)
Pe 2-7	7	6.7	12.68	12.78	-
MyCn 18	12.6	14	11.12	-	11.13(Web69)
He 2-97	<3	10	11.33[a]	-	11.44(SK89), 11.43(Web69)
He 2-107	10	12	12.21	13.17	12.26(SK89)
PC 14	7	14.1	11.83	-	11.74(SK89), 11.71(Web69)
He 2-434	<10	6.8	11.48	-	11.38(Web83), 11.48(VP85)

Notes. The slit length was 18.4 arcsec. [a]Mean flux from two wide-slit runs adopted. [b]Flux from deepest wide-slit run adopted. [c]'Circular' weighting method used for He II flux from narrow-slit spectrum (see spectrum 2.3 of Kingsburgh & Barlow 1992).
References: CSC83 - Carrasco, Serrano & Costero (1983); GMC85 - Gutiérrez-Moreno, Moreno & Cortés (1985); Ka83 - Kaler (1983); SK89 - Shaw & Kaler (1989); Web69 - Webster (1969); Web83 - Webster (1983); VP85 - Viadana & de Freitas Pacheco (1985).

3.2 Reddening

Before proceeding with the diagnostic and abundance analyses, the observed line fluxes were corrected for the effects of interstellar extinction. The extent of interstellar extinction is described by $c(\mathrm{H}\beta)$, which is the logarithmic difference between observed and dereddened Hβ fluxes, in dex. One of the best methods for deriving $c(\mathrm{H}\beta)$ is to use the ratio of the (optically thin) radio free–free flux continuum to the observed absolute Hβ flux, $F(\mathrm{H}\beta)$, since a very long baseline is employed, and the radio-frequency flux measurements are virtually free from extinction. The method used most frequently for optical spectra of PN is the comparison of the observed ratios of two or more lines of the Balmer series with their theoretically predicted ratios. However, $c(\mathrm{H}\beta)$s derived by this method are more uncertain than $c(\mathrm{H}\beta)$s derived by the radio method. The wavelength separation between lines of the strongest members of the Balmer series is quite short, compared with the radio-Hβ baseline. Also, the Balmer line ratios can be sensitive to any wavelength-dependent steps in data calibration, particularly the correction for atmospheric extinction, since mean extinction coefficients for a particular site are generally adopted, whereas the atmospheric extinction can vary from night to night, as well as during a night. However, by using a $c(\mathrm{H}\beta)$ derived from Balmer line ratios, one effectively compensates for errors that may be introduced by calibration; if the final strengths of the Balmer lines are in accord with those predicted by theory, the final corrected spectra as a whole will approximate what was emitted. Walton, Barlow & Clegg (1993) have recently found that the reddening law towards the Galactic Bulge is steeper than that found by Seaton (1979) for the local Galactic disc. There, the $c(\mathrm{H}\beta)$s derived from Balmer line ratios tend to be higher than $c(\mathrm{H}\beta)$s derived by the radio-Hβ method, because of variations in R_V. When adopting a reddening to derive the global properties of a PN, the radio-Hβ method is to be preferred.

The ratio of the integrated He II 1640-Å flux, from UV spectra, to the integrated 4686-Å flux can also be used to estimate reddening. The $c(\mathrm{H}\beta)$s derived by this method show good agreement with those derived from the radio-Hβ method. Another way to derive the reddening using *IUE* spectra is to find the $c(\mathrm{H}\beta)$ that effectively nulls the 2200-Å extinction feature.

In this work, $c(\mathrm{H}\beta)$ was derived from the optical spectra by comparing the observed Balmer decrement ratios with their theoretical values at $T_e = 10^4$ K, $n_e = 10^4$ cm^{-3} (Hummer & Storey 1987), and is denoted as $c(\mathrm{H}\beta)^{\mathrm{Ba}}$. This $c(\mathrm{H}\beta)^{\mathrm{Ba}}$ was then used to deredden the observed optical line fluxes. One could iterate and use the derived electron temperature and density to re-calculate $c(\mathrm{H}\beta)^{\mathrm{Ba}}$ explicitly, rather than assuming a constant T_e and n_e each time; however, this was found to result in a negligible change for $c(\mathrm{H}\beta)^{\mathrm{Ba}}$.

For the UV spectra, if the angular diameter of the nebula was less than the *IUE* aperture size, the ratio of He II λ1640 to λ4686 was used to derive a $c(\mathrm{H}\beta)$, denoted as $c(\mathrm{H}\beta)^{1640}$. Integrated He II 4686-Å fluxes were either taken from our wide-slit spectra (see Table 2) or derived from the $F(4686)/F(\mathrm{H}\beta)$ ratio, with $F(\mathrm{H}\beta)$ taken from the literature. The relative line fluxes from the UV spectrum were then scaled to the optical narrow-slit relative fluxes using the dereddened He II 4686-Å and 1640-Å large-aperture line fluxes. If the nebula was larger than the *IUE* aperture, the UV line fluxes were first dereddened using the value of $c(\mathrm{H}\beta)$ derived by the radio-Hβ method, denoted as $c(\mathrm{H}\beta)^{\mathrm{rad}}$, or by adopting the value of $c(\mathrm{H}\beta)$ that most effectively nulled the 2200-Å feature (in the cases of NGC 5882 and Tc 1), then scaled to the optical spectrum using $I(1640) = 6.25\,t^{0.27}\,I(4868)$ (Seaton 1978; t is $T_e/10^4$ K).

For two bright PN (NGC 6751 and 7009), the optical narrow-slit spectra were heavily saturated and fluxes for the strongest lines had to be obtained from wide-slit spectra. The scaling is quite uncertain, and, in order to compensate for this, two different reddening parameters were adopted, one for wavelengths >5411 Å and one for wavelengths <5411 Å, in order to bring the Balmer line intensities into accord with their theoretical values. The final adopted fluxes for NGC 7009 are generally within 5 per cent of those of position 1 of Barker (1983); our [O III] 4959-Å flux was adopted from Barker. Our final adopted fluxes for NGC 6751 are generally within 10 per cent of those of Aller & Czyzak (1979), except for $I(4959)$, where our value is a factor of 1.8 higher than the value of Aller & Czyzak (1979). For M 3-1, M 1-13 and NGC 2867, the strongest Balmer lines were saturated in the spectra, and it was not possible to derive a reliable $c(\mathrm{H}\beta)^{\mathrm{Ba}}$. For these three objects, $c(\mathrm{H}\beta)^{\mathrm{rad}}$ was used to deredden the spectral line intensities, which were then scaled via Hδ. Fluxes for the strongest lines were adopted from higher resolution spectra.

In cases where the He II 4686-Å line was very strong [$F(4686) \geq 75$, where $F(\mathrm{H}\beta) = 100$][3], the He II Pickering series begins to contribute significantly to the hydrogen Balmer series. For objects of high excitation, the He II 8–4 contribution to Hβ was estimated using $I(8\text{–}4) = 0.05016\,I(4686)$ (Hummer & Storey 1987), and subtracted from $I(\mathrm{H}\beta)$ before performing further analysis.

The observed line fluxes were dereddened using the mean UV and optical reddening laws of Seaton (1979) and Howarth (1983). After dereddening, the fluxes of components of unresolved blends were estimated. The contribution of He I 4713 Å to the [Ar IV] 4711-Å feature was estimated as $0.0915\,I(4471)$ at $T_e = 10^4$ K, $n_e = 10^4$ cm^{-3} (Brocklehurst 1971). The strongest reliable He I 4471-Å flux relative to H$\beta = 100$ is ~ 7 for He 2-111. This corresponds to He I $I(4713) = 0.6$. Subtraction of this makes a 2 per cent difference to the flux of [Ar IV] 4711 Å; hence the effect of errors introduced in subsequently derived electron densities based on the [Ar IV] 4711/4740-Å ratio is minimal. Typical $I(4471)$ fluxes are ~ 4, so a typical $I(4713)$ is 0.3. In the PN where [Ne IV] 4725 Å was observed, the contribution of [Ne IV] 4714 + 4716 Å to [Ar IV] 4711 Å was removed, where $I(4714+16) = 0.623\,I(4724+26)$ (Zeippen 1982).[4] [Ne IV] 4725 Å is always very weak compared with [Ar IV] 4711 Å, so again the errors introduced into n_e(Ar IV) will be minimal.

[3]All line fluxes are presented on a scale relative to Hβ, where $F(\mathrm{H}\beta)$ [or $I(\mathrm{H}\beta)$] is 100. Observed fluxes are denoted by $F(\lambda)$ and dereddened fluxes by $I(\lambda)$.

[4]Although the strengths of the [Ne IV] 4714, 16-Å and 4724, 26-Å features are extremely temperature sensitive, the ratio $I(4714+16)/I(4725+26) = 0.623$ remains unchanged over the temperature range of 5000–20 000 K, for densities less than 10^6 cm^{-3}.

The O III 3428-Å contribution to [Ne v] 3426 Å was estimated from the O III 3444-Å line, where $I(3428) = 0.336I(3444)$ (Saraph & Seaton 1980). Recently, O'Dell & Miller (1992) have investigated the effect of charge exchange on intensities of the O III Bowen lines in PN. No change was found for the O III 3428/3444-Å ratio from that of Saraph & Seaton. No correction for O III Bowen line contamination was made to the [Ne v] 3426-Å fluxes of He 2-111, He 2-29 or He 2-112 as O III 3444 Å is very weak compared with [Ne v] 3428 Å in these objects.

Table 3 presents the reddening functions $f(x)$ as a function of wavelength, the dereddened line fluxes relative to $H\beta = 100$, and $c(H\beta)^{Ba}$, the extinction derived from the Balmer decrement, and also $c(H\beta)^{rad}$ and $c(H\beta)^{1640}$ for the PN with UV measurements. The observed fluxes relative to $H\beta$ can be calculated by multiplying the dereddened intensities by $10^{-c(H\beta)f(x)}$. Fluxes followed by two colons were not used in any subsequent analysis. Fluxes followed by one colon are used, but with caution. The total [O II] 3726 + 3729-Å flux is presented; the ratios of the two components can be found in Kingsburgh & Barlow (1992) and Kingsburgh & English (1992). The IDS spectrum of Me 2-1 was of poor quality; therefore, the observed optical fluxes were adopted from Aller, Keyes & Czyzak (1981). For a few PN that only had IDS spectral coverage to ~5200 Å, [N II] 6584-Å fluxes were adopted from the literature in order to enable the derivation of nitrogen abundances. References are given in the notes following Table 3. Fluxes for A30 are presented relative to $I(5007) = 100$, and can be compared to those of Knot 4 in Jacoby & Ford (1983). A30 is further discussed in Section 6.

The observed fluxes for Mz 2, A65, K 1-2, Pe 1-3, IC 972 and ESO 223-10 are presented in Table 4. The spectra have poor S/N, and no further analysis is done.

4 NEBULAR ELECTRON TEMPERATURES AND DENSITIES

Electron temperatures and densities have been derived using the following ratios:

T_e(O III): $I(4959)/I(4363)$,

T_e(N II): $I(6584 + 6548)/I(5755)$,

n_e(S II): $I(6717)/I(6731)$,

n_e(Ar IV): $I(4711)/I(4740)$,

n_e(Cl III: $I(5517)/I(5537)$.

The atomic data used in the diagnostic and abundance analyses are listed in Table 5. The diagnostic ratios for T_e(O III), T_e(N II), n_e(S II), n_e(Ar IV) and n_e(Cl III) are presented in Table 6. The errors on the temperature-sensitive ratios are based on the error associated with either the [O III] 4363-Å flux or the [N II] 5755-Å flux; errors on the fluxes of these weak auroral transitions are the major source of error for subsequently derived temperatures. The errors on the density diagnostic ratios are based on the errors on each member of the doublet, with the cross term subtracted. The programs EQUIB and RATIO (written by I. D. Howarth and modified by S. Adams) were then used to solve the equations of statistical equilibrium to obtain n_e as a function of T_e for each diagnostic ratio. Temperatures and densities were derived as follows: T_e(O III) and T_e(N II) were derived using n_e(O II) [or n_e(S II) if no n_e(O II) was available]; n_e(S II) was derived using T_e(N II), provided that $I(5755)$ was of good S/N, otherwise T_e(O III) was used; n_e(Ar IV) and n_e(Cl III) were derived using T_e(O III). Table 7 presents the derived values of t(O III), t(N II), n_e(S II), n_e(O II), n_e(Ar IV) and n_e(Cl III) with associated errors (t is $T_e/10^4$ K). The ratios for the [O II] 3726/3729-Å doublet can be found in Kingsburgh & Barlow (1992) and Kingsburgh & English (1992), but the derived densities are presented here again for completeness. Temperature values that were adopted based on nebular excitation are in parentheses; the calibration is described in Section 4.2.

The ratios of [O II] 3727/7325 Å and [S II] 4070/6725 Å are also temperature and density diagnostics. Their diagnostic loci were generally found to lie in the same range as those of the above diagnostics. However, because of the sometimes uncertain fluxes for the [O II] 7325-Å multiplet (due to its location at the edge of the detector) and for [S II] 4068 + 4076 Å (due to the intrinsic weakness of the lines) and because of the long wavelength separation, which makes these ratios sensitive to reddening, these two diagnostics are less accurate than the other diagnostic ratios; hence they are not presented here.

4.1 High-density objects

Values of the electron density for He 2-97 from various doublet ratios appear discrepant. The value of n_e(O II) given by Kingburgh & Barlow (1992) is 17 000 cm^{-3}, derived from a 'circular' weighted mean 3726/3729-Å ratio of 2.57 ± 0.064. In Kingsburgh & English (1992), however, the n_e(O II) obtained by a trailed exposure is 6170^{+640}_{-590} cm^{-3} and n_e(S II) is 9550^{+1800}_{-1500} cm^{-3}. Tylenda et al. (1989) give $n_e = 8000$ cm^{-3}; Shaw & Kaler (1989) list $n_e = 6300$ cm^{-3}. The angular diameter for He 2.97 is given as < 3 arcsec by Milne & Aller (1982); as it is a compact PN, it is more likely to have a higher rather than lower density. The [O II] and [S II] emission is likely to come from an outer region of lower density, as in the cases of IC 4997, Vy 2-2 and Hb 12, which were discussed by Kingsburgh & Barlow in section 5.2. Indeed, inspection of the [O II] doublet ratios for each spatial cros-section in the long-slit spectrum (table 3 of Kingsburgh & Barlow 1992) reveals that two of the three cross-sections show [O II] doublet ratios that are at the high-density limit. The other cross-section shows $I(3726)/I(3729) = 2.16$, which is equal to the [O II] doublet ratio found from the trailed exposure [where $I(3726)/I(3729) = 2.18$, see Kingsburgh & English 1992]. In this work, we find the [Ar IV] 4711/4740-Å ratio to be at the high-density limit (Table 7). Also, the [N II] 6584 + 6548/5755-Å ratio is 35, which indicates that the upper levels are undergoing collisional de-excitation, and hence the ratio is more appropriate for use as a density rather than temperature diagnostic. Thus, with T_e(O III) = 9200 K, n_e(N II) = 76 000 cm^{-3} is derived and adopted for the subsequent analysis.

A similar situation is found for the very low-excitation nebula, H 2-1 [VLE; where a VLE PN is defined as having $F(5007) < F(H\beta)$]. H 2-1 is also a compact PN, whose angular diameter is given as 2.2 arcsec by Zijlstra, Pottasch & Bignell (1989). Table 3 of Kingsburgh & Barlow (1992) reveals that the [O II] 3726/3729-Å ratio is approaching its

Table 3. Dereddened line intensities.

	f(x)	IC 2003	J 900	M 3-1	M 1-11	M 1-13	NGC 2371-2	NGC 2440'	NGC 2438	NGC 2452
$c(H\beta)^{Ba}$		0.64	0.80		1.68		0.00	0.65	0.67	0.68
$c(H\beta)^{Rad}$			0.71	0.16	1.34	0.35	0.00	0.68	0.23	0.69
$c(H\beta)^{1640}$		0.42								
N V 1240	1.648	25:		–	75::	–	80.8	164	–	–
C II 1335	1.422	–		–	–	–	17.5	–	89.0	–
O IV 1401	1.312	20.8	–	–	–	–	101	67.7	–	–
N IV] 1486	1.233	22.0	–	–	13::	6.5:	110	225	110::	85.8
C IV 1550	1.185	423	1030	–	12::	–	416	438	301	310
He II 1640	1.138	392	310	–	–	–	792	267	673	563
O III] 1663	1.130	31.9	–	–	–	–	15.3	22.1	–	–
N III] 1750	1.121	14.8	–	5.08	–	6.7:	25.0:	163	92::	58.5
C III] 1908	1.230	416	1570	23.2	6::	–	166	302	412	415
C II] 2326	1.358	29.3	228	–	–	–	–	123	–	–
[Ne IV] 2423	1.120	44.9	66.9	–	–	–	345	172	–	135
[O II] 2470	1.025	–	–	–	–	–	–	17.9	–	–
He II 2734	0.696	–	–	–	–	–	–	16.3	–	13.2
O III 3133	0.447	–	–	–	–	–	43.4	63.8	–	60.3
[Ne V] 3426	0.334	4.4:	–	–	–	–	348	315	39.5	17.9
O III 3428	0.334	(5.51)	–	–	–	–	(4.1:)	(6.60)	–	–
O III 3444	0.329	16.4	–	–	–	–	12.2	19.7	–	–
[O II] 3727	0.257	20.8	85.1	91.6	63.8	449	19.9	107	84.3	89.3
H12 3750	0.253	–	–	4.3	–	3.65	–	7.40	–	3.63
H11 3770	0.249	3.32	–	3.55	–	4.10	–	6.39	–	3.89
H10 3798	0.244	4.34	–	4.74	5.39	5.04	–	4.26	–	4.54
H9 3835	0.237	6.11	–	7.16	11.0	6.53	14.1	10.4	–	7.61
[Ne III] 3868	0.231	79.1	110	73.5	–	131	35.1	104	85.6	114
H 8+He I 3889	0.226	17.4	24.3	22.2	13.7	22.8	15.8	16.1	–	15.4
[Ne III] 3967	0.211	38.1	42.6	22.6	–	39.1	20.8	39.7	–	35.2
Hε 3970	0.210	*	*	16.5	15.6	14.3	*	*	–	17.9
He I 4026	0.198	2.79	–	2.00	–	5.19	2.02	–	–	1.77
[S II] 4068	0.189	2.09	5.12	0.97	–	3.33	–	4.58	–	3.93
[S II] 4076	0.187	–	–	–	–	–	–	–	–	–
Hδ 4101	0.182	28.3	27.7	26.3	26.8	26.1	19.9	26.0	–	26.9
Hγ 4340	0.127	46.3	47.0	46.6	51.8	50.9	40.5	38.5	47.9	37.5
[O III] 4363	0.121	12.0	13.2	6.75	–	11.5	6.35	16.7	19.3	13.8:
He I 4471	0.096	1.94	4.24	4.75	–	7.13	–	3.25	–	1.64
He II 4686	0.043	60.9	47.7	0.48	–	18.8	121	79.4	99.4	86.6
[Ar IV] 4711	0.037	5.32	1.40	1.04	–	3.09	13.5	9.36	–	8.85
[Ne IV] 4725	0.033	1.0:	1.13:	–	–	3.54	–	2.36	–	–
[Ar IV] 4740	0.030	4.60	1.90	0.82	–	3.25	11.0	9.60	–	7.05
Hβ 4861	0.000	100.0	100.0	100.0	100.0	100.0	100.0	100.0	100.0	100.0
[O III] 4959	-0.024	343	368	271	2.29	396	145	345	344	350
[N I] 5200	-0.083	–	–	0.65	–	9.60	4.67	7.24	–	–
He II 5411	-0.133	4.61	–	–	–	1.49	8.23	5.85	–	5.81
[Cl III] 5517	-0.154	0.76	–	0.57	–	–	–	–	–	–
[Cl III] 5537	-0.158	0.75	–	0.59	–	–	–	–	–	–
[N II] 5755	-0.195	0.53:	–	1.14	4.90	9.71	–	6.20	–	1.96:
He I 5876	-0.215	7.89	–	14.7	3.08	17.7	0.42:	6.45	7.32	5.99
[O I] 6300	-0.282	3.54	–	3.37	2.10	25.3	–	9.72	–	–
[S III] 6312	-0.283	0.69	–	2.27	–	1.6:	6.24	1.62	–	3.07
[Ar V] 6435	-0.291	0.46	–	–	–	–	10.4	2.76	–	–
[N II] 6548	-0.318	(5.20)	–	21.0	71.0	215	–	172	18.6	27.8
Hα	-0.320	289	–	–	294	–	279	272	286	284
[N II] 6584	-0.323	15.2	[35.4]	71.7	225	629	4.58:	507	47.3	76.0
He I 6678	-0.336	1.47	–	4.44	1.36	4.92	–	5.68	2.12	3.10
[S II] 6717	-0.342	0.83	–	6.90	–	20.7	–	3.07	7.93	8.86
[S II] 6731	-0.344	1.64	–	9.26	–	23.2	–	5.96	5.03	11.9
[Ar V] 7005	-0.380	0.42	–	–	–	–	9.85	5.36	–	–
He I 7065	-0.387	2.18	–	4.07	2.26	5.01	–	3.06	–	–
[Ar III] 7135	-0.396	5.05	–	13.5	1.28	34.6	12.0	20.5	10.2	28.7
[O II] 7325	-0.419	–	–	4.54	–	15.4	–	10.3	8.18	–

Table 3 – *continued*

	IC 2448	NGC 2792	NGC 2867	NGC 3195	Fg 1	NGC 5189	NGC 5307	NGC 5315	He 2-111
$c(H\beta)^{Ba}$	2.77::	1.5:		0.45	0.38:	0.65	0.69	1.1:	1.13
$c(H\beta)^{Rad}$	0.40	1.05	0.46	0.12	0.29	0.56	0.58	0.61	1.09
$c(H\beta)^{1640}$			0.47[a]						
N V 1240		–	–	–	–	–	–		2170::
C II 1335		–	12.5	–	–	–	–		–
O IV 1401	–	67.5	5.19	–	–	–	92.6	–	–
N IV] 1486	38.5	81:	15.9	–	–	62.5	142:	–	945::
C IV 1550	328	294	242	–	–	–	193	–	–
He II 1640	326	648	204	152	120	611	366	–	960
O III] 1663	28.7	29.9	11.1	–	–	67.9	65.1	7.34	–
N III] 1750	12.2:	58:	7.52	–	–	55.3	106:	–	790
C III] 1908	353	592	665	87.9	13::	145	179	–	852
C II] 2326	11.3	–	96.4	–	–	–	–	–	–
[Ne IV] 2423	38.3	229	24.0	–	–	122	–	–	590
[O II] 2470	–	–	6.29	–	–	–	–	10.6	–
He II 2734	14.8	20.3	6.32	–	–	19.2	–	–	–
O III 3133	14.3	–	40.9	–	–	–	–	–	–
[Ne V] 3426	66.4	130::	–	–	–	38.1	–	–	590
O III 3428	–	(25::)	(4.95)	–	–	–	–	–	–
O III 3444	–	74.1	23.3	–	–	–	–	–	38.2
[O II] 3727	7.12	–	115	208	22.8	135	19.5	47.5	250
H12 3750	–	–	4.52	4.36	3.42	–	–	4.56	–
H11 3770	2.91	–	5.52	5.50	3.56	–	–	4.02	–
H10 3798	3.11	5.19	9.03	6.22	5.09	–	5.16	3.87	7.61
H9 3835	5.22	7.22	11.1	7.32	6.94	–	–	6.93	11.1
[Ne III] 3868	121	63.1	126	85.0	63.2	137	106	64.1	231
H 8+He I 3889	15.8	15.9	21.5	23.8	20.6	12.2	14.2	13.2	17.9
[Ne III] 3967	58.7	38.8	50.6	35.8	29.3	41.7	36.4	35.1	71.1
$H\epsilon$ 3970	*	*	*	*	*	*	*	*	14.6
He I 4026	3.01:	–	2.10	3.40	1.84	–	2.65	2.21	6.93
[S II] 4068	2.03	–	2.15	5.83	–	–	0.97	5.44	14.7
[S II] 4076	–	–	0.84	–	1.67	–	–	2.62	5.97
$H\delta$ 4101	34.9	29.5	27.0	29.7	28.7	22.3	28.2	26.7	26.3
$H\gamma$ 4340	46.6	44.2	43.7	49.5	45.5	47.0	47.1	45.5	46.4
[O III] 4363	11.3	12.2	15.6	4.91	3.62	15.5	16.8	2.33	34.3
He I 4471	2.17	–	4.11	5.41	4.01	3.94	1.91:	4.60	7.53
He II 4686	51.2	100.4	32.0	24.2	19.4	93.4	56.4	–	138
[Ar IV] 4711	4.84	8.73	2.78	1.19	2.23	13.2	6.24	–	25.8
[Ne IV] 4725	–	–	0.27:	–	–	–	–	–	–
[Ar IV] 4740	3.61	7.90	2.50	0.93	2.09	9.06	4.12	–	17.6
$H\beta$ 4861	100.0	100.0	100.0	100.0	100.0	100.0	100.0	100.0	100.0
[O III] 4959	448	350	575	181	200	378	449	277	377
[N I] 5200	–	–	0.87	3.45	–	1.86	–	–	33.0
He II 5411	–	6.27	2.98	–	1.49	6.64	4.31	–	8.40
[Cl III] 5517	–	–	0.42	0.76	0.46	–	–	–	1.63
[Cl III] 5537	–	–	0.68	0.59	0.54	–	–	–	3.92
[N II] 5755	–	–	1.30	2.15	–	–	–	–	27.2
He I 5876	–	3.08	13.6	15.5	13.5	7.70	8.78	–	13.6
[O I] 6300	–	1.48	4.22	–	–	–	–	–	–
[S III] 6312	–	–	2.03	1.41:	–	5.13	–	–	12.9
[Ar V] 6435	–	–	–	–	–	–	–	–	–
[N II] 6548	–	–	27.6	80.50	3.04	69.6	–	–	474
$H\alpha$	–	285	–	294	278	287	293	–	285
[N II] 6584	[3.00]	5.26	81.2	256	7.93	230	2.08	[192]	1240
He I 6678	–	–	3.69	4.19	4.14	5.12	–	–	3.70
[S II] 6717	–	–	5.29	32.2	1.30	24.5	–	–	73.9
[S II] 6731	–	–	8.24	27.3	1.99	21.8	1.42	–	80.6
[Ar V] 7005	–	–	–	–	–	–	–	–	7.87
He I 7065	–	–	4.91	2.29	–	–	–	–	3.84
[Ar III] 7135	–	–	15.8	17.2	9.14	30.4	1.61	–	44.3
[O II] 7325	–	–	1.21	–	–	–	3.49	–	9.89

Table 3 – *continued*

	NGC 5873	NGC 5882	Me 2-1	NGC 5979	He 2-138	NGC 6153	Tc 1	He 2-434	NGC 7009
$c(H\beta)^{Ba}$	1.14:	0.5:		0	0.69	0.96	0.44	0.35	[d]
$c(H\beta)^{Rad}$	0.12	0.44		0.59	0.25	1.07	0.40	0.25	0.09
$c(H\beta)^{1640}$	0.60	0.5[b]	[c]	0.88			0.30[b]		
N V 1240			45.8		–		–	–	–
C II 1335			24.0		–		–	–	–
O IV 1401	–	31.5::	113	68.3	–	–	–	–	–
N IV] 1486	–	–	49.1	86.1	–	–	–	104	13.8
C IV 1550	366	–	1480	333	–	–	–	–	14.9
He II 1640	347	75.0	559	754	–	104	–	33.6	112
O III] 1663	25.8	20.4	38.5	32.0	–	32.2	–	–	6.99
N III] 1750	19.3	28.2	28.8	47.5	–	31.1	–	–	8.33
C III] 1908	596	168	944	519	<2	40.7	46.0	94.4	65.5
C II] 2326	–	–	55.1	–	–	–	–	–	4.74
[Ne IV] 2423	–	–	243	320	–	–	–	–	5.65
[O II] 2470	–	7.64	–	–	–	–	30.8	–	–
He II 2734	–	–	18.9	–	–	–	–	–	2.14
O III 3133	–	27.0	101	69.0	–	52.9	–	73.9	45.7
[Ne V] 3426	–	–	–	38.2	–	–	–	–	–
O III 3428	–	–	–	–	–	–	310	–	–
O III 3444	–	6.80	–	–	–	–	–	–	15.0
[O II] 3727	38.4	33.5	41.1	7.35:	44.8	20.2	–	–	13.3
H12 3750	–	5.99:	–	–	–	–	–	1.79	0.56
H11 3770	4.10	5.28:	–	2.73:	–	–	–	2.55	3.85
H10 3798	4.67	4.78	–	4.34	–	–	–	4.05	5.26
H9 3835	–	7.32	–	5.56	–	–	–	5.58	7.23
[Ne III] 3868	109	113	86.0	51.7	–	62.2	–	80.9	105
H 8+He I 3889	20.5	23.1	–	9.88	14.9	17.0	–	18.9	21.6
[Ne III] 3967	50.0	49.0	–	28.1	–	34.7	–	26.5	50.6
$H\epsilon$ 3970	*	*	–	*	–	*	–	17.9	22.7
He I 4026	1.93	4.18	–	–	–	–	–	2.10	3.16
[S II] 4068	1.80	4.66	–	–	3.49	–	–	–	1.28
[S II] 4076	–	–	–	–	*	–	–	–	0.95
$H\delta$ 4101	35:	31.3	27.7	26.2	30.2	24.6	27.2	27.2	30.6
$H\gamma$ 4340	46.9	46.9	47.8	46.1	48.4	47.2	44.1	51.1	49.9
[O III] 4363	13.6	6.60	20.7	14.6	–	5.45	0.45	8.75	7.77
He I 4471	2.33:	4.65	1.21	0.99	–	4.48	1.10	4.70	5.02
He II 4686	53.6	12.1	85.0	113	–	16.4	–	–	18.0
[Ar IV] 4711	1.97	1.90	7.63	11.4	–	–	–	3.14	4.42
[Ne IV] 4725	–	–	–	–	–	–	–	–	–
[Ar IV] 4740	2.40	2.44	5.33	7.20	–	–	–	2.55	4.78
$H\beta$ 4861	100.0	100.0	100.0	100.0	100.0	100.0	100.0	100.0	100.0
[O III] 4959	384	403	464	348	–	407	27.6	442	[393]
[N I] 5200	–	–	–	–	–	–	–	–	–
He II 5411	–	–	–	–	–	–	–	–	1.04
[Cl III] 5517	–	–	–	–	–	–	–	–	–
[Cl III] 5537	–	–	–	–	–	–	–	–	–
[N II] 5755	–	–	–	–	–	–	–	–	0.21
He I 5876	–	–	3.37	–	<1.4	–	9.01	17.9	15.6
[O I] 6300	–	–	–	–	2.41	–	–	–	–
[S III] 6312	–	–	–	–	–	–	–	–	1.50
[Ar V] 6435	–	–	–	–	–	–	–	–	–
[N II] 6548	–	–	2.77	–	66.4	–	31.7	1.19	3.40
$H\alpha$	–	–	289	–	313	–	280	307	280
[N II] 6584	[17.5]	[13.5]	8.11		196	[104]	95.1	3.62	10.0
He I 6678	–	–	1.51	–	–	–	–	5.00	4.22
[S II] 6717	–	–	1.58	–	9.65	–	3.61	–	2.86
[S II] 6731	–	–	2.18	–	15.4	–	*	–	–
[Ar V] 7005	–	–	1.68	–	–	–	–	–	–
He I 7065	–	–	–	–	–	–	–	6.31	4.57
[Ar III] 7135	–	–	8.14	–	–	–	5.29	8.29	14 7
[O II] 7325	–	–	–	–	<2.5	–	5.18	–	1.97

Table 3 – *continued*

	K 3-67	M 1-8	PB 1	SkWl 3-2	M 1-12	M 3-3	M 3-4	M 3-5	M 3-6	A 30[f]
c(Hβ)[Ba]	0.46	1.19	0.81:	0.49	1.40	0.44:	0.70	0.90	0.58	0.0
[Ne V] 3426	–	–	17.7	281	–	–	–	–	–	43.3
O III 3428	–	–	–	–	–	–	–	–	–	--
O III 3444	–	–	–	–	–	–	–	–	–	--
[O II] 3727	58.6	379	14.7	172	157	374	362	329	16.3	8.44
H12 3750	–	5.73	–	–	–	–	–	–	3.38	--
H11 3770	–	6.66	–	–	6.51	–	–	6.11:	2.85	--
H10 3798	–	6.30	–	–	6.74	–	–	5.71	4.66	--
H9 3835	–	8.67	7.05	–	7.19	5.82	–	6.83	7.33	--
[Ne III] 3868	126	162	109	–	–	109	142	134	45.6	16.1
H 8+He I 3889	–	21.1	20.6	–	15.6	31.4	–	20.0	21.3	--
[Ne III] 3967	45.1	52.2	37.9	–	–	32.8	–	51.1	33.1	3.44
Hε 3970	*	*	*	–	18.9	18.7	–	*	*	--
He I 4026	7.23	–	4.52	–	–	6.86:	–	2.51	2.95	--
[S II] 4068	–	3.21	1.74	–	4.59	5.37:	–	–	0.61:	--
[S II] 4076	–	1.75	–	–	*	–	–	2.01	–	--
Hδ 4101	22.8	26.9	33.5	–	27.6	25.9	14.6	25.1	26.0	--
Hγ 4340	47.3	51.2	50.7	–	54.2	46.7	46.5	50.3	47.7	--
[O III] 4363	16.6	13.7	11.5	–	–	11.8	14.4	14.3	2.54:	1.58
He I 4471	5.31	3.11	5.65	–	2.73	3.67	–	3.79	4.11	--
He II 4686	–	54.4	39.5	69.3	–	37.0	38.3	33.2	2.36	4.81
[Ar IV] 4711	2.63	3.89	5.95	–	–	3.81	–	–	–	3.93[g]
[Ne IV] 4725	–	0.87:	–	–	–	–	–	–	–	4.93
[Ar IV] 4740	2.93	2.05	5.19	–	–	1.68	–	–	–	–
Hβ 4861	100.0	100.0	100.0	100.0	100.0	100.0	100.0	100.0	100.0	--
[O III] 4959	360	403	394	81.0	3.95	300	431	232	208	32.4
[O III] 5007	–	–	–	–	–	–	–	–	–	100.0
[N I] 5200	–	6.02	–	–	0.36	10.2	–	4.14	–	2.39
He II 5411	–	3.84	2.70	–	–	1.99	–	2.80	–	--
[Cl III] 5517	–	–	–	–	–	–	–	–	–	--
[Cl III] 5537	–	–	–	–	–	–	–	–	–	--
[N II] 5755	–	5.66	–	–	3.41	10.3	–	8.13	–	--
He I 5876	–	10.9	10.3	–	2.80	11.1	11.9	10.7	13.1	3.06
[O I] 6300	–	–	0.68:	–	1.98	–	–	17.7	–	--
[S III] 6312	–	2.23	–	–	0.18	–	–	1.51:	–	--
[Ar V] 6435	–	–	–	–	–	–	–	–	–	--
[N II] 6548	–	103	1.40	21.0	49.1	254	76.6	128	–	--
Hα	–	292	285	283	311	284	282	279	288	--
[N II] 6584	[58.1]	332	4.08	71.8	145	792	253	382	5.02	11.0
He I 6678	–	1.48	2.48	–	0.63	1.82	3.19	2.99	–	3.43
[S II] 6717	–	13.4	–	27.3	0.67	3.14	9.62	9.77	–	–
[S II] 6731	–	12.3	–	30.8	1.51	–	5.48	8.92	–	--
[Ar V] 7005	–	–	–	–	–	–	–	–	–	--
He I 7065	–	3.45	1.03	–	1.70	–	–	2.80	–	--
[Ar III]7135	–	18.0	8.23	–	1.24	17.4	19.0	16.6	–	--
[O II] 7325		–	–	–	15.4	–	–	10.1	–	--

	He 2-15	PB 4	He 2-28	He 2-29	NGC 2899	He 2-37	Lo 4[h]	He 2-48	He 2-51	Pe 2-7
c(Hβ)[Ba]	2.07	0.60:	0.70:	0.63	0.80	1.03	–	0.61	0.88	1.37
[Ne V] 3426	105::	–	–	66.3	497	–	522	–	–	145
O III 3428	–	–	–	–	–	–	–	–	–	(11.7)
O III 3444	–	6.80	–	10.4:	–	–	–	–	–	34.7
[O II] 3727	318	11.3	457	253	287	457	84.3:	342	310	26.8
H12 3750	–	–	–	–	–	–	–	–	–	–
H11 3770	–	–	–	6.25:	–	3.59	–	–	–	6.79

Table 3 – *continued*

	He 2-15	PB 4	He 2-28	He 2-29	NGC 2899	He 2-37	Lo 4[h]	He 2-48	He 2-51	Pe 2-7
H10 3798	–	–	–	–	–	–	–	–	–	4.49
H9 3835	–	4.96	–	6.93	–	–	–	5.98	10.5	6.70
[Ne III] 3868	162	67.2	137	146	161	195	17.2	115	139	103
H 8+He I 3889	–	16.7	20.3	16.6	–	10.2	–	17.6	27.5	16.5
[Ne III] 3967	–	27.0	50.9	50.4	–	56.2	–	38.6	61.2	36.5
Hε 3970	–	*	*	*	–	*	–	*	*	*
He I 4026	–	3.27	4.14	3.84	–	–	–	2.32	6.15:	2.94
[S II] 4068	–	7.82	3.94	4.54	–	–	–	1.56	5.88:	3.20
[S II] 4076	–	blend	–	–	–	4.51	–	–	–	–
Hδ 4101	19.7	30.3	27.7	27.0	12.5	22.3	–	25.3	30.2	29.5
Hγ 4340	42.8	46.0	45.6	46.5	54.8	46.0	–	49.0	54.1	49.9
[O III] 4363	32.2	3.99	6.16	31.4	37.3	26.9	–	11.2	9.19	22.1
He I 4471	5.88	4.92	–	–	–	2.85	–	3.86	6.23	–
He II 4686	78.9	33.4	17.9	88.9	145	72.8	149	21.1	27.5	92.3
[Ar IV] 4711	11.9	2.49	–	–	12.5	4.49	–	–	2.91	11.9
[Ne IV] 4725	–	–	–	–	6.55	–	–	–	–	2.28
[Ar IV] 4740	9.71	2.13	–	–	15.6	3.74	–	–	5.32	11.1
Hβ 4861	100.0	100.0	100.0	100.0	100.0	100.0	100.0	100.0	100.0	100.0
[O III] 4959	415	333	410	425	384	689	91.2	357	281	385
[N I] 5200	18.3	–	–	3.09	6.45	3.25:	–	4.91	3.57	–
He II 5411	4.84	–	–	4.57	5.51	3.13	–	1.19	2.08	6.03
[Cl III] 5517	–	–	–	–	–	–	–	–	–	–
[Cl III] 5537	–	–	–	–	–	–	–	–	–	–
[N II] 5755	22.1	–	–	4.05	14.2	4.22	–	3.40	2.98	–
He I 5876	11.6	–	–	4.12	5.6::	7.51	–	12.0	16.6	4.99
[O I] 6300	–	–	–	11.1	–	25.5	–	–	16.9	2.57
[S III] 6312	8.00	–	–	7.06	11.7	2.65	–	2.96	1.89	3.80
[Ar V] 6435	–	–	–	–	–	–	–	–	–	1.97
[N II] 6548	363	–	–	59.7	170	76.9	–	53.2	107	5.81
Hα	281	–	–	286	297	272	305	286	302	294
[N II] 6584	990	–	–	198	574	265	33.2:	165	346	17.4
He I 6678	2.50	–	–	3.59:	–	0.87	–	1.37	4.00	1.19
[S II] 6717	47.3	–	–	12.6	45.2	21.9	21.5	12.5	35.7	2.52
[S II] 6731	54.8	–	–	13.2	34.5	17.6	22.0	9.67	36.0	3.18
[Ar V] 7005	2.68	–	–	–	–	–	–	–	–	–
He I 7065	4.83	–	–	–	–	–	–	–	–	1.88
[Ar III] 7135	27.7	–	–	14.9	31.1	28.6	–	12.4	24.7	17.0
[O II] 7325	–	–	–	–	–	–	–	–	7.60:	2.40

	He 2-55	He 2-57	IC 2621	ESO 216-02	K 1-22	PB 8	He 2-76	He 2-77	Th 2-A
c(Hβ)[Ba]	0.80	2.00	1.30:	0.51	0.44	2.7::	1.49	4.13	1.07
[Ne V] 3426	–	–	80.6	–	–	–	–	–	–
O III 3428	–	–	(6.7)	–	–	–	–	–	–
O III 3444	–	–	20.5	–	–	–	–	–	–
[O II] 3727	29.8	–	44.1	197	242	107	326	–	111
H12 3750	–	–	2.63	–	–	6.89:	–	–	–
H11 3770	–	–	2.46	–	–	7.2::	–	–	4.34:
H10 3798	–	–	2.89	–	–	3.32	–	–	–
H9 3835	6.44	11.8	4.68	–	21::	4.70	–	–	12.1
[Ne III] 3868	110	160	128	80.3	93.7	27.7	–	–	199
H 8+He I 3889	13.6	28.7	14.9	–	–	29.2	–	–	15.1
[Ne III] 3967	40.5	51.2	51.2	28.3	29.3	29.0	–	–	56.7
Hε 3970	*	*	*	*	*	*	–	–	*
He I 4026	–	–	1.52	–	–	2.31	–	–	–
[S II] 4068	2.91	–	4.71	–	–	3.6:	–	–	4.92:
[S II] 4076	–	–	2.10	–	–	blend	–	–	4.28:
Hδ 4101	25.6	34.3	27.9	23.8	38.7	27.0	–	–	22.8

Table 3 – *continued*

	He 2-55	He 2-57	IC 2621	ESO 216-02	K 1-22	PB 8	He 2-76	He 2-77	Th 2-A
Hγ 4340	44.8	49.6	45.5	40.7	57.7	44.8	–	–	40.0
[O III] 4363	13.6	71.1	21.0	18.4	12.8	1.07	–	–	18.0
He I 4471	–	7.12	3.08	–	3.40:	5.98	–	–	2.79
He II 4686	95.5	4.58	41.4	110	28.5	7.32	80.0	–	50.1
[Ar IV] 4711	3.86	–	2.38	–	–	–	–	–	3.33
[Ne IV] 4725	–	–	1.15	–	–	–	–	–	–
[Ar IV] 4740	4.23	–	7.98	–	–	0.46	–	–	4.47
Hβ 4861	100.0	100.0	100.0	100.0	100.0	100.0	100.0	100.0	100.0
[O III] 4959	323	108	598	196	314	128	439	175	568
[N I] 5200	–	–	–	15.9	–	–	–	–	–
He II 5411	6.32	–	–	–	–	–	–	–	2.60
[Cl III] 5517	0.99	–	–	–	–	–	–	–	–
[Cl III] 5537	1.79	–	–	–	–	–	–	–	–
[N II] 5755	–	–	–	–	–	–	–	–	2.00
He I 5876	3.96	13.9	–	–	26.5:	–	–	16.9	7.24
[O I] 6300	–	4.88	–	–	–	–	–	–	–
[S III] 6312	–	3.27	–	–	–	–	–	1.71	–
[Ar V] 6435	–	–	–	–	–	–	–	–	–
[N II] 6548	4.26	(7.9)	–	–	33.9	–	132	4.89	24.1
Hα	283	336	–	272	301	–	283	285	269
[N II] 6584	10.6	13.1	–	–	103	–	441	18.3	79.0
He I 6678	–	4.09	–	–	–	–	–	2.94	1.58
[S II] 6717	3.82	1.60	–	13.2	21.7	–	32.9	3.19	5.22
[S II] 6731	3.46	1.68	–	7.73	31.1	–	30.1	4.91	6.33
[Ar V] 7005	–	–	–	3.74	–	–	–	–	–
He I 7065	–	4.54	–	–	–	–	–	8.46	–
[Ar III] 7135	14.1	6.10	–	–	18.1:	–	42.2	14.6	8.39
[O II] 7325	–	1.77		–	–		–	4.85	–

	MyCn 18	He 2-97	He 2-99	He 2-105	He 2-107	He 2-112	He 2-119	He 2-141	He 2-142
$c(H\beta)^{Ba}$	1.28	0.73	0.86	0.46	1.98	1.47	0.93	0.11:	2.0:
[Ne V] 3426	–	2.28:	–	–	–	172	–	–	–
O III 3428	–	0.71:	–	–	–	–	–	–	–
O III 3444	–	2.11	–	–	–	19.5	–	–	–
[O II] 3727	70.6	20.9	451	31.6	96.2	103	321	119	125
H12 3750	4.06	2.12	–	4.94	–	3.54	–	–	–
H11 3770	3.15:	3.33	–	4.52	–	3.34	5.10	–	–
H10 3798	–	4.31	–	5.70	–	6.30	6.40	–	–
H9 3835	4.39	6.51	–	8.60	–	7.95	10.8	–	–
[Ne III] 3868	14.5	43.0	–	29.1	15.8	153.8	109	60.2	2.91
H 8+He I 3889	13.6	17.1	–	22.1	–	16.0	25.2	10.3	18.0
[Ne III] 3967	18.2	12.3	–	19.4	–	46.2	41.7	22.3	14.4
Hε 3970	*	24.6	–	*	–	13.9	*	*	*
He I 4026	2.50	2.13	–	2.37	–	2.60	3.40	–	2.1::
[S II] 4068	2.66	1.92	–	1.91	–	5.54	6.56	–	8.5::
[S II] 4076	1.46	0.92	–	0.61	–	1.97	2.97	–	–
Hδ 4101	25.6	25.1	29.7	25.4	35.8	25.7	25.6	15.9	23.5
Hγ 4340	46.8	40.2	45.5	45.5	45.8	45.1	47.4	46.8	46.8
[O III] 4363	0.45::	3.22	2.59	2.03	–	29.2	5.38	21.3	3.33::
He I 4471	4.03	5.02	4.95	4.39	11.7	4.74	5.39	4.29	2.07
He II 4686	–	–	–	–	17.8	58.5	32.8	35.9	–
[Ar IV] 4711	0.23	0.60	–	–	–	6.52	1.55	7.04	–
[Ne IV] 4725	–	–	–	–	–	1.87	–	–	–
[Ar IV] 4740	0.05	0.40	–	–	–	7.49	1.04	4.52	–
Hβ 4861	100.0	100.0	100.0	100.0	100.0	100.0	100.0	100.0	100.0
[O III] 4959	109	204	–	122	13.0	575	263	631	4.52
[N I] 5200	0.41	0.55	–	–	–	1.53	6.02	–	–

Table 3 – *continued*

	MyCn 18	He 2-97	He 2-99	He 2-105	He 2-107	He 2-112	He 2-119	He 2-141	He 2-142
He II 5411	–	–	–	–	–	4.56	1.34	–	–
[Cl III] 5517	0.43	–	–	–	–	–	–	–	–
[Cl III] 5537	0.60	–	–	–	–	1.21	–	–	–
[N II] 5755	3.51	1.76	1.91	–	–	7.03	3.54	–	–
He I 5876	14.6	15.1	–	14.2	17.2	13.1	15.3	–	–
[O I] 6300	1.46	1.86	–	–	–	–	3.39	–	–
[S III] 6312	0.99	1.02	–	–	–	5.50	–	–	–
[Ar V] 6435	–	–	–	–	–	1.58	1.08	–	–
[N II] 6548	89.8	15.0	65.5	2.63	63.7	[99.8]	283	–	–
Hα	326	273	284	283	285	–	356	–	–
[N II] 6584	261	44.6	191	7.70	183	[300]	3.08	–	–
He I 6678	2.80	3.25	–	3.45	2.38	4.12	36.5	–	–
[S II] 6717	1.77	0.35	22.8	1.62	–	9.69	32.5	–	–
[S II] 6731	3.87	0.84	29.9	1.09	5.40	13.9	–	–	–
[Ar V] 7005	–	–	–	–	–	2.67	1.93	–	–
He I 7065	4.10	5.12	–	–	–	6.46	22.1	–	–
[Ar III] 7135	8.91	1.00	–	5.58	7.82	26.5	–	–	–
[O II] 7325	5.65	15.5	–	–	–	–		–	–

	NGC 6026	PC 14	H 2-1	IC 4642	M 1-26	IC 4673	NGC 6751	NGC 6905	IC 5148-50
$c(H\beta)^{Ba}$	0.52	0.71	1.28	0.60:	1.59	1.58	[e]	0.27	0.38
[Ne V] 3426	–	–	–	241	–	(35.2)	–	–	–
O III 3428	–	–	–	–	–	8.43	–	–	–
O III 3444	–	–	–	–	–	25.1	–	–	–
[O II] 3727	–	51.6	169	7.83	100	35.8	205	12.8	–
H12 3750	–	2.67	4.00	–	2.39	–	3.20	6.98	–
H11 3770	–	3.45	5.37	–	2.73	–	2.27	6.24	–
H10 3798	–	5.00	5.80	–	3.54	–	3.64	–	–
H9 3835	–	7.25	9.65	5.84	5.24	–	5.83	9.42	–
[Ne III] 3868	34.2	106	–	59.8	0.14	157	80.1	89.9	66.2
H 8+He I 3889	–	19.5	17.4	17.0	9.87	19.8	27.8	14.7	26.1
[Ne III] 3967	–	43.2	–	21.8	–	40.7	45.1	42.1	17.6
Hε 3970	–	*	18.8	*	12.3	*	*	*	–
He I 4026	–	1.71	–	–	0.70	–	2.35	–	–
[S II] 4068	–	3.44	5.40	–	3.86	–	3.06	–	–
[S II] 4076	–	*	*	–	1.23	3.55	1.23	–	–
Hδ 4101	39.9	26.5	26.8	27.4	28.6	30.4	25.4	24.9	32.5
Hγ 4340	55.5	46.0	45.9	45.5	48.8	48.8	46.1	43.3	46.9
[O III] 4363	8.81	3.86	0.82:	10.7	0.33:	16.3	8.03	10.2	10.6
He I 4471	7.44	4.55	2.70	1.81	3.23	6.73	5.52	–	8.15
He II 4686	71.5	2.64:	–	99.5	–	90.9	18.8:	103	46.3
[Ar IV] 4711	–	0.58	–	10.8:	–	11.4	–	4.09	5.19
[Ne IV] 4725	–	–	–	–	–	3.35	–	–	–
[Ar IV] 4740	–	0.84	–	6.96	–	9.63	–	4.98	9.12
Hβ 4861	100.0	100.0	100.0	100.0	100.0	100.0	100.0	100.0	100.0
[O III] 4959	150	516	17.9	230	14.7	368	478	335	177
[N I] 5200	–	–	–	–	–	–	1.19	–	–
He II 5411	–	0.78	–	–	–	3.79	0.60	–	–
[Cl III] 5517	–	–	–	–	–	–	–	–	–
[Cl III] 5537	–	–	–	–	–	–	–	2.87	–
[N II] 5755	–	–	1.9	–	4.17	–	1.70	–	–
He I 5876	<14.3	16.1	6.0	–	6.47	9.49	12.4	2.44	–
[O I] 6300	–	2.69	1.92	–	1.82	–	7.71	–	–
[S III] 6312	–	1.43	1.61	–	1.58	2.88	2.26	–	–
[Ar V] 6435	–	–	–	–	–	–	–	–	–

Table 3 – *continued*

	NGC 6026	PC 14	H 2-1	IC 4642	M 1-26	IC 4673	NGC 6751	NGC 6905	IC 5148-50
[N II] 6548	–	12.6	18.7	–	40.0	–	58.1	–	23.6
Hα	297	290	286	–	312	297	283	277	266
[N II] 6584	16.8	35.3	57.5	–	116	27.6	199	4.96	69.1
He I 6678	–	3.29	1.46	–	1.70	2.68	2.49	–	–
[S II] 6717	–	3.59	2.13	–	1.05	3.78	7.73	–	7.14
[S II] 6731	–	5.61	3.44	–	2.88	3.35	9.92	–	10.4
[Ar V] 7005	–	–	–	–	–	–	–	–	–
He I 7065	–	3.20	3.51	–	3.73	–	–	–	–
[Ar III] 7135	–	10.4	2.90	–	4.67	19.7	14.7	9.75	–
[O II] 7325	–	–	39.0	–	45.9	–	6.04	–	–

Notes. ':' indicates ~ 50 per cent uncertainty in the measured flux. '::' indicates greater than a factor of 2 uncertainty in the measured flux; flux not used for abundance analysis. *indicates that the listed line is present in blend with the above-listed line, i.e. Hε is blended with [Ne III] 3967 Å; [S II] 4076 Å is blended with [S II] 4068 Å. ( ) values in parentheses are predicted from line ratios. [ ] values in square brackets are adopted from the literature as follows: He 2–107 – fluxes are from the wide-slit run, [N II] 6584/Hα ratio from Kaler 1983; NGC 5882–I(6584) adopted from TPP77; NGC 7009 – I(4959) adopted from Ba78; NGC 5315 – I(6584) adopted from TPP77; NGC 5873 – I(6584) adopted from TPP77; IC 2448 – I(6584) adopted from TPP77; J900 – I(6584) adopted from AK87; NGC 6153 – I(6584) adopted from Pottasch et al. (1986). $c(H\beta)^{Ba}$ was derived from Balmer line ratios. $c(H\beta)^{Rad}$ was derived from the 5-GHz to Hβ ratio. $c(H\beta)^{1640}$ was derived from an integrated He II 1640- to 4686-Å ratio. [a] $c(H\beta)^{1640}$ for NGC 2867 derived via He II 1640- to 2734-Å ratio. [b] $c(H\beta)^{1640}$ for NGC 5882 and Tc 1 derived via nulling of the 2200-Å feature. [c] $c(H\beta)^{1640}$ for Me 2-1 derived via weighted mean of $c(H\beta)=0.21$ (1640/4686 ratio); $c(H\beta)=0.46$ (1640/2734 ratio); $c(H\beta)=0.26$ (2734/4686 ratio). [d] $c(H\beta)^{Ba}$ adopted for NGC 7009 is 0.0 for $\lambda<5411$ Å and 0.19 for $\lambda>5411$ Å (see text). [e] $c(H\beta)^{Ba}$ adopted for NC 6751 is 0.54 for $\lambda<5411$ Å and 1.25 for $\lambda>5411$ (see text). [f] Fluxes for A 30 are presented relative to I(5007) = 100 (see text). [g] λ4711 feature entirely due to [Ne IV] in A30. [h] Observed fluxes presented for Lo 4, but He^{++} contribution removed from Balmer lines. [i] See discussion in Section 4.6 on the UV fluxes for NGC 2440. [j] Fluxes for Mz 2 and K 1-2 presented relative to Hα = 100.

Table 4. Observed fluxes.

	Mz 2[j]	A 65	K 1-2[j]	Pe 1-3	IC 972	ESO 223-10
[O II] 3727	26	–	–	368	100	–
[Ne III] 3868	33	–	–	72	70	–
[Ne III] 3968+Hε	–	–	–	–	26	69
Hδ 4101	–	–	–	22	–	44
Hγ 4340	–	–	–	41	28:	86
[O III] 4363	–	–	–	4.8	16::	50
He I 4471	–	–	–	5.6	–	14
He II 4686	17	109:	27	15	40	117
[Ar IV] 4711	–	45:	–	–	–	
Hβ 4861	–	100	–	100	100	100
[O III] 4959	131	388	73	400	346	272
[N II] 6548	25	–	–	–	–	–
Hα 6563	100	675:	100	–	–	–
[N II] 6584	87	–	–	–	–	–
[S II] 6716	14.9	–	–	–	–	–
[S II] 6731	22.4	–	–	–	–	–

Notes: see notes to Table 3.

high-density limit in the central cross-section (spatially corresponding to 2.3 arcsec), whereas the two remaining outer cross-sections give [O II] doublet ratios corresponding to a lower density (5400 cm^{-3} for $T_e = 10\,000$ K). The [N II] (6584 + 6548)/5755-Å ratio is 40, which, for an adopted T_e of 10 000 K, gives n_e(N II) = 45 000 cm^{-3}.

The density derived from the [N II] 6584 + 6548/5755-Å ratio was used for another compact VLE PN, M 1-26. Here, for T_e(O III) = 10 000 K, n_e(N II) = 53 000 cm^{-3}. A final high-density object, He 2-57, is more fully discussed in Section 6.

4.2 Electron temperatures

Electron temperatures in PN have been extensively studied by Kaler (1986a), who compiled temperature diagnostic ratios for many PN from the literature and re-derived

Table 5. References for atomic data.

Ion	Transition Probabilities	Collision Strengths
O^{+}	Zeippen 1982	Pradhan 1976
O^{2+}	Nussbaumer & Storey 1981b	Aggarwal 1983
O^{3+}	Nussbaumer & Storey 1982b	Hayes & Nussbaumer 1984
N^{+}	Nussbaumer & Storey 1979a	Nussbaumer & Storey 1979a, 1982a, Butler & Storey (unpubl.)
N^{3+}	Nussbaumer & Storey 1979b	Mendoza 1983
N^{4+}	Wiese et al. 1966	Osterbrock & Wallace 1977
C^{+}	Nussbaumer & Storey 1981a	Hayes & Nussbaumber 1984
C^{2+}	Nussbaumer & Storey 1978	Dufton et al. 1978
C^{3+}	Wiese et al. 1966	Gau & Henry 1977
Ne^{2+}	Mendoza 1983	Butler (unpubl.)
Ne^{3+}	Zeippen 1982	Giles 1981
Ne^{4+}	Nussbaumer & Rusca 1979	Lennon & Burke 1991
Ar^{2+}	Mendoza & Zeippen 1983	Johnson & Kingston 1990
Ar^{3+}	Mendoza & Zeippen 1982a	Zeippen et al. 1987
Ar^{4+}	Mendoza & Zeippen 1982b	Mendoza 1983
S^{+}	Mendoza & Zeippen 1982a	Mendoza 1983
S^{2+}	Mendoza & Zeippen 1982b	Mendoza 1983
Cl^{2+}	Mendoza & Zeippen 1982a	Butler & Zeippen 1989

temperatures using the most recent atomic data. For the objects in common, the temperatures derived here are almost all within 1000 K of those found by Kaler. [The largest discrepancy is for NGC 2438, where we derive $t(\mathrm{O\,III})=1.5$ and Kaler derives $t(\mathrm{O\,III})=1.09$ from the line ratios listed in TPP77.] It is instructive to look at how a large data set of well-determined electron temperatures behaves, in order to establish relations that can be used for objects that are less well observed. Errors in derived abundances from collisionally excited lines are primarily due to errors in adopted electron temperatures. It is thus worth investigating relationships between $t(\mathrm{O\,III})$ and $t(\mathrm{N\,II})$ for objects that have a reliable [N II] 5755-Å flux, as this line is generally very weak and $t(\mathrm{N\,II})$ underivable in other PN; this enables a more accurate derivation of abundances for singly ionized species.

To examine how $t(\mathrm{O\,III})$ behaves with nebular excitation, Kaler (1986a) plotted $t(\mathrm{O\,III})$ versus He II $I(4686)$.[5] Fig. 1 plots this for the objects in the current sample. [Recall that $I(4686)$ is expressed relative to Hβ on a scale where $I(\mathrm{H}\beta)=100$.] A trend of increasing $t(\mathrm{O\,III})$ with increasing $I(4686)$ is seen. Considerable scatter is also seen; inspection of the error bars for $t(\mathrm{O\,III})$ shows that the scatter is real and not attributable to errors in electron temperature. The real variations in $t(\mathrm{O\,III})$ for a given $I(4686)$ probably reflect the variations in oxygen abundance in PN. Errors for $I(4686)$ are not given, as the errors in $t(\mathrm{O\,III})$ would tend to dominate the relationship between the two quantities. A least-squares fit to the 48 points of Fig. 1, weighted according to the mean errors on the electron temperatures given in Table 7, yields

$$T_e(\mathrm{O\,III})=(9400\pm47)+(54\pm7)\,I(4686)\,\mathrm{K}, \quad (1)$$

with a correlation coefficient of 0.76. Kaler (1986a) obtained $T_e(\mathrm{O\,III})=9700+58\ I(4686)$ K for his sample. The two relations show excellent agreement. The current sample contains more very high-excitation objects; thus we are able to see how the trend behaves for larger $t(\mathrm{O\,III})$ and $I(4686)$. Fig. 2 plots $t(\mathrm{N\,II})$ versus $I(4686)$. An error-weighted least-squares fit to the 18 points in this figure yields

$$T_e(\mathrm{N\,II})=(9100\pm46)+(17\pm7)\,I(4686)\,\mathrm{K}, \quad (2)$$

with a correlation coefficient of 0.79. However, given the flatness of the slope for this distribution, one may also interpret $t(\mathrm{N\,II})$ as being essentially independent of nebular excitation. Fig. 2 shows considerably less scatter than the same plot made by Kaler (his fig. 9); our $t(\mathrm{N\,II})$s are between 0.8 and 1.1, whereas Kaler has $t(\mathrm{N\,II})$s between 0.75 and $\gtrsim 1.5$. The increased scatter found by Kaler may well be due to observational error, as the only $t(\mathrm{N\,II})$s plotted in Fig. 2 were obtained with a good quality 5755-Å flux. The mean $t(\mathrm{N\,II})$ for this sample of 22 PN is 0.99 ± 0.13 [four PN included in this average have $I(4686)=0$ and hence were not plotted in Fig. 2]. This value is in good agreement with the value of 1.03 found by Kaler (1986a).

The ratio $t(\mathrm{O\,III})/t(\mathrm{N\,II})$ versus $I(4686)$ is plotted in Fig. 3, where a trend is seen. The points all lie in the range found by Kaler (see his fig. 12). In both cases there is considerable scatter. A least-squares fit to the 18 points in Fig. 3 yields

$$\frac{T_e(\mathrm{O\,III})}{T_e(\mathrm{N\,II})}=(1.15\pm0.06)+(0.0037\pm0.0009)\,I(4686), \quad (3)$$

with a correlation coefficient of 0.69. TPP77 found that, for lower excitation PN with $I(4686)<25$, $t(\mathrm{O\,III})=t(\mathrm{N\,II})$, and, for higher excitation PN, $t(\mathrm{O\,III})/t(\mathrm{N\,II})=1.25$. Fig. 3 shows that adoption of a ratio of 1.25 would be acceptable for PN of medium excitation with $I(4686)\lesssim 75$, given the observed scatter, in order to estimate $t(\mathrm{N\,II})$ when only $t(\mathrm{O\,III})$ is available. In these cases, one may also use the mean $t(\mathrm{N\,II})=0.99$ derived above. For PN of low and medium excitation, differences of only $\lesssim 1000$ K are found between these two estimation methods. For high-excitation and very high-excitation PN, equation (3) should be preferred for deriving $t(\mathrm{N\,II})$ when only $t(\mathrm{O\,III})$ is available. Equation (3) can be used in all cases anyway, and has been adopted for this analysis.

4.3 Electron densities

In this section we compare densities derived from various ions. Kingsburgh & English (1992) showed that $n_e(\mathrm{O\,II})$ and $n_e(\mathrm{S\,II})$ are the same within the errors for a sample of 57 PN having densities between ~ 500 and 10 000 cm^{-3}. Densities derived for a large sample of PN were examined by Stanghellini & Kaler (1989), who found that densities derived from the [O II], [S II], [Ar IV] and [Cl III] doublet ratios agree to within ~ 30 per cent. It is desirable to compare densities derived from diagnostics that are observed in the same spectra, in order to compare the same volume in the nebula.

[5] Kaler used the He II 4686-Å line strength to indicate the extent of nebular excitation when the line was observed. For objects of lower excitation that do not show any He II lines, Kaler used the temperature of the central star to parametrize excitation. Here we restrict our discussion to objects with $I(4686)>0$.

Table 6. Line ratios used for temperature and density diagnostics.

Object	$\frac{I(4959)}{I(4363)}$	$\frac{I(6584+6548)}{I(5755)}$	$\frac{I(6717)}{I(6731)}$	$\frac{I(4711)}{I(4740)}$	$\frac{I(5517)}{I(5537)}$
IC 2003	28.6±1.46	39:	0.51±0.12	1.16±0.11	1.07±0.29
K 3-67	21.7±0.88			0.90±0.092	
J 900	27.9±0.59			0.74±0.19	
M 1-8	29.4±1.49	76.9±1.5	1.09±0.073		
PB 1	34.3±1.83			1.15±0.58	
M 3-1	40.2±1.42	81.3±4.1	0.75±0.017	1.27±0.18	0.97±0.24
M 1-11		60.3±5.4			
SkWl 3-2			0.89±0.25		
M 1-12		56.9±14.0	0.44±0.20		
M 1-13	34.3±2.60	86.9±1.3	0.89±0.024	0.95±0.19	
NGC 2371-2	22.8±3.41			1.2:	
M 3-3	25.9±3.09	101.1±2.0		2.3:	
NGC 2440	20.6±0.67	109.6±1.6	0.52±0.051	0.98±0.065	
NGC 2438	17.8±6.70		1.15±0.033		
NGC 2452	25:	53:	0.74±0.013	1.26±0.032	
M 3-4	29.9±5.39		1.76±0.30		
M 3-5	16.3±0.85	62.8±1.0	1.10±0.075		
M 3-6	82:				
A 30	21.6:				
He 2-15	12.9±2.06	61.2±1.8	0.86±0.012	1.22±0.043	
IC 2448	39.7±2.27			1.34±0.20	
NGC 2792	28.6±1.49			1.10±0.066	
PB 4	83.4±12.6			1.2:	
NGC 2867	36.8±0.75	83.7±2.9	0.64±0.10	1.11±0.026	
He 2-28	66.5±15				
He 2-29	13.5±0.44	63.7±22.3	0.96±0.092		
NGC 2899	10.3±1.24	52.4±1.6	1.31±0.057	0.80±0.072	
He 2-37	25.6±1.21	81.1±4.1	1.24±0.050	1.20±0.072	
Lo 4			0.98±0.25		
NGC 3195	36.9±2.91	156.5±3.3	1.18±0.014	1.28±0.34	1.29±0.45
He 2-48	31.9±2.65	64.0±4.5	1.29±0.088		
He 2-51	30.5±2.60	152 ±38	0.99±0.035	0.55:	
Pe 2-7	17.4±0.41		0.79±0.066	1.08±0.027	
He 2-55	5.82±0.93		1.10±0.22	0.91±0.25	0.55±0.28
He 2-57	1.70±0.52				
IC 2621	28.4±0.80			0.30±0.015	

Table 6 – *continued*

Object	$\frac{I(4959)}{I(4363)}$	$\frac{I(6585+6548)}{I(5755)}$	$\frac{I(6717)}{I(6731)}$	$\frac{I(4711)}{I(4740)}$	$\frac{I(5517)}{I(5537)}$
ESO 216-02	10.6±2.22		1.71±0.92		
K 1-22	24.5±4.41		0.70±0.38		
Fg 1	55.4±5.91		0.65±0.085	1.07±0.11	0.85±0.26
PB 8	120:				
He 2-76			1.09±0.28		
He 2-77			0.64±0.13		
Th 2-A	26.3±0.57	51.6±18.0	0.82±0.070	0.74±0.12	
NGC 5189	24.3±0.17		1.12±0.048	1.45±0.055	
MyCn 18		100.0±1.8	0.46±0.010		0.72±0.29
He 2-97	63.3±5.05	35±5	0.42±0.11	1.50±0.15	
NGC 5307	26.8±3.61			1.51±0.042	
He 2-99		134:	0.76±0.061		
NGC 5315	119.1±11.9				
He 2-105	60.2±8.43		1.49:		
He 2-111	11.0±1.98	63.0±1.3	0.92±0.014	1.47±0.10	0.42:
He 2-112	19.7±1.19	56.9±3.1	0.70±0.013	0.87±0.053	
He 2-119	49.0±3.09	131.1±2.6	1.12±0.025	1.49±0.42	
NGC 5873	28.2±3.87			0.82±0.13	
NGC 5882	61.1±9.17			0.78±0.12	
Me 2-1	22.4		0.72	1.43	
NGC 5979	23.8±5.46		1.59±0.24		
He 2-138			0.63±0.12		
He 2-141	29.7±1.67		1.56±0.62		
NGC 6026	22.3				
NGC 6153	74.8±19.5				
PC 14	133.8±5.21		0.60±0.037	0.69±0.11	
H 2-1		39.9±7.3	0.62±0.10		
IC 4642	21.5±5.59			1.5:	
Tc 1	240±30				
M 1-26	171:	37.4±6.4	0.36±0.15		
IC 4673	22.6±1.39		1.13±0.15	1.18±0.12	
NGC 6751	59.5±1.85	151.3±19.7	0.78±0.012		
He 2-434	50.6±0.95		1.23±0.074		
NGC 6905	32.8±1.55				
NGC 7009	50.6±0.75	63.8±19.1		0.92±0.11	
IC 5148-50	16.7±6.70		0.69:	0.57±0.086	

1994MNRAS.271..257K

Table 7. Electron temperatures and densities.

Object	t(O III)	t(N II)	n_e(S II)	n_e(O II)	n_e(Ar IV)	n_e(Cl III)
IC 2003	$1.20^{+0.02}_{-0.01}$	(0.99)	8900^{+hdl}_{-5700}	13200:	1910^{+1060}_{-840}	1910^{+1140}_{-1400}
K 3-67	$1.31^{+0.03}_{-0.02}$			30200:	$5500^{1400\ f}_{1050}$	
J 900	$1.20^{+0.04}_{-0.02}$	(0.99)		3980^{+790}_{-650}	8240^{+7000}_{-3600}	
M 1-8	$1.21^{+0.01}_{-0.04}$	1.09±0.01	400^{+130}_{-110}	140±60		
PB 1	$1.16^{+0.01}_{-0.05}$				2000^{+7700}_{-ldl}	
M 3-1	$1.06^{+0.04}_{-0.01}$	$1.00^{+0.01}_{-0.05}$	1600^{+160}_{-140}	1070^{+100}_{-90}	950^{+1400}_{-ldl}	2150^{+4460}_{-1690}
M 1-11		$1.03^{+0.04}_{-0.03}$		12000^{+6600}_{-3500}		
SkWl 3-2	(1.36)		990^{+2000}_{-570}			
M 1-12		1.00±0.04	10^5	13200±1700		
M 1-13	$1.16^{+0.01}_{-0.04}$	$0.95^{+0.02}_{-0.01}$	860^{+40}_{-50}	890±40	4240^{+2020}_{-1380}	
NGC 2371-2	1.34±0.10		230:	810		
M 3-3	$1.26^{+0.08}_{-0.05}$	0.91± 0.01		330±40		
NGC 2440	$1.39^{+0.02}_{-0.04}$	0.86±0.02	7200^{+10000}_{-2900}		$4200^{+700\ f}_{-650}$	
NGC 2438	$1.50^{+0.40}_{-0.20}$	(1.25)	350±50			
NGC 2452	1.26:	1.20:	1820±80	1170^{+210}_{-170}	1070^{+80}_{-70}	
M 3-4	1.21±0.10	(0.99)	ldl(100)			
M 3-5	1.56±0.05	1.11±0.02	400^{+160}_{-120}			
M 3-6	0.88:			3020^{+370}_{-330}		
A 30	1.36		[200][a]			
He 2-15	$1.67^{+0.16}_{-0.14}$	1.11±0.02	1020±20		1520±140	
IC 2448	$1.10^{+0.02}_{-0.04}$				490^{+290}_{-180}	
NGC 2792	1.20±0.03				2380^{+420}_{-350}	
PB 4	$0.88^{+0.05}_{-0.03}$				1550:	
NGC 2867	1.11±0.02	$0.96^{+0.04}_{-0.02}$	2700^{+50}_{-70}		2270^{+330}_{-190}	
He 2-28	$0.91^{+0.10}_{-0.03}$		(1000)			
He 2-29	$1.71^{+0.05}_{-0.06}$	$1.10^{+0.35}_{-0.25}$	720^{+300}_{-240}			
NGC 2899	1.95±0.20	1.21±0.02	130±20		8500^{+1720}_{-1420}	
He 2-37	$1.26^{+0.04}_{-0.02}$	$1.01^{+0.02}_{-0.05}$	190±30		1600^{+280}_{-240}	
Lo 4	(1.75)		300^{+250}_{-100}			
NGC 3195	$1.11^{+0.04}_{-0.02}$	0.76±0.02	240±20	280±20	900±60	470^{+850}_{-300}
He 2-48	$1.16^{+0.05}_{-0.02}$	1.11±0.05	150±40			
He 2-51	$1.20^{+0.05}_{-0.02}$	$0.82^{+0.39}_{-0.08}$	660±30		14500:	
Pe 2-7	1.50±0.02	(1.25)	1600^{+280}_{-240}		3100^{+220}_{-200}	
He 2-55	$1.31^{+0.05}_{-0.07}$		420^{+250}_{-160}		5060^{+3650}_{-2180}	9840:
He 2-57[b]	1.7					
IC 2621	1.16±0.02				44400^{+4100}_{-6300}	
ESO 216-02	1.95±0.30	(1.40)	200			

Table 7 – *continued*

Object	t(O III)	t(N II)	n_e(S II)	n_e(O II)	n_e(Ar IV)	n_e(Cl III)
K 1-22	1.25±0.10		2280^{+hdl}_{-1800}			
Fg 1	$0.96^{+0.04}_{-0.02}$		2600^{+530}_{-490}	2340±170	2540^{+800}_{-600}	3140^{+3100}_{-1570}
PB 8	[0.80][c]			2190^{+170}_{-140}		
He 2-76	(1.40)	(1.15)	450^{+1100}_{-400}			
He 2-77	[0.88][d]		3000±1050			
Th 2-A	1.25±0.01	1.21:	1220^{+210}_{-180}		8240^{+1000}_{-1060}	
NGC 5189	1.31±0.05	(1.0)	390±60	620±60	*ldl*	
MyCn 18	–	0.90±0.02	2290±600	3820±220		4700:
He 2-97[e]	$0.94^{+0.02}_{-0.04}$		9550		*hdl*	
NGC 5307	1.25±0.05	(0.99)		3390^{+280}_{-190}	*ldl*	
He 2-99		0.81	1380^{+200}_{-180}	300±30		
NGC 5315	$0.81^{+0.02}_{-0.03}$			2820^{+150}_{-110}		
He 2-105	0.96±0.04		*ldl*(300)			
He 2-107	[1.03][c]			1950±150		
He 2-111	$1.90^{+0.30}_{-0.20}$	1.10±0.02	800±30	790±70	*ldl*	17000:
He 2-112	1.40±0.04	1.15±0.02	2180±80	2880±150	6040^{+720}_{-770}	
He 2-119	$1.01^{+0.02}_{-0.04}$	0.81±0.02	330±30	280±30	*ldl*	
NGC 5873	$1.20^{+0.10}_{-0.05}$	(0.99)		3310±160	1550^{+450}_{-350}	
NGC 5882	0.95±0.05			2950±160	6620^{+1890}_{-1490}	
Me 2-1	1.35	(1.19)	2080	1820^{+540}_{-410}	*ldl*	
NGC 5979	$1.31^{+0.04}_{-0.10}$	(1.09)	*ldl*	1410±140		
He 2-138	0.84[g]		3090±1000	4570±350		
He 2-141	$1.20^{+0.16}_{-0.10}$	(0.99)	*ldl*	2090±100		
He 2-142				7240^{+1100}_{-960}		
NGC 6026	1.36:		[300][c]			
NGC 6153	0.90±0.06			3020±280		
PC 14	0.78±0.02		2550^{+240}_{-290}	1590±200	7930^{+2280}_{-1780}	
H 2-1[e]	(1.0)		3160			
IC 4642	$1.36^{+0.20}_{-0.10}$		2550	940^{+660}_{-520}	*ldl*	
Tc 1	0.96±0.04		1800	1300±100	*ldl*	
M 1-26[e]	1.00		*hdl*			
IC 4673	$1.36^{+0.03}_{-0.02}$		370^{+150}_{-110}	1080^{+350}_{-300}	1820^{+580}_{-440}	
NGC 6751	0.98±0.02	$0.80^{+0.03}_{-0.05}$	1250±40	1050±150		
He 2-434	1.00±0.02		1250±190	3550±310		
NGC 6905	1.16±0.02			1550^{+600}_{-430}		
NGC 7009	1.00±0.02	$1.07^{+0.20}_{-0.11}$		4350^{+660}_{-550}	4370^{+1130}_{-900}	
IC 5148-50	1.45:	(1.21)	2000:	60±20	15000^{+45000}_{-12000}	

Notes: ( ) values in parentheses are adopted, based on excitation (see text). [a]n_e for A 30 has been adopted from Jacoby & Ford (1983). [b]See text for discussion on diagnostics for He 2-57. [c]Values have been adopted from Shaw & Kaler (1989). [d]t(O III) for He 2-77 adopted from Caswell & Haynes (1987); see text. [e]See discussion in Section 4.1 on n_e for He 2-97, H 2-1 and M 1-26. [f]n_e(Ar IV) was adopted for abundance analysis of NGC 2440. [g]t for He 2-138 derived from [O II] 3727/7325-Å ratio. *ldl* indicates the diagnostic ratio is at its low-density limit. *hdl* indicates the diagnostic ratio is at its high-density limit.

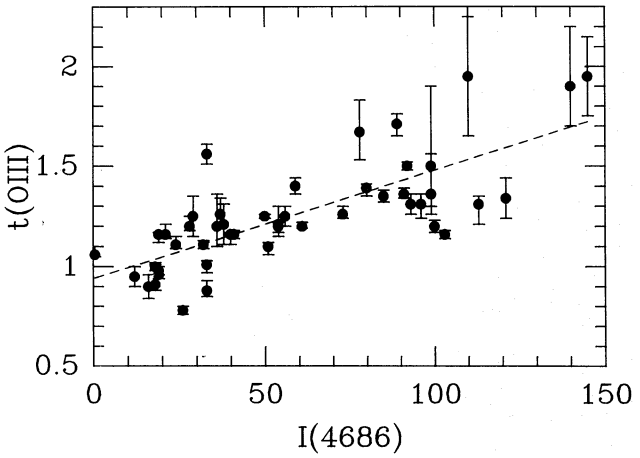

Figure 1. t(O III) versus I(4686). An error-weighted least-squares fit to the 48 points is given in equation (1).

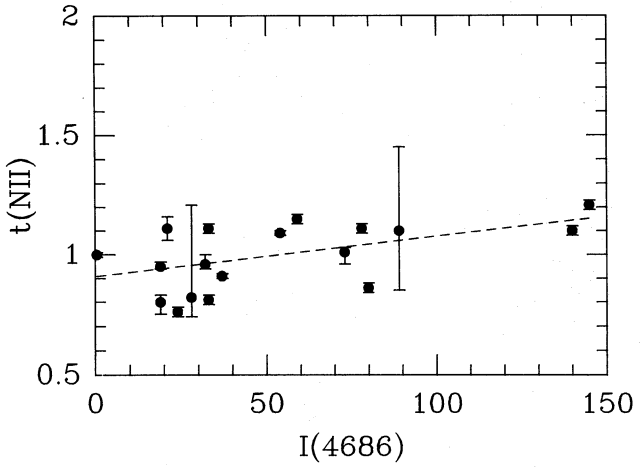

Figure 2. t(N II) versus I(4686). An error-weighted least-squares fit to the 18 points is given in equation (2).

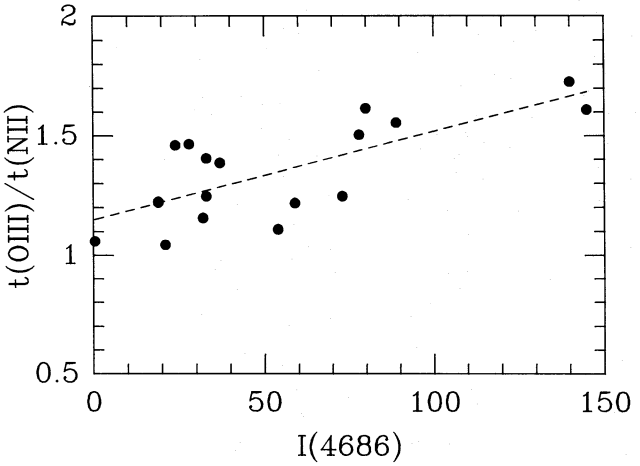

Figure 3. t(O III)/t(N II) versus I(4686). A least-squares fit to the 18 points is given in equation (3).

In this sample, 20 objects have n_e(S II), n_e(Ar IV) and/or n_e(Cl III) which can be compared with each other. Six objects have all densities equal within the formal observational errors. Another eight objects do not have densities that are equal within the formal observational errors; however, the densities are the same to within a factor of 2. It is therefore conceivable that they may be equal. So, for these 14 objects one may conclude that the nebulae are roughly homogeneous.

The remaining six objects: NGC 2899, He 2-37, Th 2-A, He 2-112, PC 14 and IC 4673 all have n_e(Ar IV) > n_e(S II). NGC 2899 shows the greatest variation, with n_e(Ar IV) ~ $60n_e$(S II). NGC 2899 is a Type I PN, with extreme bipolar morphology and filamentary structure, and hence extreme local variations in density are not surprising. The ionization potential to obtain Ar^{3+} is 40.7 eV, far higher than the ionization potential to obtain S^+, which is 10.4 eV. Thus, for density distributions that decrease with radius, the [Ar IV] lines would trace the innermost denser parts of the nebula, whereas the [S II] lines would originate from the outermost regions. The [Ar IV] and [S II] densities found in these six objects are consistent with this scenario. Thus in this data set we see evidence both for essentially homogeneous density distributions and for density distributions that decrease with increasing radius.

5 ABUNDANCE ANALYSIS

5.1 Helium

He II λ4686 is produced by radiative recombination, while the observed He I lines are produced predominantly by radiative recombination; however, for He I, there is also a collisional contribution to the He I line fluxes. Helium ionic abundances are derived assuming Case B recombination relative to H^+ using

$$\frac{n(\mathrm{He}^{m+})}{n(\mathrm{H}^+)} = (I_\lambda/I_{\mathrm{H}\beta})(\alpha_{\mathrm{eff}}^{\mathrm{H}\beta}/\alpha_{\mathrm{eff}}^{\mathrm{He}^{m+}})(\lambda/4861), \quad (4)$$

where the effective recombination coefficients $\alpha_{\mathrm{eff}}^{\mathrm{H}\beta}$ and $\alpha_{\mathrm{eff}}^{\mathrm{He}^{m+}}$ are functions of electron temperature and density, and were taken from Hummer & Storey (1987, Hβ and He^{2+}) and Brocklehurst (1971, He^+).

Line strengths of the He I lines were first corrected for the effect of collisional population of their upper states, which can occur via excitation from the 2^3S state (as it is metastable). The collisional contribution was estimated following Clegg (1987). If these collisional corrections are not made, the resultant He/H ratio is typically 9 per cent higher (see Clegg 1989). In order to derive final He^+/H^+ abundances, a weighted average of the He^+/H^+ abundances derived from $\lambda\lambda$4471, 5876 and 6678 Å was taken. Weighting was based on the S/N of the line and the quality of the spectrum used. For cases where the He I lines were of good S/N, agreement between He^+/H^+ derived from the three lines is generally within a few per cent of the final adopted He^+/H^+. Table 8 presents the He^+/H^+ and He^{2+}/H^+ ionic abundance ratios, and the adopted He/H ratios, by number, for PN that had good S/N spectra.

5.2 Collisionally excited lines

In order to derive ionic abundances of collisionally excited species, the equations of statistical equilibrium were solved

Table 8. Abundances.

		IC 2003	K 3-67	J 900	M 1-8	PB 1	M 3-1	SkWl 3-2
4471	He^+/H^+	0.0366 (2)	0.0987 (1)	0.0820 (1)	0.0647 (1)	0.1124 (2)	0.0958 (1)	0.0000 (-)
5876	He^+/H^+	0.0480 (2)	0.0000 (0)	0.0000 (0)	0.0829 (4)	0.0704 (4)	0.1041 (3)	0.0000 (-)
6678	He^+/H^+	0.0359 (1)	0.0000 (0)	0.0000 (0)	0.0398 (0)	0.0628 (1)	0.1141 (1)	0.0000 (-)
Avg.	He^+/H^+	0.0410	0.0987	0.0820	0.0792	0.0813	0.1044	0.0000
4686	He^{2+}/H^+	0.0514	0.0000	0.0402	0.0459	0.0329	0.0004	0.0596
	He/H	0.092	0.099	0.122	0.125	0.114	0.105	>0.060
3727	$10^5 \times O^+/H^+$	3.49	1.26	8.48	10.1	1.26	4.07	2.32
4959	$10^4 \times O^{2+}/H^+$	1.95	1.19	2.14	2.31	2.99	2.07	0.312
1401	$10^4 \times O^{3+}/H^+$	2.19	–	–	–	–	–	–
	ICF(O)	1.00	1.00	1.30	1.36	1.25	1.00	–
	$10^4 \times O/H$	4.49	1.32	3.89	4.49	3.91	2.48	>0.544
6584	$10^6 \times N^+/H^+$	4.73	5.74	9.44	49.6	1.10	13.3	6.41
1750	$10^5 \times N^{2+}/H^+$	4.59	–	–	–	–	3.25	–
1486	$10^5 \times N^{3+}/H^+$	4.75	–	–	–	–	–	–
1240	$10^5 \times N^{4+}/H^+$	1.83	–	–	–	–	–	–
	ICF(N)	1.00	10.4	4.59	4.47	31.2	1.00	–
	$10^4 \times N/H$	1.16	0.60	0.433	2.21	0.341	0.458	>0.064
2326	$10^5 \times C^+/H^+$	12.1	–	–	–	–	–	–
1908	$10^4 \times C^{2+}/H^+$	2.74	–	10.9	–	–	0.293	–
1550	$10^4 \times C^{3+}/H^+$	1.41	–	3.64	–	–	–	–
	ICF(C)	1.74	–	1.39	–	–	1.20	–
	$10^4 \times C/H$	9.32	–	20.3	–	–	0.352	–
3868	$10^5 \times Ne^{2+}/H^+$	3.85	4.26	5.53	7.92	7.27	5.07	–
2423	$10^5 \times Ne^{3+}/H^+$	2.05	–	–	–	–	–	–
3426	$10^6 \times Ne^{4+}/H^+$	1.09	–	–	–	5.86	–	51.6
	ICF(Ne)	1.00	1.10	1.82	1.95	1.50	1.20	–
	$10^4 \times Ne/H$	0.601	0.471	1.01	1.54	1.18	0.608	>0.516
7135	$10^7 \times Ar^{2+}/H^+$	4.48	–	–	11.4	7.61	10.4	–
4740	$10^7 \times Ar^{3+}/H^+$	3.69	–	1.71	2.10	5.92	0.995	–
7005	$10^7 \times Ar^{4+}/H^+$	0.796	–	–	–	–	–	–
	ICF(Ar)	1.04	–	1.82	1.29	1.03	1.41	–
	$10^6 \times Ar/H$	0.935	–	0.311	1.74	1.39	1.61	–
6725	$10^7 \times S^+/H^+$	3.30	–	18.7	4.84	8.48	4.27	–
6312	$10^7 \times S^{2+}/H^+$	16.9	–	–	31.9	–	45.8	–
	ICF(S)	1.67	–	8.93	1.23	21.2	1.34	–
	$10^6 \times S/H$	3.37	–	(16.7)	4.54	(18.0)	6.70	–

		M 1-13	NGC 2371-2	M 3-3	NGC 2440	NGC 2440[a]	NGC 2438	M 3-4	NGC 2452
4471	He^+/H^+	0.1443 (1)	0.0000 (0)	0.0759 (1)	0.0608(1)	0.0608(1)	0.0000(0)	0.0000(0)	0.0329 (3)
5876	He^+/H^+	0.1263 (3)	0.0030 (1)	0.0860 (3)	0.0388(0)	0.0388(0)	0.0549(1)	0.0908(1)	0.0417 (1)
6678	He^+/H^+	0.1277 (1)	0.0000 (0)	0.0489 (0)	0.1413(0)	0.1413(0)	0.0587(0)	0.0859(0)	0.0809 (0)
Avg.	He^+/H^+	0.1302	0.0030	0.0835	0.0608	0.0608	0.0549	0.0908	0.0373
4686	He^{2+}/H^+	0.0157	0.1038	0.0314	0.0684	0.0684	0.0869	0.0323	0.0735
	He/H	0.146	0.107	0.115	0.129	0.129	0.142	0.123	0.111
3727	$10^5 \times O^+/H^+$	24.5	1.93	22.6	12.7	12.7	3.50	18.0	1.92
4959	$10^4 \times O^{2+}/H^+$	2.60	0.550	1.52	1.37	1.37	0.913	2.47	1.76
1401	$10^4 \times O^{3+}/H^+$	–	4.51	–	2.63	–	–	–	–
	ICF(O)	1.08	1.00	1.24	1.00	1.70	1.88	1.23	2.07
	$10^4 \times O/H$	5.45	5.25	4.68	5.28	4.37	2.38	5.24	4.04
6584	$10^6 \times N^+/H^+$	138.0	–	192.0	149.0	149.0	9.36	55.4	9.48
1750	$10^5 \times N^{2+}/H^+$	3.03	3.47	–	31.4	–	–	–	13.6
1486	$10^5 \times N^{3+}/H^+$	2.04	10.6	–	29.5	–	5.69	–	13.9
1240	$10^5 \times N^{4+}/H^+$	–	2.68	–	10.4	–	–	–	–
	ICF(N)	1.00	1.00	2.07	1.00	3.40	1.50	2.90	1.00
	$10^4 \times N/H$	1.89	1.68	3.98	8.61	5.13	0.998	1.61	2.84
2326	$10^5 \times C^+/H^+$	–	–	–	–	–	–	–	–
1908	$10^4 \times C^{2+}/H^+$	–	0.524	–	3.52	–	0.748	–	2.09
1550	$10^4 \times C^{3+}/H^+$	–	0.612	–	1.38	–	0.238	–	0.771
	ICF(C)	–	1.76	–	2.00	–	1.37	–	1.11
	$10^4 \times C/H$	–	2.00	–	9.70	–	1.35	–	3.17
3868	$10^5 \times Ne^{2+}/H^+$	7.64	1.17	4.64	3.36	3.36	2.11	6.92	4.83
2423	$10^5 \times Ne^{3+}/H^+$	–	8.64	–	2.03	–	–	–	4.72
3426	$10^6 \times Ne^{4+}/H^+$	–	64.0	–	55.9	55.9	5.57	–	4.09
	ICF(Ne)	2.09	1.00	3.08	1.00	1.50	1.50	2.12	1.00
	$10^4 \times Ne/H$	1.60	1.62	1.43	1.10	1.34	0.401	1.47	0.996
7135	$10^7 \times Ar^{2+}/H^+$	28.1	10.1	13.9	16.3	16.3	6.26	15.0	15.5
4740	$10^7 \times Ar^{3+}/H^+$	3.59	8.60	1.57	6.59	6.59	–	–	6.32
7005	$10^7 \times Ar^{4+}/H^+$	–	–	–	3.71	3.71	–	–	–
	ICF(Ar)	3.73	1.00	1.94	1.22	1.41	1.87	1.87	1.03
	$10^6 \times Ar/H$	11.8	1.87	3.00	3.24	3.75	1.17	2.81	2.26
6725	$10^7 \times S^+/H^+$	14.1	–	1.83	5.26	5.26	3.23	4.08	3.81
6312	$10^7 \times S^{2+}/H^+$	36.3	146.0	–	33.0	33.0	–	–	32.1
	ICF(S)	1.06	–	6.89	1.22	1.20	9.94	7.62	1.94
	$10^6 \times S/H$	5.36	>14.6	(1.26)	4.68	4.43	(3.21)	(3.11)	6.97

Table 8 — *continued*

		M 3-5	M 3-6	He 2-15	IC 2448	NGC 2792	PB 4	NGC 2867	He 2-28
4471	He^+/H^+	0.0783(1)	0.0814 (1)	0.1145(0)	0.0443 (1)	0.0000 (0)	0.0978 (1)	0.0811 (1)	0.0000(-)
5876	He^+/H^+	0.0793(4)	0.0896 (3)	0.0763(3)	0.0000 (0)	0.0204 (1)	0.0000 (0)	0.0911 (3)	0.0000(-)
6678	He^+/H^+	0.0830(2)	0.0000 (0)	0.0671(1)	0.0000 (0)	0.0000 (0)	0.0000 (0)	0.0927 (1)	0.0000(-)
Avg.	He^+/H^+	0.0802	0.0876	0.0740	0.0443	0.0204	0.0978	0.0894	0.0000
4686	He^{2+}/H^+	0.0293	0.0019	0.0703	0.0427	0.0847	0.0270	0.0267	0.0145
	He/H	0.109	0.090	0.144	0.087	0.105	0.125	0.116	>0.015
3727	$10^5\times O^+/H^+$	9.09	1.67	9.09	0.741	–	0.966	7.46	30.9
4959	$10^4\times O^{2+}/H^+$	0.661	2.61	1.01	3.29	1.92	5.44	4.15	5.88
1401	$10^4\times O^{3+}/H^+$	–	–	–	–	7.15:	–	1.10	–
	ICF(O)	1.23	1.01	1.56	1.57	2.98	1.18	1.00	–
	$10^4\times O/H$	1.93	2.82	2.99	5.28	5.74	6.52	6.00	>8.9:
6584	$10^6\times N^+/H^+$	56.9	1.41	14.8	1.01	1.05	–	11.7	–
1750	$10^5\times N^{2+}/H^+$	–	–	–	–	18.0	–	4.47	–
1486	$10^5\times N^{3+}/H^+$	–	–	–	15.8	17.4	–	6.52	–
1240	$10^5\times N^{4+}/H^+$	–	–	–	–	–	–	–	–
	ICF(N)	2.12	16.9	3.29	1.50	1.00	–	1.00	–
	$10^4\times N/H$	1.21	0.237	4.89	2.39	3.55:	–	1.28	–
2326	$10^5\times C^+/H^+$	–	–	–	6.18	–	–	21.0	–
1908	$10^4\times C^{2+}/H^+$	–	–	–	4.18	3.88	–	7.89	–
1550	$10^4\times C^{3+}/H^+$	–	–	–	2.10	0.977	–	1.55	–
	ICF(C)	–	–	–	1.25	1.73	–	1.09	–
	$10^4\times C/H$	–	–	–	8.63	8.39	–	12.6	–
3868	$10^5\times Ne^{2+}/H^+$	2.96	7.95	2.98	8.07	3.08	11.7	8.39	20.5
2423	$10^5\times Ne^{3+}/H^+$	–	–	–	2.39	9.77	–	1.55	–
3426	$10^6\times Ne^{4+}/H^+$	–	–	–	–	–	–	–	–
	ICF(Ne)	2.92	1.07	2.97	1.00	1.00	1.20	1.00	–
	$10^4\times Ne/H$	0.865	0.858	0.885	1.05	1.29	1.40	0.995	>21:
7135	$10^7\times Ar^{2+}/H^+$	8.70	–	13.6	–	–	–	13.0	–
4740	$10^7\times Ar^{3+}/H^+$	–	–	5.18	4.41	7.32	4.43	2.78	–
7005	$10^7\times Ar^{4+}/H^+$	–	–	1.31	–	–	–	–	–
	ICF(Ar)	1.87	–	1.44	1.70	2.98	1.20	1.16	–
	$10^6\times Ar/H$	1.63	–	2.89	(0.748)	(2.18)	(0.530)	1.83	–
6725	$10^7\times S^+/H^+$	3.65	–	21.8	21.7	–	–	5.64	22.1
6312	$10^7\times S^{2+}/H^+$	15.1	–	70.6	–	–	–	44.6	–
	ICF(S)	1.05	–	1.15	3.13	–	–	1.45	–
	$10^6\times S/H$	1.97	–	10.6	(6.80)	–	–	7.28	>2.21:

		He 2-29	NGC 2899	He 2-37	Lo 4	NGC 3195	He 2-48	He 2-51	Pe 2-7
4471	He^+/H^+	0.0000(0)	0.0000(0)	0.0594 (1)	0.0000 (-)	0.1111(1)	0.0799(1)	0.1273 (1)	0.0000(0)
5876	He^+/H^+	0.0283(1)	0.0000(0)	0.0571 (3)	0.0000 (-)	0.1154(3)	0.0904(3)	0.1205 (4)	0.0322(3)
6678	He^+/H^+	0.0985(0)	0.0000(0)	0.0235 (0)	0.0000 (-)	0.1099(1)	0.0365(0)	0.1056 (1)	0.0311(1)
Avg.	He^+/H^+	0.0283	0.0000	0.0576	0.0000	0.1134	0.0878	0.1192	0.0319
4686	He^{2+}/H^+	0.0796	0.1337	0.0618	0.1344	0.0201	0.0177	0.0232	0.0807
	He/H	0.108	0.134	0.119	0.134	0.134	0.105	0.142	0.113
3727	$10^5\times O^+/H^+$	7.19	5.08	16.9	0.475	30.8	8.44	32.9	1.58
4959	$10^4\times O^{2+}/H^+$	0.980	0.631	3.49	0.178	1.39	2.21	1.60	1.06
1401	$10^4\times O^{3+}/H^+$	–	–	–	–	–	–	–	–
	ICF(O)	2.44	6.01	1.63	34.3	1.11	1.13	1.13	2.32
	$10^4\times O/H$	4.15	6.84	8.42	7.73	4.99	3.45	5.51	2.83
6584	$10^6\times N^+/H^+$	28.8	66.0	47.4	2.46	107.0	23.7	114.0	3.27
1750	$10^5\times N^{2+}/H^+$	–	–	–	–	–	–	–	–
1486	$10^5\times N^{3+}/H^+$	–	–	–	–	–	–	–	–
1240	$10^5\times N^{4+}/H^+$	–	–	–	–	–	–	–	–
	ICF(N)	5.77	13.5	4.99	163	1.62	4.09	1.67	17.9
	$10^4\times N/H$	1.66	8.89	2.36	4.01	1.74	0.970	1.90	0.583
2326	$10^5\times C^+/H^+$	–	–	–	–	–	–	–	–
1908	$10^4\times C^{2+}/H^+$	–	–	–	–	1.11	–	–	–
1550	$10^4\times C^{3+}/H^+$	–	–	–	–	–	–	–	–
	ICF(C)	–	–	–	–	3.59	–	–	–
	$10^4\times C/H$	–	–	–	–	3.98	–	–	–
3868	$10^5\times Ne^{2+}/H^+$	2.53	2.01	8.29	0.230	5.87	6.51	6.80	2.54
2423	$10^5\times Ne^{3+}/H^+$	–	–	–	–	–	–	–	–
3426	$10^6\times Ne^{4+}/H^+$	6.76	49.9	–	50.4	–	–	–	20.3
	ICF(Ne)	1.50	1.50	2.41	1.50	3.59	1.56	3.45	1.50
	$10^4\times Ne/H$	0.481	1.05	2.00	0.790	2.10	1.02	2.34	0.686
7135	$10^7\times Ar^{2+}/H^+$	7.30	12.5	19.7	–	20.6	7.88	24.0	10.2
4740	$10^7\times Ar^{3+}/H^+$	–	7.32	3.51	–	1.18	–	5.33	7.03
7005	$10^7\times Ar^{4+}/H^+$	–	–	–	–	–	–	–	2.29
	ICF(Ar)	1.87	1.08	1.25	–	2.62	1.87	2.49	1.06
	$10^6\times Ar/H$	1.37	2.14	2.91	–	5.71	1.48	7.30	2.07
6725	$10^7\times S^+/H^+$	7.01	11.8	9.08	3.40	30.5	4.01	31.0	1.65
6312	$10^7\times S^{2+}/H^+$	61.7	71.7	43.9	–	65.1	42.5	58.2	47.8
	ICF(S)	1.32	1.69	1.27	28.2	1.02	1.21	1.02	1.85
	$10^6\times S/H$	9.07	14.1	6.73	(9.60)	9.75	5.62	9.15	9.14

Table 8 – *continued*

		He 2-55	He 2-57	IC 2621	Fg 1	PB 8	He 2-76	He 2-77	Th 2-A
4471	He^+/H^+	0.0000 (0)	0.1093(1)	0.0575(1)	0.0797(1)	0.1177(1)	0.0000 (-)	0.0000(0)	0.0559 (1)
5876	He^+/H^+	0.0293 (1)	0.0603(0)	0.0000(0)	0.0929(3)	0.0000(0)	0.0000 (-)	0.1157(1)	0.0503 (3)
6678	He^+/H^+	0.0000 (0)	0.0917(1)	0.0000(0)	0.1028(1)	0.0000(0)	0.0000 (-)	0.0721(0)	0.0411 (1)
Avg.	He^+/H^+	0.0293	0.1005	0.0575	0.0922	0.1177	0.0000	0.1157	0.0496
4686	He^{2+}/H^+	0.0818	0.0041	0.0348	0.0159	0.0059	0.0687	0.0000	0.0425
	He/H	0.111	0.105	0.092	0.108	0.124	>0.069	0.116	0.092
3727	$10^5\times O^+/H^+$	2.15	0.145[b]	20.7	1.42	16.1	7.42	9.06	2.33
4959	$10^4\times O^{2+}/H^+$	1.40	3.97	3.96	2.41	3.10	1.70	2.87	2.86
1401	$10^4\times O^{3+}/H^+$	–	–	–	–	–	–	–	–
	ICF(O)	2.43	–	1.37	1.11	1.03	–	1.00	1.51
	$10^4\times O/H$	3.93	>3.98	8.27	2.84	4.86	>2.44	3.77	4.67
6584	$10^6\times N^+/H^+$	3.01	99.7	–	1.78	–	57.4	4.55	9.24
1750	$10^5\times N^{2+}/H^+$	–	–	–	–	–	–	–	–
1486	$10^5\times N^{3+}/H^+$	–	–	–	–	–	–	–	–
1240	$10^5\times N^{4+}/H^+$	–	–	–	–	–	–	–	–
	ICF(N)	18.3	–	–	20.0	–	–	4.20	20.1
	$10^4\times N/H$	0.549	>0.997	–	0.356	–	>0.574	0.190	1.86
2326	$10^5\times C^+/H^+$	–	–	–	–	–	–	–	–
1908	$10^4\times C^{2+}/H^+$	–	–	–	–	–	–	–	–
1550	$10^4\times C^{3+}/H^+$	–	–	–	–	–	–	–	–
	ICF(C)	–	–	–	–	–	–	–	–
	$10^4\times C/H$	–	–	–	–	–	–	–	–
3868	$10^5\times Ne^{2+}/H^+$	3.94	4.56	7.21	7.51	7.60	–	–	8.69
2423	$10^5\times Ne^{3+}/H^+$	–	–	–	–	–	–	–	–
3426	$10^6\times Ne^{4+}/H^+$	–	–	22.3	–	–	–	–	–
	ICF(Ne)	2.80	–	1.50	1.18	1.57	–	–	1.63
	$10^4\times Ne/H$	1.10	>0.46	1.42	0.885	1.19	–	–	1.47
7135	$10^7\times Ar^{2+}/H^+$	11.3	5.34	–	8.37	–	17.6	15.7	4.50
4740	$10^7\times Ar^{3+}/H^+$	3.51	–	6.27	3.34	1.21	–	–	4.06
7005	$10^7\times Ar^{4+}/H^+$	–	–	–	–	–	–	–	–
	ICF(Ar)	1.06	–	2.07	1.05	1.57	–	1.87	1.00
	$10^6\times Ar/H$	1.57	>0.534	(1.29)	1.23	(0.191)	>1.76	2.92	0.860
6725	$10^7\times S^+/H^+$	7.76	44.9	10.5	1.20	–	11.2	3.88	2.10
6312	$10^7\times S^{2+}/H^+$	–	9.27	–	–	–	–	61.4	–
	ICF(S)	1.86	–	8.38	17.4	–	–	1.20	16.5
	$10^6\times S/H$	11.4	>45.4	(8.80)	(2.09)	–	>1.12	7.89	(3.47)

		NGC 5189	MyCn 18	He 2-97	NGC 5307	He 2-99	NGC 5315	He 2-105	He 2-111
4471	He^+/H^+	0.0813 (1)	0.0796 (1)	0.0972 (1)	0.0369 (0)	0.0977 (1)	0.0905 (1)	0.0887 (2)	0.1455 (0)
5876	He^+/H^+	0.0571 (3)	0.0996 (3)	0.0970 (3)	0.0561 (1)	0.0000 (0)	0.0000 (0)	0.1022 (4)	0.0891 (3)
6678	He^+/H^+	0.1380 (0)	0.0685 (0)	0.0779 (1)	0.0000 (0)	0.0000 (0)	0.0000 (0)	0.0875 (1)	0.1019 (1)
Avg.	He^+/H^+	0.0632	0.0946	0.0932	0.0561	0.0977	0.0905	0.0966	0.0923
4686	He^{2+}/H^+	0.0797	0.0000	0.0000	0.0478	0.0000	0.0[c]	0.0000	0.1263
	He/H	0.143	0.095	0.093	0.104	0.098	0.091	0.097	0.219
3727	$10^5\times O^+/H^+$	5.41	6.66	11.3	2.59	61.1	7.14	1.56	7.16
4959	$10^4\times O^{2+}/H^+$	1.71	1.81	2.89	2.28	–	5.66	1.48	0.684
1401	$10^4\times O^{3+}/H^+$	–	–	–	7.63:	–	–	–	–
	ICF(O)	1.72	1.00	1.00	1.68	1.00	1.00	1.00	2.03
	$10^4\times O/H$	3.88	2.48	4.02	4.26	6.11	6.37	1.64	2.84
6584	$10^6\times N^+/H^+$	42.6	69.1	18.7	0.515	70.2	68.4	1.69	192.0
1750	$10^5\times N^{2+}/H^+$	–	–	–	–	–	–	–	16.2
1486	$10^5\times N^{3+}/H^+$	–	–	–	24.2:	–	–	–	17.1
1240	$10^5\times N^{4+}/H^+$	–	–	–	–	–	–	–	19.3
	ICF(N)	7.20	3.72	3.55	1.50	1.00	8.92	10.5	1.00
	$10^4\times N/H$	3.06	2.57	0.664	>3.65:	0.702	6.11	0.177	7.18
2326	$10^5\times C^+/H^+$	–	–	–	–	–	–	–	–
1908	$10^4\times C^{2+}/H^+$	0.574	–	–	0.951	–	–	–	0.473
1550	$10^4\times C^{3+}/H^+$	–	–	–	0.507	–	–	–	–
	ICF(C)	2.30	–	–	1.11	–	–	–	4.15
	$10^4\times C/H$	1.30	–	–	1.62	–	–	–	1.96
3868	$10^5\times Ne^{2+}/H^+$	5.13	2.29	5.53	4.62	–	16.6	3.62	3.04
2423	$10^5\times Ne^{3+}/H^+$	3.57	–	–	–	–	–	–	5.05
3426	$10^6\times Ne^{4+}/H^+$	7.79	–	1.21	–	–	–	–	62.4
	ICF(Ne)	1.00	1.37	1.50	1.70	–	1.13	1.11	1.00
	$10^4\times Ne/H$	0.948	0.313	0.847	0.776	–	1.87	0.400	1.43
7135	$10^7\times Ar^{2+}/H^+$	1.42	9.57	0.958	1.28	–	–	5.25	19.8
4740	$10^7\times Ar^{3+}/H^+$	7.77	0.091	0.536	3.47	–	–	–	8.31
7005	$10^7\times Ar^{4+}/H^+$	–	–	–	–	–	–	–	3.99
	ICF(Ar)	1.27	1.37	1.39	1.00	–	–	1.87	1.37
	$10^6\times Ar/H$	1.17	1.32	0.207	>0.476	–	–	0.983	4.39
6725	$10^7\times S^+/H^+$	11.4	2.78	4.13	1.65	28.1	–	0.744	35.2
6312	$10^7\times S^{2+}/H^+$	42.0	35.4	25.0	–	–	–	–	96.1
	ICF(S)	1.40	1.18	1.17	14.4	10.5	–	13.1	1.20
	$10^6\times S/H$	7.48	4.50	3.40	(2.37)	(29.5)	–	(0.971)	15.7

		He 2-112	He 2-119	NGC 5873	NGC 5882	Me 2-1	NGC 5979	He 2-141	NGC 6153
4471	He^+/H^+	0.0906 (1)	0.1095 (1)	0.0452(1)	0.0921 (1)	0.0237(1)	0.0197 (1)	0.0838 (1)	0.0887 (1)
5876	He^+/H^+	0.0824 (3)	0.1116 (3)	0.0000(0)	0.0000 (0)	0.0222(3)	0.0000 (0)	0.0000 (0)	0.0000 (0)
6678	He^+/H^+	0.1049 (1)	0.0791 (1)	0.0000(0)	0.0000 (0)	0.0390(1)	0.0000 (0)	0.0000 (0)	0.0000 (0)
Avg.	He^+/H^+	0.0885	0.1047	0.0452	0.0921	0.0258	0.0197	0.0838	0.0887
4686	He^{2+}/H^+	0.0505	0.0270	0.0453	0.0099	0.0730	0.0962	0.0302	0.0134
	He/H	0.139	0.132	0.091	0.102	0.099	0.116	0.114	0.102
3727	$10^5\times O^+/H^+$	3.05	34.7	3.76	2.33	2.10	0.776	8.70	1.24
4959	$10^4\times O^{2+}/H^+$	2.31	2.68	2.07	4.94	1.94	1.57	3.66	4.48
1401	$10^4\times O^{3+}/H^+$	–	–	–	–	5.29	4.01	–	–
	ICF(O)	1.35	1.17	1.59	1.07	1.00	1.00	1.23	1.10
	$10^4\times O/H$	3.53	7.16	3.89	5.54	7.44	5.65	5.57	5.06
6584	$10^6\times N^+/H^+$	41.0	121.0	4.76	–	1.62	–	–	21.6
1750	$10^5\times N^{2+}/H^+$	–	–	5.63	62.5	4.18	8.43	–	52.1
1486	$10^5\times N^{3+}/H^+$	–	–	–	–	4.97	10.7	–	–
1240	$10^5\times N^{4+}/H^+$	–	–	–	–	1.60	–	–	–
	ICF(N)	11.6	2.06	1.00	1.00	1.00	1.00	–	1.00
	$10^4\times N/H$	4.74	2.49	0.611	6.25	1.09	1.91	–	5.43
2326	$10^5\times C^+/H^+$	–	–	–	–	9.24	–	–	–
1908	$10^4\times C^{2+}/H^+$	–	–	3.70	6.55	3.11	2.05	–	1.24
1550	$10^4\times C^{3+}/H^+$	–	–	1.14	–	2.29	0.631	–	–
	ICF(C)	–	–	1.26	1.12	1.65	1.81	–	1.13
	$10^4\times C/H$	–	–	7.21	7.34	10.5	5.08	–	1.40
3868	$10^5\times Ne^{2+}/H^+$	4.66	10.5	5.18	14.0	2.92	1.93	3.02	13.3[d]
2423	$10^5\times Ne^{3+}/H^+$	–	–	–	–	(6.36)	9.48	–	–
3426	$10^6\times Ne^{4+}/H^+$	29.0	–	–	–	–	7.77	–	–
	ICF(Ne)	1.50	2.67	1.88	1.12	3.83	1.00	1.52	1.13
	$10^4\times Ne/H$	1.13	2.81	0.973	1.56	1.12[e]	1.22	0.459	1.50[d]
7135	$10^7\times Ar^{2+}/H^+$	14.1	26.0	–	–	5.46	–	–	–
4740	$10^7\times Ar^{3+}/H^+$	5.18	1.60	2.13	3.92	4.05	5.91	4.19	–
7005	$10^7\times Ar^{4+}/H^+$	1.93	–	–	–	1.12	–	–	–
	ICF(Ar)	1.09	1.94	1.88	1.12	1.02	7.47	1.52	–
	$10^6\times Ar/H$	2.31	5.37	(0.399)	(0.439)	1.08	4.41	0.637	–
6725	$10^7\times S^+/H^+$	5.70	29.8	7.38	15.4	1.19	–	–	–
6312	$10^7\times S^{2+}/H^+$	55.5	149.0	–	–	–	–	–	–
	ICF(S)	1.61	1.05	12.1	3.38	19.0	–	–	–
	$10^6\times S/H$	9.89	18.8	(8.94)	(5.20)	(2.26)	–	–	–

		IC 4642	PC 14	IC 4673	NGC 6751	He 2-434	NGC 6905	NGC 7009	IC 5148-50
4471	He^+/H^+	0.0364 (1)	0.0896 (1)	0.1348 (0)	0.1108 (1)	0.0928 (1)	0.0000 (0)	0.0988 (1)	0.1742 (0)
5876	He^+/H^+	0.0000 (0)	0.1101 (3)	0.0658 (1)	0.0873 (3)	0.1208 (3)	0.0168 (1)	0.1046 (3)	0.0991 (1)
6678	He^+/H^+	0.0000 (0)	0.0793 (1)	0.0706 (1)	0.0628 (1)	0.1239 (1)	0.0000 (0)	0.1041 (1)	0.0000 (0)
Avg.	He^+/H^+	0.0364	0.0999	0.0682	0.0871	0.1158	0.0168	0.1033	0.0991
4686	He^{2+}/H^+	0.0855	0.0021	0.0781	0.0154	0.0000	0.0862	0.0148	0.0402
	He/H	0.122	0.102	0.146	0.103	0.116	0.103	0.118	0.139
3727	$10^5\times O^+/H^+$	0.357	7.96	2.44	26.6	0.444	0.634	0.836	1.61
4959	$10^4\times O^{2+}/H^+$	0.922	13.5	1.53	2.78	4.40	2.16	4.10	0.696
1401	$10^4\times O^{3+}/H^+$	–	–	–	–	–	–	–	–
	ICF(O)	2.24	1.01	1.66	1.11	1.00	3.34	1.09	1.25
	$10^4\times O/H$	2.14	14.5	2.94	6.07	4.45	7.43	4.58	1.08
6584	$10^6\times N^+/H^+$	–	14.0	6.85	70.2	0.691	0.984	2.00	8.25
1750	$10^5\times N^{2+}/H^+$	–	–	–	–	–	–	11.7	–
1486	$10^5\times N^{3+}/H^+$	–	–	–	–	–	–	13.2	–
1240	$10^5\times N^{4+}/H^+$	–	–	–	–	–	–	–	–
	ICF(N)	–	18.2	12.1	2.28	100	117	1.00	6.70
	$10^4\times N/H$	–	2.54	0.827	1.60	0.693	1.15	2.51	0.553
2326	$10^5\times C^+/H^+$	–	–	–	–	–	–	0.514	–
1908	$10^4\times C^{2+}/H^+$	–	–	–	–	2.28	–	1.71	–
1550	$10^4\times C^{3+}/H^+$	–	–	–	–	–	–	0.224	–
	ICF(C)	–	–	–	–	1.01	–	1.05	–
	$10^4\times C/H$	–	–	–	–	2.30	–	2.08	–
3868	$10^5\times Ne^{2+}/H^+$	1.98	32.0	5.33	8.75	7.79	5.10	10.5	1.48
2423	$10^5\times Ne^{3+}/H^+$	–	–	–	–	–	–	0.633	–
3426	$10^6\times Ne^{4+}/H^+$	44.3	–	6.59	–	–	–	–	–
	ICF(Ne)	1.50	1.07	1.50	2.18	1.01	3.44	1.00	1.54
	$10^4\times Ne/H$	0.962	3.44	0.898	1.91	0.787	1.75	1.11	0.229
7135	$10^7\times Ar^{2+}/H^+$	–	0.162	14.9	18.2	6.73	7.38	12.2	–
4740	$10^7\times Ar^{3+}/H^+$	5.40	2.41	7.54	–	3.44	5.24	6.46	6.53
7005	$10^7\times Ar^{4+}/H^+$	–	–	–	–	–	–	–	–
	ICF(Ar)	5.59	1.06	1.09	1.87	1.01	1.01	1.01	1.54
	$10^6\times Ar/H$	(3.02)	2.72	2.45	3.41	1.03	1.27	1.88	1.01
6725	$10^7\times S^+/H^+$	–	5.35	2.51	8.95	–	–	3.21	2.55
6312	$10^7\times S^{2+}/H^+$	–	103.0	55.3	56.4	–	–	33.2	–
	ICF(S)	–	1.86	1.64	1.10	–	–	2.65	10.0
	$10^6\times S/H$	–	20.2	9.46	6.98	–	–	9.66	(2.56)

Notes. [a]Abundances for NGC 2440 derived from optical spectra only are adopted, and included in final PN abundance averages. [b] O^+/H^+ derived from the 7325-Å line for He 2-57. [c]Presence of nebular He II 4686-Å emission swamped by stellar emission for NGC 5315 (see text). [d]t(Ne III) adopted to derive ionic abundances of neon for NGC 6153 (see text). [e]Ne/H derived from I(3868) and ICF = O/O^{2+} for Me 2-1.

using the program EQUIB to derive the relative population of level i of ion X^{m+}. The dereddened line intensities of Table 3 were then used to derive ionic abundances, where the ionic abundance of an ion X^{m+} is given by

$$\frac{n(X^{m+})}{n(H^+)} = \frac{I_\lambda}{I_{H\beta}} \frac{\alpha^{\rm eff}_{H\beta}}{A_{ij}} \frac{n(X^{m+})}{n_i} \frac{\lambda}{4861}. \quad (5)$$

In order to calculate total abundances of a given ion, either all stages of ionization present must be observed, or unseen stages of ionization need to be accounted for. The standard ionization correction factor (ICF) scheme is from Barker (1980), which relies primarily on the similarity of ionization potentials between various ions. The ICF scheme of WBCM adopted here (see Appendix) not only takes into account the similarity of ionization potentials, but is also based on the results of 10 detailed photoionization models which take into account physical processes that the old ICF scheme cannot, for example the effects of charge exchange, dielectronic recombination, etc. In addition, higher stages of ionization are more accurately estimated. This scheme is more fully described in the appendix.

Generally, when deriving abundances, t(N II) is used for neutral and singly ionized species, and t(O III) is used for all other ions. However, for several ions this assumption is not valid; inspection of the ionization potentials reveals that they would not be coincident with either the N^+ or O^{2+} ions. Errors in adopted electron temperature propagate exponentially into errors in abundances, thus careful consideration must be made concerning which temperature to adopt for a given ion. For the current analysis, ionic species with ionization potentials between those of N^+ and O^{2+} had an intermediate temperature adopted, based on relative ionization potentials. For species with ionization potentials higher than that of O^{2+}, temperatures were adopted based on the aforementioned photoionization models. T_e(N II) was adopted for all singly ionized species. A temperature one-third of the way between t(N II) and t(O III) was adopted for S^{2+} and Ar^{2+}, when t(N II) was measured. T_e(O III) was adopted for all other doubly ionized species. T_e(O III) + 1000 K was adopted for all triply ionized species, except for C^{3+}, where T_e(O III) + 650 K was used instead. Finally, T_e(O III) + 2270 K was used for all 4-times ionized species. n_e(O II) was used whenever possible, otherwise n_e(S II) was adopted. Abundances of neutral species were not derived; fractions of neutral oxygen or neutral nitrogen were assumed to be the same as that of neutral hydrogen, in which case the final abundance ratios with respect to hydrogen would not be affected. Table 8 presents the abundances for all observed ionic species of O, N, C, Ne, Ar and S, together with the adopted ICFs and total abundances. Table 9 presents the ionic abundances for the VLE PN. Total abundances for these objects could not be obtained, and there is a significant amount of neutral material present. The VLE PN are discussed at the end of Section 6. Note that the abundance limits derived for these objects are not included in any final abundance average for the sample of PN.

The C II 1335-Å line was not used to derive abundances, as it can be affected by interstellar line absorption. There is a well-known discrepancy between carbon abundances derived from the optical C II 4267-Å recombination line and the UV C III] 1909-Å collisionally excited line, in that abundances derived from C II λ4267 are often significantly higher than those derived from the λ1909 line (Barker 1980; Kaler 1986b). In this study, for internal consistency we used the C III] 1909-Å line only to derive C^{2+} abundances. The C^+ abundances derived from the [C II] 2326-Å line can be somewhat uncertain, as λ2326 lies in a region of low sensitivity of the *IUE* camera. Also, the dereddened flux of this line is sensitive to the adopted UV extinction law and thus is strongly dependent on the degree of reddening to an object. The C^+ abundances derived from this line for J 900 and for NGC 2440 were not used to derive their C/H ratios. The λ1401 feature was assumed to be entirely due to O IV]; the Si IV contribution was assumed to be negligible (see, for example, Harrington et al. 1982). To derive the O^+/H^+ abundance, we used the [O II] 3727-Å line flux, and not the

Table 9. Ionic abundances for VLE PN.

λ		M 1-11	M 1-12	He 2-138	H 2-1	Tc 1	M 1-26
4471	He^+/H^+	0.0000 (0)	0.0530 (0)	0.0000 (0)	0.0520 (0)	0.0221 (0)	0.0623 (0)
5876	He^+/H^+	0.0198 (1)	0.0181 (3)	0.00947(3)	0.0380 (3)	0.0632 (1)	0.0409 (3)
6678	He^+/H^+	0.0330 (0)	0.0153 (1)	0.0000 (0)	0.0351 (1)	0.0000 (0)	0.0408 (1)
Avg.	He^+/H^+	0.0198	0.0174	0.00947	0.0373	0.0632	0.0409
6300	$10^6 \times O^o/H^+$	3.76	3.94	9.50	3.89	–	3.70
3727	$10^4 \times O^+/H^+$	0.579	1.53	0.658	4.67	1.70	2.94
4959	$10^5 \times O^{2+}/H^+$	0.240	0.420	–	1.99	3.33	1.64
5200	$10^6 \times N^o/H^+$	–	1.04	–	–	–	–
6584	$10^5 \times N^+/H^+$	4.44	3.19	6.43	1.67	2.03	3.63
1908	$10^5 \times C^{2+}/H^+$	–	–	2.26	–	16.5	–
3868	$10^5 \times Ne^{2+}/H^+$	1.22	–	–	–	–	0.014
7135	$10^7 \times Ar^{2+}/H^+$	0.992	1.03	–	2.40	4.85	3.86
6725	$10^7 \times S^+/H^+$	–	1.65	16.7	11.1	2.59	8.98
6312	$10^7 \times S^{2+}/H^+$	–	3.84	–	31.7	–	30.6
	N^+/O^+	0.77	0.21	0.98	0.036	0.12	0.12
	$10^4 \times (O^{2+}+O^+)/H^+$	0.603	1.57	0.657	4.87	2.04	3.10
	$10^6 \times (S^{2+}+S^+)/H^+$	–	0.549	1.67	4.27	0.259	3.96

[O II] 7325-Å line flux. The [Ne IV] 4725-Å feature is very temperature sensitive and hence was not used to derive abundances. To derive the S^+/H^+ abundance, the [S II] 6717, 31-Å fluxes were used, rather than the [S II] 4068-Å flux. The λ4068 line is generally weak, and was only used to estimate S^+/H^+ when $\lambda\lambda$6717, 31 were unavailable. When both [Ar V] 6435 and 7005 Å were present in a spectrum, an equally weighted mean of the Ar^{4+} abundance derived from each line was adopted.

The effect that any temperature fluctuations (Peimbert 1967, and more recently Peimbert, Storey & Torres-Peimbert 1993 and Liu & Danziger 1993) may have on the derived nebular abundances was not taken into account.

6 DISCUSSION OF INDIVIDUAL OBJECTS

IC 5148-50 (=PK 2−52°1). This object is a large, presumably old, PN and has been studied by Kaler, Shaw & Kwitter (1990). We find good agreement between our fluxes, reddening and abundances compared with those of Kaler et al. (1990). As the He I line fluxes from our spectra were uncertain (λ5876 is blended with the NaD night sky lines, and λ4471 is of extremely poor S/N), we adopted the observed λ5876 flux from Kaler et al. (1990). Overall abundances for this object are somewhat low compared with the average ($O/H = 1.1 \times 10^{-4}$ by number), perhaps because of the high electron temperature used; we derived T_e(O III) = 14 500 K. More 'normal' abundances cannot be ruled out, as Kaler et al. derived a lower T_e(O III) of 12 000 K, which, if adopted here, would increase the oxygen, nitrogen and neon abundances by a factor of 2.

K 3-67 (=PK 165−9°1). K 3-67 has been studied by Tamura & Shaw (1987, hereafter TS87) and by AK87. We find good agreement between our fluxes and those of TS87 and AK87. TS87 have classified this object as a Type I PN, based on an N/O ratio of 0.78 and an He/H ratio of 0.13. We, unfortunately, do not have [N II] λ6584 within our wavelength coverage, and have adopted $I(6584) = 58.1$ from AK87, essentially the same value as listed by TS87. With this flux, we derive $N/H = 6.0 \times 10^{-5}$, which is a little below the abundance for the 'average' PN. We have adopted the derived values of t(O III) = 1.35 and n_e(Ar IV) = 5500 cm^{-3} for the abundance analysis. This t(O III) was adopted to calculate the abundances of all ionic species, as the fluxes listed in AK87 yield t(O III) = t(N II) = 1.31 (for n_e = 5500 cm^{-3}). TS87 list slightly higher temperatures; t(O III) = 1.45 and t(N II) = 1.5. The oxygen abundances derived in all three studies are below average; we derive $O/H = 1.3 \times 10^{-4}$, AK87 derive $O/H = 1.8 \times 10^{-4}$ and TS87 derive $O/H = 1.4 \times 10^{-4}$. As our t(O III) was derived from a high S/N [O III] 4363-Å flux, and is in good agreement with AK87, the low oxygen abundance does not seem to arise from an overestimated temperature, but is presumably due to the progenitor star for K 3-67 having formed from a lower metallicity environment. TS87 confirmed kinematically the population II status of K 3-67, from its deviation in radial velocity from a galactic circular orbit. Our optically thick distance of 9.6 kpc (Kingsburgh & Barlow 1992), towards the galactic anticentre, establishes the distant nature of this object. We derive a helium abundance of 0.099 by number, whereas TS87 derive 0.13; TS87 did not take the collisional corrections for He I fluxes into account. If collisional corrections are applied to the He I line fluxes of TS87, their He/H ratio drops to 0.114. Thus, given our N/O = 0.45 and He/H = 0.099, we cannot conclude that this object is a Type I PN. Indeed, the neon abundance that we derive ($Ne/H = 4.71 \times 10^{-5}$) is also lower than the 'average' PN; the lower abundances are consistent with the population II status of K 3-67, possibly pointing to Type IV or intermediate Type III–IV status for this object. The derived abundances for K 3-67 were not included in arriving at the average PN abundances given in Tables 13 and 14. It is interesting to note that both TS87 and AK87 found central star C IV + He II 4658 + 86-Å features; this object merits further study.

NGC 2371-2 (=PK 189+19°1). This object is an extreme bipolar PN, with an O VI central star, and has been classified as Type I by Peimbert & Torres-Peimbert (1983). It has been studied by TPP77 (who examined two areas) and by AC79. Our optical spectra were obtained with the slit positioned at 60° east of north, compared with the nebula's major axis PA of 135° east of north. We find N/O = 0.32 and He/H = 0.107, which does not place it in the Type I class. However, the line fluxes presented here, in TPP77 (both areas) and in AC79, are quite varied, indicating that this object is highly inhomogeneous, with extreme local variations. In our own spectra, we are looking at a higher region of excitation, compared with both regions examined by TPP77 and compared with AC79, as judged by the strength of nebular He II 4686 Å and other lines of high ionization in our spectra, and the weakness of low-ionization lines like [O II] 3727 Å. In addition, our spectra show extremely weak [N II] 6584 Å, as compared with TPP77 and AC79. Our He^+/H^+ abundance is uncertain, as He I 5876 Å is blended with the NaD night sky lines; He^+/H^+ derived from this line is 0.003. Our He^{2+}/H^+ abundance is 0.104, thus He/H = 0.107. If we adopted the He I and He II line fluxes from AC79, a He^+/H^+ ratio of 0.042 would be derived (taking the collisional corrections into account) and a He^{2+}/H^+ ratio of 0.059; thus He/H = 0.101. Adoption of the He I and He II fluxes from a region 'a' of TPP77 yields $He^+/H^+ = 0.028$ and $He^{2+}/H^+ = 0.095$, hence He/H = 0.123. (Region 'b' of TPP77 exhibited no He I lines.)

IUE spectra are available for NGC 2371-2, but the line fluxes are found to vary from spectrum to spectrum. As none of the position angles for the *IUE* spectra matched the position angle for our optical spectra, we chose the spectra with the highest S/N. The abundances for NGC 2371-2 presented in Table 8 are uncertain, due to these local variations, and hence a Type I status is not completely ruled out. Adoption of N^+/H^+ from TPP77, together with the higher ionization stages seen in the *IUE* spectra, would increase the N/H ratio, but the final N/H ratio would still be uncertain due to the clumpiness of this nebula. Because this object shows such extreme variations in various line strengths, the use of optical spectra obtained at the same position as UV spectra would be required in order to derive accurate total abundances and to confirm its Type I status.

J 900 (=PK 194+2°1). J 900 has the highest C/O ratio (=5.21) of all the PN in our sample. J 900 has also been studied by AC83. We find generally good agreement between our fluxes, reddening and abundances and theirs, including a high C/O ratio (their modelling fit gave C/O = 5.92).

A 30 (= PK 208 + 33°1). A30 is an unusual PN, which has hydrogen-deficient inner knots, as indicated by the absence of Balmer lines. Our slit had a PA of 60° east of north and would have passed through Knots 2 and 4 of Jacoby (1979). Our relative line intensities can be compared with those listed for Knot 4 by Jacoby & Ford (1983). A30 has also been observed with the *IUE*, however, most spectra are of the central star, and the one part of the nebula that has been studied in the UV (Harrington & Feibelman 1984) corresponds to Knot 3 of Jacoby (1979). Thus no *IUE* spectra are appropriate for combining with our IPCS spectrum. Our IPCS spectrum reveals no hydrogen lines, but strong He II 4686 Å and [Ne V] 3426 Å. It is somewhat noisy, so the fluxes of weak lines are uncertain. The fluxes for A30 presented in Table 3 are relative to $I(5007)$, which has been set equal to 100.0; an $E(B-V)$ of 0.0 has been adopted, based on the H I reddening maps of Burstein & Heiles (1982). Jacoby & Ford adopted $c(H\beta)=0.44$, based on the extinction derived for the central star by Cohen et al. (1977); however, this extinction is likely to be due to dust within the nebula and may not be appropriate for our nebular spectrum. Harrington et al. (1993) found evidence for the presence of a ring of hot dust in Knots 2 and 4 listed by Jacoby & Ford, based on *K*-band images. We derived a T_e(O III) of 13 600 K, which can be favourably compared with T_e(O III) = 13 400 K derived by Jacoby & Ford for Knot 4. We adopted n_e(rms) = 200 cm^{-3} from Jacoby & Ford. The [Ne IV] 4715, 4725-Å lines are particularly strong, which indicates that the temperature must be quite high in the Ne^{3+} zone. The feature at 4715 Å is entirely due to [Ne IV]; the He I 4713-Å contribution as predicted by the He I 5876-Å flux is ~1 per cent of the total flux in λ4715 and hence is negligible. We assumed that the Ne^{3+} abundance was halfway between the Ne^{2+} and Ne^{4+} abundances, and used the strength of [Ne IV] 4715 + 4725 Å to derive the temperature; in this way, T_e(Ne IV) is estimated to be 20 000 K. Borkowski et al. (1993) constructed photoionization models for the dusty, hydrogen-poor gas of A30, and found that the primary heating mechanism for this gas is ejection of photoelectrons from the dust grains.

Table 10 presents the ionic abundances, relative to the $O^+ + O^{2+}$ abundance, for A30. Since the He I λ6678 flux was anomalously stronger than the higher S/N λ5876 flux, we derived the He^+ abundance from the λ5876 line alone. Total abundances are also presented in Table 10, relative to oxygen, where an ICF for oxygen has been derived via the He^+/He^{2+} ratio; ICF(O) = 1.15. Abundances relative to oxygen for the 'average' non-Type I PN (see Table 14) are also presented. The He/O number ratio of 780 that we derive is consistent with the complete conversion to helium of all the original hydrogen, with no destruction or creation of oxygen, in material with an original He/H ratio of ~0.11 and O/H ratio of 4.8×10^{-4} (the last two ratios correspond to those of a typical PN – see Table 13). In contrast to the unchanged oxygen abundance, A30 is enriched by a factor of 3.5 in nitrogen, and by a factor of 4.1 in neon, relative to 'normal' PN (Table 13). The enhancement in the abundances of these two elements may have been caused by envelope burning of dredged-up carbon into nitrogen by the CN cycle operating at the base of a convective hydrogen envelope, during an earlier stage of evolution, followed by α-particle capture in the helium shell by the then-subducted ^{14}N, giving ^{22}Ne. Jacoby & Ford (1983) derived a similar O/He ratio for Knot 4 to that found here, but derived nitrogen and neon abundances that were 2–3 times lower than those found here. Their lower neon abundance can be attributed to the lack of coverage of [Ne V] λ3426 by their spectra. Note that, due to possible internal extinction within the nebula, which would affect the relative line intensities, the derived abundances for A30 have some degree of uncertainty.

Table 10. Relative abundances derived for A30.

ionic ratio	A 30	'Avg.' PN
$He^+/(O^+ + O^{2+})$	628	–
$He^{2+}/(O^+ + O^{2+})$	277	–
$N^o/(O^+ + O^{2+})$	0.023	–
$N^+/(O^+ + O^{2+})$	0.068	–
$Ne^{2+}/(O^+ + O^{2+})$	0.26	–
$Ne^{4+}/(O^+ + O^{2+})$	0.53	–
O^{2+}/O^+	13.9	–
ICF(O)	1.15	–
$N/O = N^+/O^+$	1.01	0.29
Ne/O*	1.03	0.25
He/O	780	200

Notes: *ICF = 1.5 adopted for Ne, in order to account for Ne^{3+}.

NGC 2440 (= PK 234 − 3°1). NGC 2440 is a Type I PN, with extremely clumped and filamentary structure. Recent *HST* imaging of this object in the light of [O III] (Heap 1993) shows the complicated structure of this object. NGC 2440 was extensively studied by Shields et al. (1981, hereafter SAKC), who utilized optical and UV spectra and constructed a photoionization model for this object. Our spectrum samples a region of higher excitation as compared with SAKC's, in that our He II 4686-Å flux is a factor of 1.3 higher, our [Ne V] 3426-Å flux is a factor of 3.2 higher, our [O II] 3727-Å flux is a factor of 1.3 lower and our [N II] 6584-Å flux is a factor of 1.4 lower than those of SAKC. Our other relative line fluxes are within ~20 per cent of those of SAKC. The ionization stratification present in this nebula is exemplified by the variations in line strength seen in the *IUE* spectra. We have used SWP and LWP spectra taken in 1988 for our analysis, as they had the highest S/N. Our derived abundances show good agreement with those derived by the photoionization model of SAKC, except for the case of carbon, where we derived a C/O ratio of 1.8, whereas SAKC had 0.56. The main reason for this difference lies in the C^{2+} abundance derived from the C III] 1909-Å line, where our C^{2+}/H^{2+} ratio is a factor of 5.3 times larger than that of SAKC. Possibly, the result represents a real variation in carbon abundance in different areas of the nebula, but errors in scaling the *UV* spectra to the optical spectra via the He II 1640/4686 ratio could give errors in the derived abundances, if different areas of excitation are combined. The position angle of the *IUE* spectra used was 250° east of

north, while the position angle of the IPCS spectra was 90° east of north. Our derived C/H ratio could be inaccurate, due to slightly different parts of the nebula being sampled. The second entry for NGC 2440 in Table 8 presents abundances derived using the optical spectra only. These abundances are the ones adopted for NGC 2440 and plotted in Figs 4–14, and were included in arriving at the average Type I PN abundances listed in Tables 13 and 14.

M 3-6 (=PK 254+5°1). The abundances presented in Table 8 for M 3-6 are somewhat low compared with the 'average' PN; O/H is 2.82×10^{-4} by number. We believe that the low abundances result from adopting an unreliable temperature, as our [O III] 4363-Å flux is uncertain. We derived a temperature of 8800 K, from an $I(5007+4959)/I(4363)$ ratio of 318 and n_e(O II)=3020 cm^{-3}. This object has also been studied by Acker et al. (1989). After dereddening their observed fluxes with $c(H\beta)=0.68$, we find the agreement between our fluxes and their fluxes to be within 10 per cent, except for [O III] 4959 Å, where we have derived $I(4959)=208$, whereas the spectrum of Acker et al. gives $I(4959)=273$. Thus Acker et al. derive a lower temperature for M 3-6, of 7200 K (however, they also flag their $I(4363)$ with a colon, so their temperature must also be considered uncertain). By adopting $T_e=7200$ K, the O/H ratio rises to 6.57×10^{-4} by number, which is within the range of the 'average' PN. Thus the seemingly low abundances for M 3-6 can probably be attributed to the uncertainty in the adopted temperature.

Lo 4 (=PK 274−9°1). Our central star spectra of Lo 4, obtained in 1978 February, show the O VI 3811, 34-Å lines in emission. The nucleus is known to pulsate non-radially, and has recently undergone a dramatic mass-loss event (see Werner et al. 1992). Werner et al. find its spectrum to be that of a PG 1159 star (i.e. an extremely hot hydrogen-deficient pre-white dwarf) during its 'low' state, and its spectrum shows Wolf–Rayet wind features during its 'high' state. We find our nebular spectrum to be of extremely high excitation, where $I(4686)=150$. The nebular spectrum is of somewhat poor S/N, as the nebula is of low surface brightness. Fluxes for Lo 4 are presented uncorrected for reddening relative to Hβ in Table 3 (as the spectrum was of poor S/N); however, the contribution of the He II Pickering series to the Balmer decrement has been removed (Section 3.2). The observed Hα/Hβ ratio is 3.05, which is close to the intrinsic ratio of 2.85 (Hummer & Storey 1987). No λ4363 emission was detected in this spectrum, and hence t(O III)=1.75 was adopted from the λ4686 flux and equation (1). The oxygen-to-hydrogen abundance ratio derived for this object is 7.73×10^{-4}, and is roughly a factor of 1.7 higher than that found for the average non-Type I PN (Table 9). We find an N/O ratio of 0.52 and an Ne/O ratio of 0.10 for this object.

NGC 2899 (=PK 277−3°1). NGC 2899 has been studied by López et al. (1991), who examined its kinematic structure with echelle measurements and obtained other physical parameters using low-resolution spectra. We derive $c(H\beta)=0.80$, in good agreement with the value of $c(H\beta)=0.71$ found by López et al. (1991). Our spectra, however, probe a region of higher excitation than that studied by López et al. (1991); none the less, we find similar abundances, except for He/H. In our spectrum, the helium is all doubly ionized and we derive He/H=0.134, whereas López et al. (1991) saw both He I and He II lines and derived a higher overall He/H ratio of 0.182. However, we do derive a similar N/O ratio to that of López et al. (1991); we obtain N/O=1.3, and they obtained N/O=1.8 (they adopted t(O III) to calculate all ionic abundances; the adoption of t(N II) for the O^+ and N^+ zones would drop their N/O ratio into even closer accord with the value that we derive).

He 2-57 (=PK 289−1°1). He 2-57 is quite a heavily reddened object; a value of $c(H\beta)=2.00$ was used to obtain the dereddened relative line intensities listed in Table 3. It is an unusual object, possibly related to high-density PN with binary companions, such as Cn 1-1 (Lutz 1984), PC 11 (Gutiérrez-Moreno, Moreno & Cortés 1987) or AS 201 (Kohoutek 1987), although no absorption lines indicating the presence of a companion are seen. The [O III] temperature diagnostic ratio is quite low; $I(5007+4959)/I(4363)=6.6$. This indicates collisional de-excitation of the uppermost level for λ4363; the ratio is more appropriately used as a density rather than temperature diagnostic. The temperature for He 2-57 has been estimated by finding the temperature that is consistent with the average oxygen abundance for PN; $T_e=17\,000$ K gives O/H=4.1×10^{-4} from the λ4363 line, which should not be collisionally suppressed. For this temperature, a density of $10^{6.3}$ cm^{-3} is derived from the above [O III] ratio. No [O II] 3727-Å emission is seen in the on-star spectrum, in accord with the expectation that the line should be collisionally de-excited, at such a high density. Similar temperatures and densities are also found in Cn 1-1 ($T_e=15\,000$ K, $n_e=10^6$ cm^{-3}; Lutz 1984), PC 11 ($T_e=20\,000$ K, $n_e=10^5$ cm^{-3}; Gutiérrez-Moreno et al. 1987) and AS 201 ($T_e=15\,000$ K, $n_e=10^6$ cm^{-3}; Kohoutek 1987). He 2-57 also contains a low-density region, extending across all eight of the 2.3-arcsec spatial increments along our slit, from which the [S II] emission seen in the on-star spectrum originates. The spectrum of this outer region reveals strong [O II] λ3727 emission; here the [S II] 6717, 31-Å doublet ratio is 1.3, consistent with its low-density limit. In this regard, He 2-57 resembles the planetary nebula EGB 6, which has a very large low-density shell surrounding an unresolved very high-density nebula and hot central star (Liebert et al. 1989). Table 11 presents the observed and dereddened line fluxes from the outer nebula of He 2-57, where $c(H\beta)=1.7$ was derived from the Hα/Hβ ratio and was used to deredden the observed fluxes. This value of $c(H\beta)$ may be more appropriate for dereddening the on-star spectrum than the value 2.0 yielded by the on-star Hα/Hβ ratio, in which case the on-star ratio is probably enhanced by collisional effects.

Table 11. Line fluxes for the outer region of He 2-57.

line	F/F(Hβ=100)	I/I(Hβ=100)
[O II] 3727	297	810
Hβ	100	100
[O III] 5007	103	90
He I 5876	29	12.5
Hα	995	285
[S II] 6717	122	32.0
[S II] 6731	91.7	23.9

As the density appropriate for the on-star spectrum of He 2-57 is so high, the ICF scheme is found to break down, and only ionic abundances are presented in Table 8. He 2-57 could be a symbiotic star, or it could be a planetary nebula whose central star has recently undergone another mass-loss event which has given rise to the high-density nebular material revealed by the on-star spectrum.

Fg 1 (=PK 290+7°1). López, Meaburn & Palmer (1993a) and López, Roth & Tapia (1993b) have taken deep images of Fg 1, revealing jet-like structures along the minor axis of the nebula. Two symmetric strings of ionized knots are located 2 arcmin either side of Fg 1, along an axis ~15° east of north, at equal distances from the central star. López et al. (1993b) found that the radial expansion velocity of the innermost knots was ±43 km s^{-1}. Our IPCS optical spectra of Fg 1 were obtained with a slit PA of 90° east of north, 15° from the major axis of the nebula. The *IUE* spectrum that we obtained in 1991 April revealed a central star wind with the N v 1240-Å and O v 1371-Å line showing P Cygni structure and with stellar He II 1640-Å emission present. We find a lower than average nitrogen abundance for the central region of this object, N/H = 3.6×10^{-5}. The [N II] 6584-Å feature is weak [I(6584) = 7.9] and no strong lines of nitrogen are revealed in the *IUE* spectrum (although it has a somewhat poor S/N). Spectra of the north and south knots of Fg 1 by López et al. (1993b) reveal strong [N II] lines, where F(6584)/F(Hα) = 2.72 in the north knot, and F(6584)/F(Hα) = 1.87 in the south knot; possibly the strength of these lines is due to shock excitation. The knots are interpreted by López et al. (1993b) as resulting from episodic mass outflows from a previous evolutionary stage. This objects merits further study.

He 2-77 (=PK 298−0°1). He 2-77 is the most heavily reddened object in this sample, with a c(Hβ) of 4.13. Extensive dust is present around this object, as it is heavily obscured in the optical region and has a strong far-infrared flux as measured by *IRAS*. The status of He 2-77 has been debated in the literature, as to whether it is a PN or an H II region. Cohen & Barlow (1980) argued that it was a heavily reddened compact H II region, based on its large radio flux and reddening and its 10-μm spectrum. Jourdain de Muizon et al. (1987) argued that it was a PN, based mainly on the presence of [S IV] 10.5-μm and [Ne III] 15.5-μm lines in its *IRAS* LRS spectrum. However, Jourdain de Muizon et al. (1990) subsequently showed that [S IV] and [Ne III] emission was present in the *IRAS* LRS spectra of a number of other galactic H II regions and included He 2-77 in this group. Caswell & Haynes (1987) determined a radio recombination temperature of 8800 K for He 2-77 (≡G298.187−0.782). They derived a kinematic distance of 10 kpc from its recombination line radial velocity and noted that it was the most distant H II region in the Galaxy possessing an optical counterpart. We have derived abundances for He 2-77, but have not included it in the PN averages.

We find good agreement between our observed line fluxes and reddening, and those of Jourdain de Muizon et al. (1987). We derive n_e(S II) = 3000 cm^{-3}, identical to the value found by Jourdain de Muizon et al. (1987). As our spectrum was too heavily reddened to observe [O III] 4363 Å, and as no [N II] 5755-Å emission was present, we have adopted the value of T_e = 8800 K derived from the radio recombination line spectrum by Caswell & Haynes (1987). Jourdain de Muizon et al. (1987) obtained a value of T_e = 9000 K from the ratio of the [S III] 6312-Å to 18.7-μm fluxes. Our abundances are generally in good agreement with their values, except for N/H, where they derived a value 3.3 times higher than ours, as they adopted a higher ICF for nitrogen. Our N/H ratio of 2×10^{-5} is more consistent with the nitrogen abundances generally found for galactic H II regions (Dufour 1984). The Ar^{2+}/H^+ abundance ratio derived from our λ7136 flux is a factor of 2 higher than the Ar^{2+}/H^+ ratio derived by Jourdain de Muizon et al. (1987) from the 8.99-μm [Ar III] line in the *IRAS* LRS spectrum.

NGC 5189 (=PK 307−3°1). This object is a Type I PN, with an O VI central star. It shows bipolar morphology, and is of very high excitation. We find reasonable agreement between our relative line fluxes and those of de Freitas Pacheco et al. (1991), except for the important [O III] 4959-Å line, for which our flux is a factor of 1.2 lower. Hence de Freitas Pacheco et al. derived a lower t(O III) of 1.03, whereas we derive t(O III) = 1.3.

We have also observed this object at medium resolution, and presented the [O II] 3726/29-Å doublet ratio as a function of angular distance from the central star (Kingsburgh & Barlow 1992). In our highest resolution spectrum (10 Å mm^{-1}), each component of [O II] 3726, 3729 Å and [Ne III] 3868 Å is split and reveals velocity structure. This long-slit spectrum was aligned in the north–south direction, along the minor axis of the nebula, and contains 11 increments, each 2.2-arcsec wide. Velocity structure is only seen in the components of the [O II] doublet south of the central star. The wavelength, FWHM and flux for each velocity component of [O II] λλ3726, 3729 and [Ne III] 3868 Å were measured using the ELF routine in DIPSO. The differences between the measured and laboratory wavelengths were used to derive radial velocities, which were converted to heliocentric velocities ($V_\odot$). Table 12 presents the positive and negative heliocentric velocities for λλ3626, 3729 and for 3868 Å, the FWHM of each velocity component, and twice the projected expansion velocity, for each spatial increment. The expansion velocities listed for the [O II] doublet were derived from the flux-weighted means of each 3726-Å and 3729-Å component.

He 2-99 (=PK 309−4°1): He 2-99 has a WC9 central star and has been extensively studied by Kaler et al. (1989). *IUE* spectra are available for this object, but few nebular lines are present, and, as He II 1640 Å is stellar in origin, there is no way to scale the UV fluxes to our optical spectra. Thus we present results from the optical nebular spectrum only. The nebular spectrum is a sum of the spatial increments located 3.3–7.7 arcsec west of the central star and 3.3–7.7 arcsec east of the central star. The position angle for the spectrum was 80° east of north. The nebular temperature is quite cool. All the oxygen appears to be in O^+, as no [O III] 4959-Å or 5007-Å emission is seen. An electron temperature of 8100 K was derived from the [N II] 6584/5755-Å ratio, and used in deriving the abundances for all the observed ionic species. No He II λ4686 emission is present in our offset nebular spectrum.

He 2-111 (=PK 315−0°1). He 2-111 is the most extreme Type I object in our sample, with N/O = 2.53 and He/H = 0.219. Its extreme bipolar morphology and extended structure were revealed by Webster (1978), who found areas of the outer nebula to be expanding at ~400 km s^{-1}, con-

Table 12. Velocity structure in [O II] 3726, 29 Å and [Ne III] 3868 Å for NGC 5189.

	[O II] λ3726				[O II] λ3729				[O II]$_{avg}$			[Ne III] λ3868			
D[a]	FWHM	$V_\odot^-$	FWHM	$V_\odot^+$	FWHM	$V_\odot^-$	FWHM	$V_\odot^+$	$\overline{V_\odot^-}$	$\overline{V_\odot^+}$	$\Delta V_{(OII)}$	FWHM	$V_\odot^-$	$V_\odot^+$	$\Delta V_{(NeIII)}$
+11.0	0.61	−33.87			0.61	−33.86			−33.87			0.58	−26.43	42.81	69.24
+8.8	0.59	−30.65			0.59	−33.05			−31.87			0.56	−26.18	42.81	68.99
+6.6	0.57	−29.04			0.57	−29.03			−29.04			0.58	−23.85	28.09	51.94
+4.4	0.58	−28.23			0.58	−29.03			−28.60			0.56	−22.30	29.64	51.94
+2.2	0.56	−27.43			0.56	−30.64			−29.06			0.58	−26.43	30.41	55.04
0	0.64	−37.09	0.64	10.40	0.64	−30.64	0.64	31.29	−37.09	10.40	47.49	0.56	−26.95	31.16	58.14
−2.2	0.65	−38.70	0.65	23.28	0.58	−35.46	0.58	25.66	−37.02	24.40	61.42	0.55	−30.05	24.21	54.26
−4.4	0.62	−35.48	0.62	23.28	0.55	−33.85	0.55	23.45	−34.67	23.37	58.04	0.54	−35.48	23.43	58.91
−6.6	0.59	−40.31	0.59	24.08	0.59	−39.48	0.59	23.25	−39.89	23.65	63.54	0.60	−38.58	21.88	60.46
−8.8	0.70	−41.11	0.70	23.28	0.79	−37.08	0.79	23.25	−39.36	23.27	62.63	0.68	−47.11	22.66	69.77
−11.0												0.57	−33.93	24.21	58.14

Notes. Units: FWHM are expressed in Å; velocities are expressed in km s^{-1}. [a]D is the distance from the central star in arcseconds, and the slit was oriented N–S. $V_\odot^-$, $V_\odot^+$ are the radial expansion velocities of the blue and red components of each line, respectively. $V_\odot^{+,-}$ is the flux-weighted average of the two velocity components for λλ3726 and 3729. $\Delta V = |V_\odot^+ - V_\odot^-|$ is twice the expansion velocity.

siderably faster than any other PN. Meaburn & Walsh (1989) performed echelle observations of He 2-111 and found expansion velocities ranging from a few tens of km s^{-1} for areas close to the central star, to velocities close to 400 km s^{-1} for material towards the edges of the faint outer nebula. Our dereddened line intensities show good agreement with those of de Freitas Pacheco et al. (1991), except for He II 4686 Å; our flux is a factor of 2 larger than theirs, presumably because our spectrum of the central zone traced a region of higher excitation. He 2-111 has been observed recently with the *IUE* satellite (see Table 1), but, as it is very heavily reddened, the UV spectrum is very noisy and the line fluxes are uncertain. The abundances derived from the UV lines are, however, fortuitously in agreement with those derived from the optical lines and ICFs.

NGC 6153 (=PK 341 − 5°1). Pottasch, Dennefeld & Mo (1986) examined NGC 6153 at optical, UV and IR wavelengths, and concluded that it was overabundant in many elements, particularly neon. We find a He/H ratio of 0.102, whereas Pottasch et al. found He/H = 0.13. Pottasch et al. derived t(Ne III) from the 3868-Å/15.5-μm line ratio and adopted an electron temperature of 8100 K for their abundance analysis, based on the approximate intersection of their derived diagnostic loci (see their fig. 4), where they strongly weighted t(Ne III) compared with t(O III). In order to derive t(Ne III), Pottasch et al. scaled up a λ3868 flux from a spectrum observed with a 4 × 4 arcsec^2 slot and adopted $I(3868) = 93$, on a scale where $I(H\beta) = 100$. As the diameter of this PN is 20 arcsec, their [Ne III] 3868-Å flux was not an integrated value, whereas the *IRAS* 15.5-μm flux was. Using our wider slit spectra (6.7 × 18.4 arcsec^2), we estimated the integrated 3868-Å flux using the 'circular' integral method (as described in Kingsburgh & Barlow 1992) and obtained $I(3868) = 106$, in reasonable agreement with Pottasch et al. Using this flux, we derived t(Ne III) = 0.81 from the 3868/15.5 flux ratio and Ne/H = 2.5 × 10^{-4}, in agreement with the values derived by Pottasch et al. This neon abundance is enhanced by about a factor of 2 relative to other PN (Table 14). We used $n_e = 3090$ cm^{-3}, from the [O II] doublet ratio, to derive the abundances for all ions and used the value of t(O III) = 0.98 from the $I(5007+4959)/I(4363)$-Å ratio to calculate abundances for all ionic species other than Ne^{2+}, whereas Pottasch et al. used the lower temperature of t(Ne III) = 0.81 for all ions. We find that the derived N/H ratio is enhanced (5.4 × 10^{-4}); however, the N III] 1750-Å flux is of poor S/N, so the N/H ratio could easily be out by a factor of 3. The O/H ratio is about 'average' when t(O III) = 0.98 is adopted (5.1 × 10^{-4}), whereas Pottasch et al. found O/H ~ 1 × 10^{-3} when they adopted the lower value of t = 0.81. Similarly, our carbon abundance is 'average' when t(O III) = 0.98 is used. We conclude that this object is possibly enriched in nitrogen and neon, but that uncertainties in the electron temperature are enough to give this PN 'normal' abundances. The conclusion that NGC 6153 has an enhanced neon abundance rests on the reliability of the *IRAS* LRS 15.5-μm line flux. If the 15.5-μm line flux is correct, then this may provide further evidence for the presence of temperature fluctuations within planetary nebulae and that optical forbidden line temperature diagnostics may provide inappropriately high temperatures for determining abundances from collisionally excited lines. We emphasize that accurate electron temperatures are crucial for the derivation of accurate abundances, particularly when temperatures are ≲ 9000 K.

VLE PN Six VLE PN are present in this sample, and their ionic abundances, together with N^+/O^+, $(O^{2+}+O^+)/H^+$ and $(S^{2+}+S^+)/H^+$ ratios, are presented in Table 9. Total abundances could not be derived, because of the presence of significant neutral hydrogen and helium in these objects. Note that the He^+/H^+ ratios are all more than a factor of 2 smaller than the He/H ratios found for the PN in Table 8. We have not attempted to estimate the fraction of neutral helium in these nebulae. Fig. 4 of Kaler (1978b) plots He/H ratios as a function of stellar effective temperature, and a trend is seen for log $T_{eff} < 4.7$. This type of trend could be used to estimate the neutral helium abundance; however, we have not derived T_{eff} in the present analysis. A future paper will be devoted to properties of the central stars for this sample, where such trends will be investigated.

Two of these objects, M 1-11 and He 2-138, have high N^+/O^+ ratios – 0.77 and 0.98, respectively. Whether these

Table 13. Abundance summary.

Object	He/H	O/H[a]	N/O	C/O	N/C	Ne/O	Ar/O ($\times10^3$)	S/O ($\times10^2$)
IC 2003	0.092	8.65	0.26	2.07	0.13	0.13	2.1	0.74
(K 3-67)[b]	0.099	8.12	0.45	–	–	0.36	–	–
J 900	0.122	8.59	0.11	5.21	0.021	0.26	(0.80)	4.3
M 1-8	0.125	8.65	0.49	–	–	0.34	3.9	1.0
PB 1	0.144	8.59	0.087	–	–	0.30	3.5	4.6
M 3-1	0.105	8.39	0.18	0.14	1.30	0.25	6.5	2.7
M 1-13	0.146	8.74	0.35	–	–	0.29	22	0.98
NGC 2371-2	0.107	8.72	0.32	0.38	0.84	0.31	3.6	–
*M 3-3	0.115	8.67	0.85	–	–	0.31	6.4	0.27
*NGC 2440	0.129	8.64	1.17	–	–	0.31	8.8	1.01
NGC 2438	0.142	8.38	0.42	0.57	0.74	0.17	4.9	1.4
NGC 2452	0.111	8.61	0.70	0.76	0.89	0.25	5.6	1.7
M 3-4	0.123	8.72	0.31	–	–	0.28	5.4	0.59
M 3-5	0.110	8.29	0.63	–	–	0.45	8.4	1.0
M 3-6	0.090	8.45	0.084	–	–	0.30	–	–
*He 2-15	0.144	8.48	1.63	–	–	0.30	9.7	3.5
IC 2448	0.087	8.72	0.45	1.63	0.28	0.20	(1.4)	1.3
NGC 2792	0.105	8.76	0.62:	1.46	1.05	0.22	(3.8)	–
PB 4	0.125	8.81	–	–	–	0.21	(0.81)	–
NGC 2867	0.116	8.78	0.21	2.1	0.10	0.17	3.1	1.2
He 2-29	0.108	8.62	0.40	–	–	0.12	3.3	2.2
*NGC 2899	0.134	8.83	1.3	–	–	0.15	3.2	2.1
He 2-37	0.119	8.93	0.28	–	–	0.24	3.5	0.80
NGC 3195	0.134	8.70	0.35	0.80	0.44	0.42	11	2.0
He 2-48	0.106	8.54	0.28	–	–	0.30	4.3	1.6
He 2-51	0.142	8.74	0.35	–	–	0.42	13	1.7
Pe 2-7	0.113	8.45	0.21	–	–	0.24	7.4	3.2
He 2-55	0.111	8.59	0.14	–	–	0.28	4.0	2.9
IC 2621	0.092	8.92	–	–	–	0.17	1.6	1.0
Fg 1	0.108	8.45	0.13	–	–	0.31	4.3	0.74
PB 8	0.123	8.69	–	–	–	0.24	0.39	–
(He 2-77)[c]	0.116		0.050	–	–	–	7.7	0.21
Th 2-A	0.092	8.67	0.40	–	–	0.31	1.8	0.74
*NGC 5189	0.143	8.59	0.79	0.34	2.35	0.24	3.0	1.9
*MyCn 18	0.095	8.39	1.04	–	–	0.13	5.3	1.8
He 2-97	0.093	8.60	0.17	–	–	0.21	0.52	0.85
(*)NGC 5307[d]	0.104	8.63	>0.86	0.38	>2.2	0.18	1.1	0.56
He 2-99	0.098	8.79	0.11	–	–	–	–	4.8
*NGC 5315	0.091	8.80	0.96	–	–	0.31	–	–
He 2-105	0.097	8.21	0.11	–	–	0.24	6.0	0.59
*He 2-111	0.219	8.45	2.53	0.69	1.44	0.50	15	5.5
*He 2-112	0.139	8.55	1.34	–	–	0.32	6.5	2.8
He 2-119	0.132	8.85	0.35	–	–	0.39	7.5	2.6
NGC 5873	0.091	8.59	0.16	1.85	0.085	0.25	(1.0)	2.3
*NGC 5882	0.102	8.74	1.13	1.32	0.85	0.28	(0.79)	0.94
Me 2-1	0.099	8.87	0.15	1.41	0.10	0.15	1.5	0.30
NGC 5979	0.116	8.75	0.34	0.90	0.38	0.22	(7.8)	–
He 2-141	0.114	8.75	–	–	–	0.09	(1.1)	–
*NGC 6153	0.102	8.70	1.07	0.28	3.88	0.30	–	–
IC 4642	0.122	8.33	–	–	–	0.45	(14)	–
PC 14	0.102	9.16	0.18	–	–	0.24	1.9	1.4
IC 4673	0.146	8.47	0.28	–	–	0.31	8.3	3.2
NGC 6751	0.103	8.78	0.26	–	–	0.31	5.6	1.1
He 2-434	0.116	8.65	0.16	0.57	0.30	0.18	2.3	–
NGC 6905	0.103	8.87	0.16	–	–	0.24	1.7	–
NGC 7009	0.118	8.66	0.55	0.45	1.21	0.24	4.1	2.1
Avg. all PN	0.115	8.68	0.47	1.15	0.41	0.26	4.79	1.71
±	0.022	0.15	0.47	1.15	0.41	0.17	4.79	1.43
Avg. non Ty I PN	0.112	8.69	0.28	1.31	0.22	0.25	4.91	1.64
±	0.015	0.16	0.22	1.23	0.22	0.17	4.91	1.45
Avg. Ty I PN	0.129	8.65	1.20	0.68	1.76	0.28	5.93	1.84
±	0.037	0.15	0.60	0.68	1.76	0.14	5.81	1.21
HII regions	0.100	8.70	0.074	0.58	0.13	0.16	5.24	2.29
solar	0.098	8.93	0.12	0.47	0.25	0.15	4.27	2.04

Notes. All ratios are by number. *Type I PN (see text). [a]O/H given in log scale, where H + 12. [b]K 3-67 is omitted from the abundance averages (as it is a possible Type IV PN). [c]He 2-77 is omitted from the abundance averages (as it is an H II region). [d]NGC 5307 is only included in the 'all PN' abundance averages, as its possible Type I status is based on an uncertain N III] 1750-Å flux. Argon abundances given in parentheses have been derived from [Ar IV] 4740-Å flux only, and are not used in final Ar/O average. References for H II region and solar abundances are given following Table 14.

objects are precursors to the Type I PN is difficult to ascertain. Although the N^+/H^+ ratios are a factor of 1.5–2 higher than those found in the other VLE PN, their O^+/H^+ and O^{2+}/H^+ ratios are a factor of 3 or more lower than those found in the other VLE PN, implying that a very large amount of neutral material is present. Under these extreme conditions, the N^+/O^+ ratio may not reflect the true N/O ratio.

7 DISCUSSION

Table 13 presents the He/H, O/H, N/O, C/O, N/C, Ne/O, Ar/O and S/O ratios for the current PN sample, together with the same values for galactic H II regions and for the Sun. Note that the argon abundances derived using only the [Ar IV] 4740-Å feature and the ICF listed in the Appendix are very uncertain; accordingly they have been flagged in Table 8, and are not included in any of the final abundance averages. Table 13 also presents the means of these quantities for the Type I PN and for the non-Type I PN samples. Values listed in Table 13 are included in Figs 4–14; objects that have only limits to their abundances, or abundances marked by a colon, are not plotted.

Table 14 presents the average C, N, O, Ne, Ar and S abundances, by number relative to hydrogen, for non-Type I and for Type I PN (excluding VLE PN), on a logarithmic scale where H = 12.0. Mean abundances for galactic H II regions, for the Sun, and for the Orion Nebula, are also presented.

7.1 Type I PN

In all PN progenitor stars, the products of nucleosynthesis have been dredged-up to the surface and the ejected nebula enriched in helium and nitrogen, but some appear to have been particularly enriched in these elements. Type I PN were defined by Peimbert & Torres-Peimbert (1983) as having $N/O \geq 0.5$ *and* $He/H \geq 0.125$. They are often bipolar, showing pronounced filamentary structure. They also show a wide range of ionization stages (e.g. [O I] to [Ne V]). Type I PN are believed to have evolved from more massive than average progenitor stars, with initial main-sequence mass $M > 2.4\ M_\odot$ (Peimbert & Serrano 1980),[6] and thus to have formed more recently out of a more enriched ISM.

Fig. 4 plots log(N/O) versus log(He/H) for the PN in our sample. There is a continuous sequence of objects, with only one object (He 2-111) clearly separated from the bulk of the sample, and objects with $N/O > 0.5$ do not appear distinct from objects with $N/O < 0.5$, presumably pointing to a continuous range of progenitor star masses. The six PN that would be classified as Type I under Peimbert & Torres-Peimbert's criteria are He 2-111, He 2-112, He 2-15, NGC 2440, 2899 and 5189 (i.e. using both the N/O and the He/H criteria). Inspection of Fig. 4 reveals there to be no correlation between N/O and He/H, although a trend of increasing N/O with increasing He/H might appear to be present if only the Type I PN were considered. Some previous investigators have argued that there is a correlation between N/O and He/H for both Type I and non-Type I PN, and that this supports the second dredge-up phase as being responsible for the increase in both N and He. However, closer inspection of Fig. 4 and of other such plots in the literature (e.g. fig. 1 of Dufour 1991) reveals that a continuous range of N/O ratios between 0.1 and 1.0 is encountered for He/H ratios between 0.09 and 0.14. Only for N/O ratios in excess of ~1.2 does there appear to be a trend for He/H to increase with increasing N/O.

Anticipating the discussion in Section 7.3 below, we note that no difference is found between the oxygen abundances of galactic H II regions or 'normal' (non-Type I) galactic planetary nebulae, compared with the oxygen abundances of galactic Type I nebulae defined either using the criteria of Peimbert & Torres-Peimbert (1983) or using our new Type I criterion defined below. There is therefore no evidence that any significant depletion of oxygen has occurred in the envelopes of the progenitor stars of these nebulae, for instance as a result of the second dredge-up. Walton et al.

[6]It is interesting to note that this mass limit roughly corresponds to the point above which helium burning proceeds non-degenerately in the cores of AGB stars (Iben & Renzini 1983).

Table 14. Average PN abundances.

ratio	all	non-Type I	Type I	HII Regions[a]	Solar[b]	Orion[e]
He/H	0.115±0.022 (55)	0.112±0.015 (43)	0.129±0.037 (11)	0.100±0.010	0.098±0.008	0.100
O/H	8.68±0.15 (54)	8.69±0.15 (42)	8.65±0.15 (11)	8.70±0.25	8.93±0.035	8.60
N/H	8.35±0.25 (47)	8.14±0.20 (36)	8.72±0.15 (11)	7.57±0.33	8.00±0.05[c]	7.83
C/H	8.74±0.30 (20)	8.81±0.30 (15)	8.48±0.30 (3)	8.46±0.20	8.60±0.05[d]	8.53
Ne/H	8.09±0.15 (52)	8.10±0.15 (41)	8.09±0.15 (11)	7.90±0.17	8.09±0.10	7.91
Ar/H	6.39±0.30 (41)	6.38±0.30 (33)	6.42±0.30 (8)	6.42		6.35
S/H	6.92±0.30 (43)	6.91±0.30 (34)	6.91±0.30 (9)	7.06	7.24	6.93

Notes: He/H ratios are by number. Abundances for O, N, C and Ne are by number on a logarithmic scale, where H = 12. The number of PN included in each average is enclosed in parentheses following each average. [a]H II region abundances from Dufour (1984). [b]Solar abundances from Grevesse & Anders (1989). [c]Solar nitrogen abundance from Grevesse et al. (1990). [d]Solar carbon abundance from Grevesse et al. (1991). [e]Orion abundances from Rubin et al. (1991).

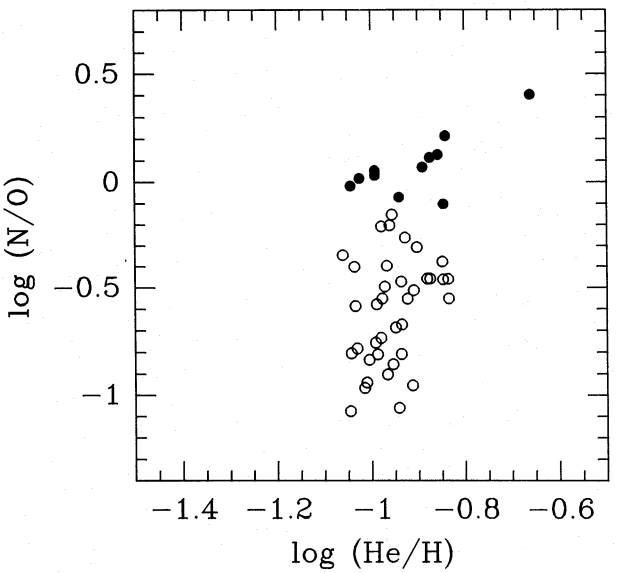

Figure 4. Log (N/O) versus log (He/H). Type I PN are filled circles, non-Type I PN are open circles in all plots. A trend of increasing N/O ratio with increasing He/H ratio is found for only the Type I PN.

(1991) and Barlow (1991) reported a similar result for Large Magellanic Cloud (LMC) planetary nebulae, with five Type I PN in the LMC exhibiting the same mean oxygen abundance as twelve LMC non-Type I PN (and LMC H II regions). Walton et al. (1991; see table 1 of Barlow 1991) found that the nitrogen abundance alone in the LMC Type I nebulae exceeded the LMC H II region C+N abundance by 0.2–0.5 dex, while the C+N abundances of the Type I PN were 0.35–1.05 dex larger than those of LMC H II regions. They concluded that the enhanced nitrogen in the Type I PN of the LMC had been largely produced by CN-cycle envelope burning (see Iben & Renzini 1983) of primary carbon brought up to the base of the hydrogen-burning layer by the third dredge-up.

We therefore propose a single criterion clearly to separate Type I nebulae from other PN: Type I PN are those objects that have experienced envelope-burning conversion to nitrogen of dredged-up primary carbon. Since CN- or CNO-cycle processed material brought to the surface layers by the first or second dredge-ups cannot increase the summed C+N+O abundance, and since oxygen abundances are not found to be significantly altered anyway, any PN whose nitrogen abundance exceeds its progenitor main-sequence star's C+N abundance (the latter is assumed to be the same as the C+N abundance of H II regions in the same galaxy) *must* have experienced envelope burning into nitrogen of dredged-up carbon.

The upper limit to the N/O ratio following the first and second dredge-ups can be taken to be equal to the original (C+N)/O ratio. The solar abundances listed in Table 14 give (C+N)/O = 0.59; the mean galactic H II region abundances of Dufour (1984; also listed in Table 14) give (C+N)/O = 0.65; the Orion Nebula abundances of Rubin et al. (1991) give (C+N)/O = 1.0; while the Orion Nebula abundances of Baldwin et al. (1991) give (C+N)/O = 0.78. We adopt the criterion that any galactic PN whose N/O ratio exceeds 0.8 is a Type I planetary nebula. Such a PN *must* have undergone envelope-burning conversion to nitrogen of primary carbon raised to the hydrogen envelope by the third dredge-up. Our Type I criterion does not involve the helium abundance.

7.2 Helium abundances

For a sample of 43 non-Type I PN, we find a mean He/H ratio of 0.112 ± 0.015 by number. By mass, their mean $Y = 0.305 \pm 0.041$. This can be compared to the mean He/H ratio for galactic H II regions, 0.100 ± 0.005 by number or 0.283 ± 0.014 by mass (see Dufour 1984). The difference between the He/H ratios for H II regions and PN is indicative of the amount of stellar processing of hydrogen to helium that has occurred in the progenitor star. The nominal excess of helium found in non-Type I PN over that in H II regions is $\Delta Y = 0.022$. Owing to the sensitivity of the helium abundances to the collisional corrections, this number must be considered provisional at present. From Becker & Iben (1980; their equation 7), the predicted surface He/H number ratio after the first dredge-up (for an initial He/H ratio of 0.100) is 0.107 for a 1.0-$M_\odot$ initial mass star, 0.105 for a 1.5-$M_\odot$ star, and 0.101 for a 2.5-$M_\odot$ star. Following the third dredge-up, the surface He/H ratios predicted for the same three models (from fig. 10 of Becker & Iben 1980) are 0.108, 0.110 and 0.112. Since their extrapolated models did not predict significant enhancements of carbon (and therefore of helium too) by the third dredge-up for initial stellar masses less than $\sim 2\ M_\odot$, and since our results for galactic PN and the results of Walton et al. (1991) and Barlow (1991) for Magellanic Cloud PN indicate that real stars undoubtedly do achieve significant carbon dredge-up for initial masses significantly lower than $2.0\ M_\odot$, our observed mean He/H number ratio of 0.112 for non-Type I PN is likely to be consistent with surface helium enhancement by the first and third dredge-ups in stars with initial masses less than $\sim 2.5\ M_\odot$.

The mean He/H abundance found for the 11 Type I PN in our sample is 0.129 ± 0.037 by number, or $Y = 0.338$ by mass. Thus the mean excess of helium found in Type I PN over H II regions is $\Delta Y = 0.055$ by mass. However, there is a very wide range in the He/H ratios found for the Type I PN. The two extreme cases are He 2-111 (He/H = 0.219) and NGC 5315 [He/H = 0.091; although swamping by the very strong stellar He II emission feature of its WC4 central star (Méndez 1991) could have prevented the detection of any nebular He II emission], while for the remainder the He/H ratio spans the range 0.095–0.144. The models of Becker & Iben (1980) for a solar abundance 5-$M_\odot$ initial mass star predict a negligible enhancement of helium after the first dredge-up, a He/H surface abundance enhancement from 0.100 to 0.113 after the second dredge-up, and a final surface He/H enhancement to 0.158 after the third dredge-up. Thus the observed He/H ratios for Type I PN appear to be consistent with those expected at the surfaces of relatively massive AGB stars after the third dredge-up. The spectra of Type I PN often simultaneously exhibit strong lines from high-ionization species (e.g. He II and [Ne V]) and strong lines from low-ionization species (e.g. [O II], [O I] and [N I]). The presence of substantial amounts of neutral material may be

indicated, and, if the helium neutral fraction differs from that of hydrogen, the $(He^+ + He^{2+})/H^+$ ratios derived from the observed ionic emission lines may not yield the true He/H abundance ratios in the nebulae. Subject to this caveat, Type I PN could be significant producers of helium for the ISM.

7.3 Oxygen abundances

Previous studies of PN abundances have found evidence for oxygen depletion in PN, particularly for the Type I nebulae (Peimbert 1985; Torres-Peimbert 1984, drawing upon the data set of PTP83; and more recently Kaler et al. 1990, for galactic PN, and Henry, Liebert & Boroson 1989, for Magellanic Cloud PN). These authors found an inverse trend between the N/O and O/H ratios. This was interpreted as indicating that the ON cycle occurred significantly in the progenitor star, whereby initial O was converted into secondary N. Products of the CNO cycle have been predicted to alter the surface abundances of sufficiently massive PN progenitor stars experiencing the second dredge-up, at the foot of the AGB, but only small oxygen depletions, of the order of 10 per cent, have been predicted for stars with initial solar abundances (Becker & Iben 1979). Fig. 5 plots log(N/O) versus log(O/H) for our sample of PN. No significant decrease in O/H is seen for higher N/O ratios, with the Type I PN having the same mean O/H ratio as the non-Type I PN. For 43 non-Type I PN, the mean oxygen abundance is found to be $O/H = (4.93 \pm 2.22) \times 10^{-4}$ by number. For 11 Type I PN in the sample, the mean $O/H = (4.42 \pm 1.44) \times 10^{-4}$, the same as the average found for non-Type I PN, within the errors, although nominally giving a 10 per cent depletion of oxygen relative to the non-Type I nebulae, consistent with the very modest surface oxygen depletions predicted by Becker & Iben (1979) in the aftermath of the second dredge-up. The Type I and non-Type I oxygen abundances lie in a reasonably narrow range and the observed spread in oxygen abundances is likely to be due to a range of metallicities of the original star-forming regions. Errors in electron temperature would also contribute to the spread in O/H ratios, although we have eliminated objects with very uncertain [O III] 4363-Å fluxes.

Another way to look for ON-cycle processing is via a negative correlation between O/H and He/H ratios, because, if the temperature is high enough for the ON cycle to occur, a further enhancement of helium should also occur. Fig. 6 plots log(O/H) versus log(He/H); no correlation is seen. Hence we see no evidence for significant ON-cycle processing in our sample, even for the Type I PN. We believe that past studies that found this trend may have included objects with uncertain abundances due to unreliable electron temperatures, or have underestimated unseen (high) stages of ionization.

Let us examine in detail some of the previous claims for the presence of oxygen depletion, where all these studies relied only on optical spectra for their abundance analyses. Fig. 2 of PTP83 plots log(N/O) versus log(O/H) for 12 Type I PN, and an inverse trend is apparent. However, this trend is weighted entirely by three objects: PB 6, Hu 1-2 and Me 2-2, all with apparent low oxygen abundances and high N/O ratios. For all three objects, the oxygen abundance was flagged with a colon (see table 1 of PTP83); for PB 6, $O/H = 2.40 \times 10^{-4}$ (by number); for Hu 1-2, $O/H = 1.66 \times 10^{-4}$; and for Me 2-2, $O/H = 2.00 \times 10^{-4}$. For PB 6, the oxygen abundance was derived using the optical spectra of TPP77. More recently, Kaler et al. (1991) studied PB 6, using UV and optical spectroscopy, and derived $O/H = (6.3\text{–}7.9) \times 10^{-4}$, within the range found for the

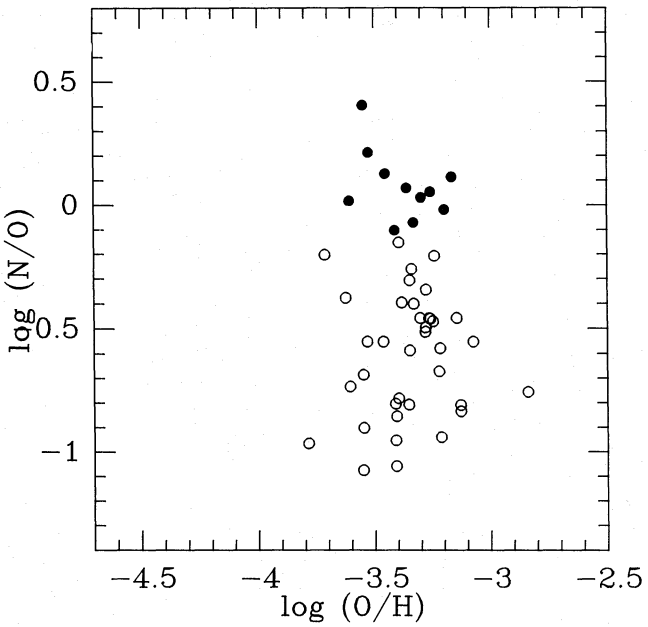

Figure 5. Log(N/O) versus log(O/H). No trend of decreasing oxygen abundance with increasing N/O ratio is seen, hence no destruction of oxygen is found as predicted by Becker & Iben (1980) for the second dredge-up phase, even for the Type I PN. The mean oxygen abundance for the 48 non-Type I PN in this sample is $(4.91 \pm 2.15) \times 10^{-4}$, and for the six Type I PN is $(4.08 \pm 1.47) \times 10^{-4}$.

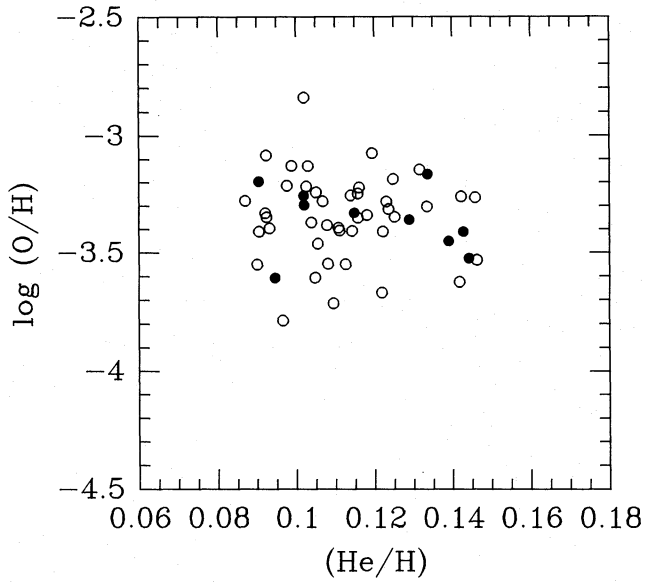

Figure 6. Log(O/H) versus log(He/H). No trend of increased helium abundance with decreasing oxygen abundance is found. A trend may be expected if the products of the second dredge-up significantly affect the surface abundances of the progenitor star whilst it is on the AGB.

'average' PN found in this sample. PTP83 adopted the fluxes for Hu 1-2 from Aller & Czyzak (1983), who found Hu 1-2 a difficult object to fit with their photoionization models, as it shows such a large range of excitation and ionization. The UV spectra reveal lines of C IV and O IV; in addition the C IV λ4658 − 5 recombination line is seen, so O^{4+}, as well as C^{4+}, needs to be accounted for. Using the fluxes listed in tables 5 and 6 of AC83, we derive $O/H = 4.53 \times 10^{-4}$, where the ICF for oxygen is estimated to be 1.23, and corrects for the presence of O^{4+}. Considering Me 2-2, a closer examination of its abundances indicates that it is likely to be an intermediate population or low-metallicity object. From the line intensities of Barker (1978), we derive $O/H = 2.46 \times 10^{-4}$ and $Ne/H = 5.60 \times 10^{-5}$. The optically thick distance derived for Me 2-2 by Kingsburgh & Barlow (1992) of 9 kpc, and the high heliocentric radial velocity given by Schneider et al. (1983; -152 km s^{-1}) also point to it being a distant metal-poor object.

More recently, Kaler, Shaw & Kwitter (1990) have also claimed to see an inverse trend between N/O and O/H ratios. Their study examined large, extended PN, where very few had reliable [O III] 4363-Å fluxes, and hence the electron temperatures and ultimately the abundances tended to be uncertain. Electron temperatures were frequently estimated based on the He II 4686-Å line strength. Also, some of their O/H ratios were derived using predicted O^+/H^+ ratios based on [S II] or [O I] line strengths, for the cases where [O II] 3727 Å was not observed. Within the errors of the $I(4686)$ versus t(O III) relation, the temperature adopted to derive abundances can be dropped enough to give abundances that lie within the 'average' range found here. Only one object in their sample, M 3-2, had a good λ4363 flux and a low oxygen abundance, $O/H = 1.2 \times 10^{-4}$. This object had a rather high ratio of t(O III)/t(N II) = 1.6, yet the O^+/H^+ and O^{++}/H^+ ratios are similar. Also, it has a high heliocentric radial velocity (84 km s^{-1}; Schneider et al. 1983), possibly pointing to intermediate population status. Further study of this object would be worthwhile.

Finally, Henry, Liebert & Boroson (1989) found an inverse trend between N/O and O/H for both LMC and SMC PN, using abundances derived from optical lines and a traditional ICF scheme. However, based on an extensive set of optical *and* ultraviolet spectra of a sample of 20 LMC and 20 SMC PN, Walton et al. (1991) and Barlow (1991) found no such trend. The underestimation of high unseen stages of ionization of oxygen by the earlier ICF schemes based on optical spectra alone appears to have been an important factor leading to low oxygen abundance estimates for some high-excitation nebulae in the past.

7.4 Nitrogen abundances

There has been much discussion in the literature as to whether the nitrogen in both Type I and non-Type I PN is enhanced by the CN cycle alone, or by the CN cycle and ON cycle together. Monk, Barlow & Clegg (1988) showed that the CN cycle, via the first dredge-up, was responsible for the enhancement of nitrogen, relative to the initial H II region values, both in Magellanic Cloud and galactic non-Type I PN. As noted above, Henry et al. (1989) and Henry (1990) argued that, for Type I PN, nitrogen was produced at the expense of O in the ON cycle, based on a negative correlation between N/O and O/H. Dufour (1991) argued for both CN and ON cycling being responsible for nitrogen production in PN. Our discussion of oxygen abundances, in Section 7.3, ruled out significant nitrogen production via the ON cycle at the time of the second dredge-up, as no decrease in oxygen abundance is found with increasing nitrogen abundance for our sample, even for the Type I PN. Products of the CN cycle may be brought to the surface by the first dredge-up, or following the third dredge-up, when CN burning of dredged-up carbon at the bottom of the hydrogen convective envelope can occur for sufficiently massive stars. In order to ascertain the relative importance of these two processes, we compare here the nitrogen abundances of non-Type I PN, and of Type I PN, with the total carbon + nitrogen abundances found for H II regions (Table 14). In order to obtain the mean N/H number ratio of $(1.40 \pm 0.88) \times 10^{-4}$ found for non-Type I PN, 36 per cent of the carbon originally present has to be converted to nitrogen. This value is consistent with the fraction predicted for the first dredge-up phase in the solar metallicity models of Becker & Iben (1980), for which it was predicted that about one-third of the initial carbon present would be converted to nitrogen. Thus for non-Type I PN, the nitrogen abundances are consistent with those predicted from the first dredge-up. For the Type I PN, however, even if all the initial carbon is converted to nitrogen, the maximum possible N/H ratio is 3.25×10^{-4} by number (assuming the initial carbon and nitrogen abundances to be the same as the galactic H II region abundances of Dufour 1984; see also Table 14), roughly a factor of 2 smaller than the N/H ratio found for the average Type I PN, for which $N/H = (5.29 \pm 1.81) \times 10^{-4}$. Since we found no evidence for significant oxygen depletion attributable to the ON cycle (Section 7.3), we noted in Section 7.1 that this implies that envelope burning of dredged-up carbon into nitrogen occurred in the progenitor AGB stars of these objects. Becker & Iben (1980) suggested that CN cycling of primary carbon at the base of the hydrogen envelope becomes important for stars of initial mass $\gtrsim 4$ M$_\odot$, consistent with the assumption that the Type I PN trace the high-mass end of the PN progenitor star mass distribution. Other evidence supporting the occurrence of envelope burning has come from the discovery of enhanced lithium abundances in luminous O-rich SMC AGB stars (Smith & Lambert 1989; Plez, Smith & Lambert 1993).

Henry (1990) found that nitrogen varies in 'lockstep' with oxygen in H II regions; hence for H II regions the nitrogen abundance indicates the metallicity of the star-forming region. The N/H ratios of PN can then be compared to N/H ratios of H II regions, for a given metallicity, in order to establish nitrogen yields into the ISM.

7.5 Carbon abundances

Fig. 7 plots log[(C + N + O)/H] versus log(C/H). There is a trend of increasing C + N + O with increasing C/H, which is in agreement with the scenario of carbon produced via the triple-α process being brought to the surface by the third dredge-up. From the mean abundances listed in Table 14, the average increase in the total C + N + O abundance over the H II region value is 0.19 dex for both the non-Type I PN and for the Type I PN (see Table 14), while the increase in the total C + N abundance over the H II value is 0.38 dex for the

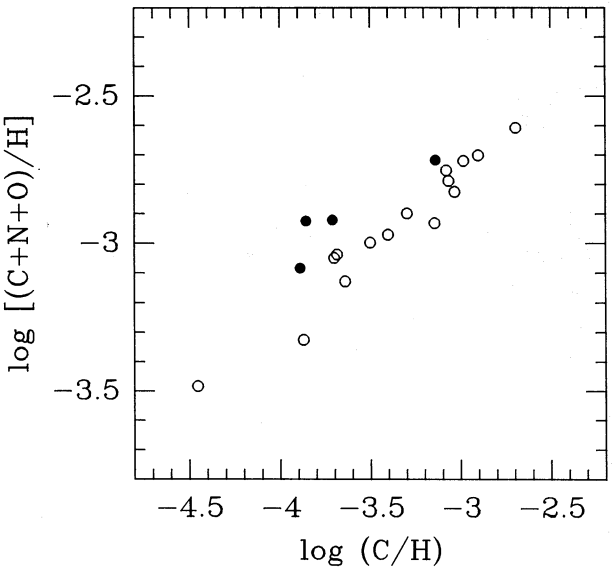

Figure 7. Log[(C + N + O)/H] versus log(C/H). A positive correlation between (C + N + O)/H versus C/H is seen. This is consistent with the prediction that carbon is produced via triple-α burning and is subsequently brought to the surface of the AGB star during the third dredge-up phase.

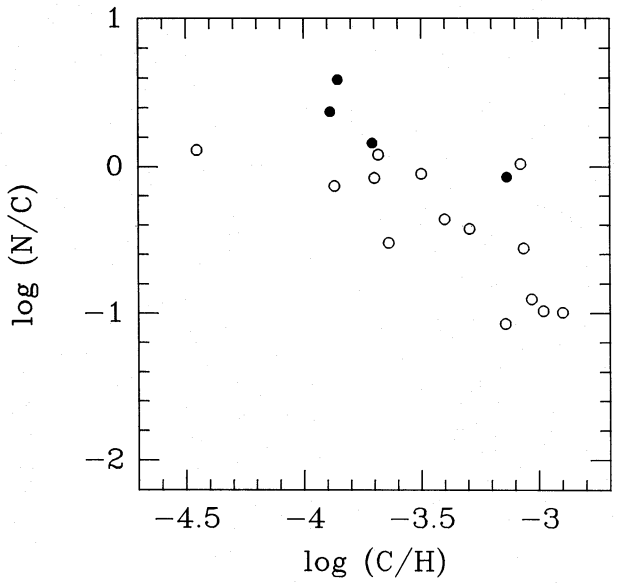

Figure 8. Log(N/C) versus log(C/H). An inverse trend is found, also consistent with carbon production being dominated by the third dredge-up.

non-Type I PN and 0.41 dex for the Type I PN. Almost all PN appear to have undergone the third dredge-up phase, but only the relatively massive progenitors of the Type I PN had high enough temperatures at the base of their hydrogen convective envelopes for envelope burning to occur at a significant level.

Fig. 8 presents log(N/C) versus log(C/H) for the 20 objects in this sample. In this figure, an inverse trend is seen, also arising from the increased carbon abundance produced by the third dredge-up.

Fig. 9 plots log(C/O) versus log(O/H) for the 20 PN for which we have derived carbon abundances. We find that eight of the 20 objects have C/O > 1 and 12 objects have C/O < 1 (NGC 2440 is not included). Therefore, in our sample, ~ 40 per cent of PN are carbon-rich, somewhat lower than the 62 per cent found by Zuckerman & Aller (1986; hereafter ZA86) for a sample of 68 galactic PN. However, ZA86 included nine objects for which the C II 4267-Å line was used to derive carbon abundances and this line is known to give systematically higher abundances than the collisionally excited C III] λ1909 line (see Rola & Stasińska 1994, and the discussion in Section 5.2). If we re-examine the sample of ZA86, and exclude the objects where the λ4267 line was used, the percentage of carbon-rich PN drops. The number of their objects with C/O > 1 is then 27, where, in addition to excluding objects for which the λ4267 line was used, we have excluded CRL 618 (as it is a proto-PN) and K 648 (as it is a halo object), and included objects that have the unidentified IR bands (arising from aromatic hydrocarbons) in their spectra. The revised number of their objects with C/O < 1 is 26, where we have again excluded PN for which the λ4267 line was used and have also excluded M 1-92 (as it is a proto-PN) and included objects where the 9.7-μm silicate feature is observed and for which only the limiting ratio of C/O < 1 can be given (He 2-108, He 2-138, Tc 1, Vy 2-2). Three objects with

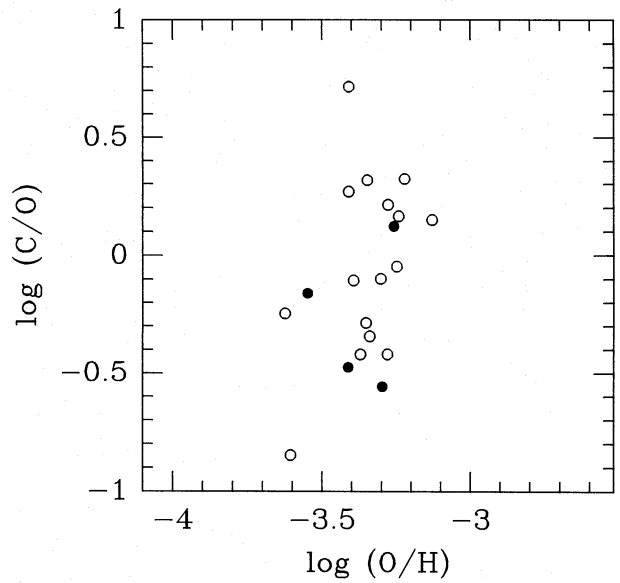

Figure 9. Log(C/O) versus log(O/H). A fraction of 40 per cent carbon-rich PN is found for this sample of 20 objects.

C/O = 1 have not been included in either group. Thus the percentage ratio of C-rich PN reduces to 46 per cent for the ZA86 sample, consistent with the 40 per cent found in our sample. Rola & Stasińska (1994) have recently rederived C/O ratios for 85 PN, using observational data published in the literature, and found that 35 per cent of the sample was carbon rich (C/O > 1). (Their re-analysis of the ZA86 sample yielded 45 per cent as being carbon-rich, in agreement with our estimate above.)

7.6 Neon abundances

Henry (1989) investigated the relation between neon and oxygen abundances for a sample of 171 PN, where he used line fluxes from the literature for PN in our own Galaxy (disc and Halo), and in the SMC, LMC and M 31, and re-derived oxygen and neon abundances. He found a 'lockstep' relation between neon and oxygen (independent of host galaxy); the slope of the relation between log(Ne/H) and log(O/H) being essentially unity. Henry found that neon and oxygen are also related in H II regions, again with a slope of unity. Kaler (1978a) argues that a relation between neon and oxygen could result from ionization effects; however, Henry (1989) investigated this possibility and did not find the effect to be significant. For PN, both neon and oxygen indicate the metallicity of the ISM at the time of formation of the PN progenitor star, since neither is created or destroyed by nucleosynthesis reactions during the lifetime of the progenitor star. Fig. 10 plots log(Ne/H) versus log(O/H) for our sample. The Type I PN do not appear to be separated from the rest of the sample, although the most extreme Type I PN, He 2-111, does have the highest Ne/O ratio (=0.50). A dashed line of slope unity is also plotted in Fig. 10, and the distribution of points is found to be consistent with this slope. The mean Ne/O ratio by number for the 48 non-Type I objects is 0.25 ± 0.17, which can be compared to the value of 0.18 ± 0.09 found by Henry (1989) for the AC83 and AK87 galactic samples. In our analysis, we have used recent 10-level collision strength calculations made by Dr K. Butler (private communication) for Ne^{2+}; relative to the older collision strengths, the new values increased the Ne^{2+}/H^+ ratios, and the Ne/H ratios, by ~10–15 per cent.

From the results of Becker & Iben (1979), the possibility exists that surface enhancements of ^{22}Ne might occur in the more massive AGB stars, via helium capture by fresh ^{14}N in the intershell region during the AGB thermal pulse phase. However, the mean Ne/H abundance for the Type I PN in our sample (Table 14) is the same as that found for the lower mass non-Type I objects. Further, if the surface enhancement of neon were significant, one would expect a correlation between the Ne and the C+N abundances of PN. Fig. 11 plots log[(C+N+O)/H] versus log(Ne/H). No significant slope is found. Hence there is no evidence for significant enhancements of neon in Type I PN.

7.7 Argon abundances

Fig. 12 plots log(N/O) versus log(Ar/H). There is considerable observational scatter in the derived argon abundances, and, neglecting an outlying Type I point, no significant correlation is found. De Freitas Pacheco et al. (1992) did find a correlation in their sample, the argon abundance seeming to be particularly enhanced in the Type I PN. Since the argon abundance is not expected to be modified by nucleosynthesis, de Freitas Pacheco et al. (1992) suggested that the correlation between Ar/H and N/O could result from the objects that have high N/O ratios also being formed more recently out of the enriched ISM, so that the Ar/H ratio traces the metallicity of the star-forming region. However, other elements that more reliably trace the metallicity of the star-forming region, oxygen and neon, show no enhancement in the Type I PN compared with the non-Type I PN. Possibly, the trend found by de Freitas Pacheco et al. arose from the ICF that they adopted for argon. Fig. 13 plots our log[ICF (Argon)] versus log(ArH), and, if we again neglect a couple of outlying points, reveals no trend, indicating that no systematic effects are present.

From Table 14, it can be seen that the mean argon abundances derived for the Type I PN and non-Type I PN in our sample are the same. The overall mean argon abundance of 6.39 ± 0.30 is in good agreement with the value of 6.42 listed by Dufour (1984) for a sample of galactic H II regions, and with the values of 6.35 and 6.32 derived for the Orion Nebula by Rubin et al. (1991) and Baldwin et al. (1991), respectively.

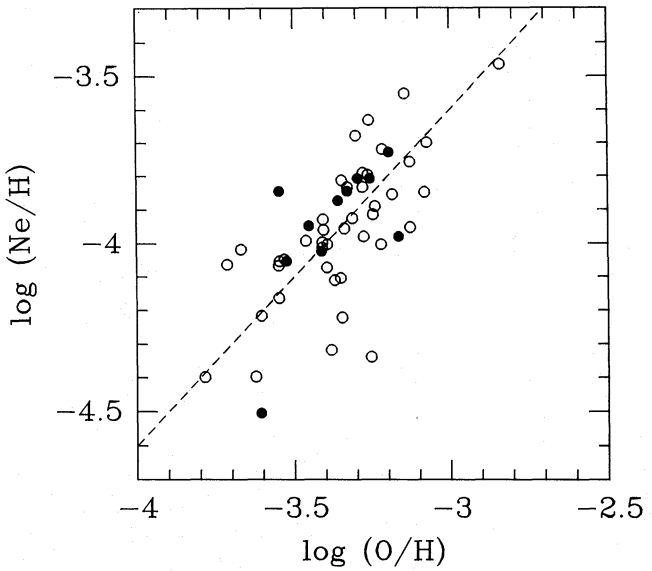

Figure 10. Log(Ne/H) versus log(O/H). The dashed line has a slope of 1, and the distribution of points is consistent with this line. Note that the Type I PN shows no signs of enhanced neon.

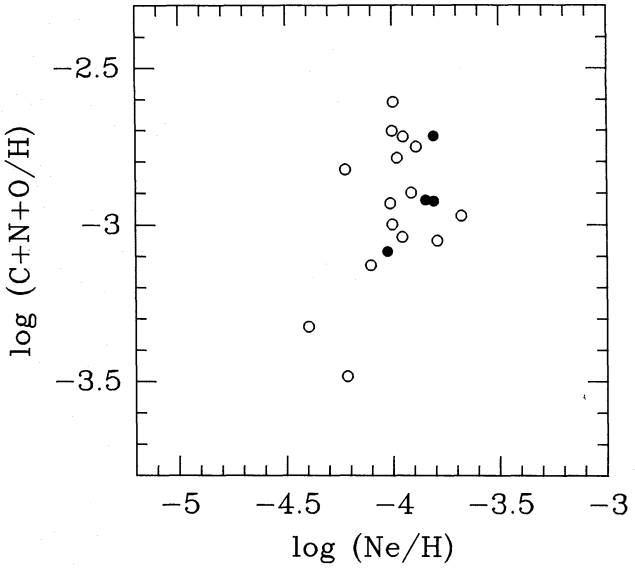

Figure 11. Log[(C+N+O)/H] versus log(Ne/H). No correlation between neon and carbon is seen, indicating that neon production has not occurred in the progenitor star to a significant extent.

7.8 Sulphur abundances

The abundances for sulphur must be considered the most uncertain amongst the elements considered here. It is expected that in most PN sulphur will be found mainly in the 3- and 4-times ionized stages, but only the singly and doubly ionized stages are observed in optical spectra. The S^{2+} abundance is usually derived from the [S III] 6312-Å line, which is an auroral transition and hence extremely temperature sensitive. In the current study, we have tried to adopt a temperature for the S^{2+} zone that will be more representative for that zone than the [N II] or [O III] electron temperature (Section 4); however, this attempt is clearly not satisfactory. It is desirable to obtain spectra covering [S III] 9069 Å as well as [S III] 6312 Å in order to derive directly the temperature appropriate for the S^{2+} zone and thus obtain accurate S^{2+} abundances. More infrared observations of [S IV] 10.5-μm line fluxes are also desirable.

Köppen et al. (1991) found a trend of increasing S with increasing O; however, we see no such trend (Fig. 14). They adopted a different ICF for sulphur, which presumably is responsible for the differences seen between the samples. We made use of Fig. 15 for our adopted ICFs (see Appendix).

Despite the uncertainties in our sulphur abundances, we find good agreement between the S abundances derived for the Type I PN and non-Type I PN (Table 14). Our overall mean sulphur abundance of 6.92 ± 0.30 can be compared with the solar value of 7.24 (Grevesse & Anders 1989) and the Orion Nebula values of 6.93 and 7.12 derived by Rubin et al. (1991) and Baldwin et al. (1991), respectively.

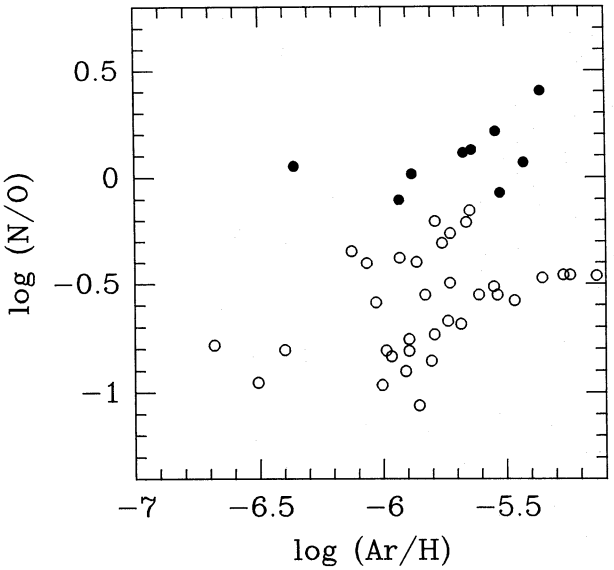

Figure 12. Log(N/O) versus log(Ar/H). A slight trend of increasing N/O ratio with increasing argon abundance is seen, particularly for the Type I PN. de Freitas Pacheco et al. (1992) have suggested that the trend results from the progenitor stars for Type I PN forming from a relatively enriched ISM; however, as no trend for increased neon or oxygen abundances is found for the Type I PN (see Fig. 10), the trend is most likely due to errors in derived argon abundances, possibly through an incorrect ICF (Fig. 13).

8 CONCLUSIONS

For this sample of 68 southern galactic PN, we find 11 objects that can be classified as Type I. We have introduced a physically based criterion for separating Type I PN from non-Type I PN: the Type Is have nitrogen abundances in excess of those that could be produced via complete conversion of original carbon into nitrogen. No evidence for oxygen depletion in these objects was found and hence the Type I PN necessarily have undergone convective envelope burning during the third dredge-up phase. This process is predicted to occur in the more massive ($\gtrsim 2.5$ $M_\odot$) progenitor stars, whose remnants would therefore be the Type I PN.

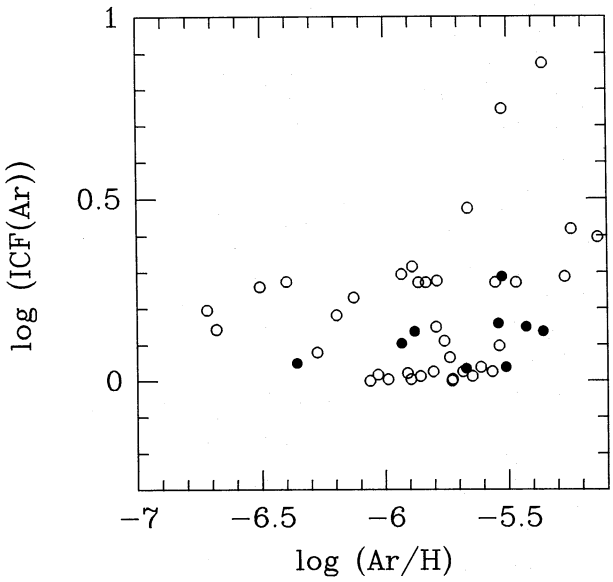

Figure 13. Log[ICF(Ar)] versus log(Ar/H). A slight trend of increasing argon abundance with increasing ICF is seen, indicating that the argon abundances may be overestimated for ON with a high ICF.

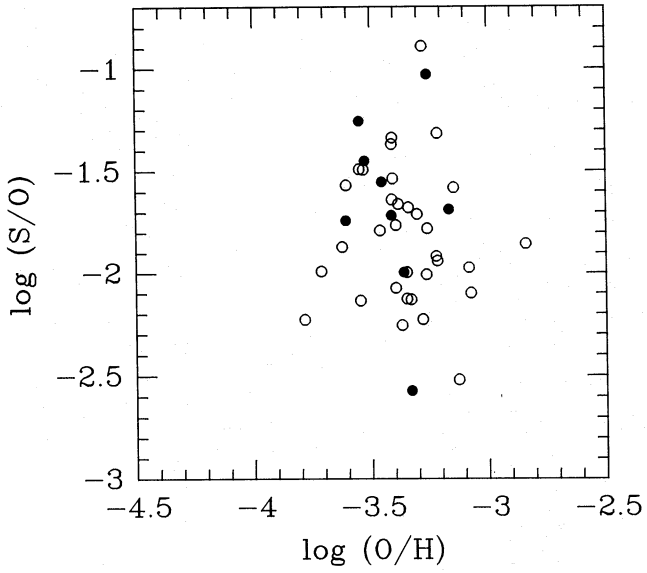

Figure 14. Log(S/O) versus log(O/H). No trend between sulphur and oxygen abundances is seen. The derivation of the total sulphur abundance using lines from optical spectra only is quite uncertain, as only trace stages of ionization are observed.

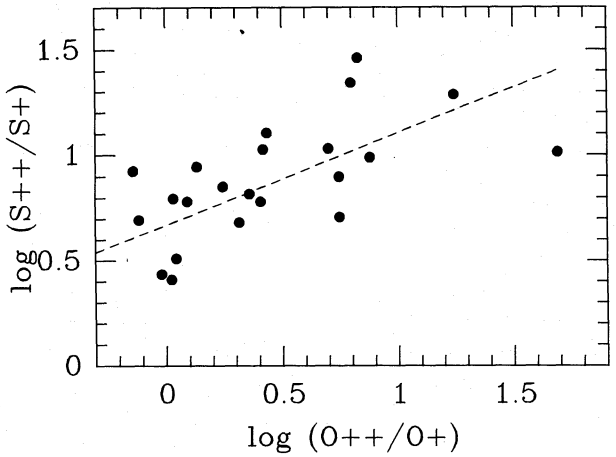

Figure 15. Log(S^{2+}/S^{+}) versus log(O^{2+}/O^{+}). A least-squares fit yields the following relation: $S^{2+}/S^{+} = 4.677 + (O^{2+}/O^{+})^{0.433}$, the relation is used in order to estimate S^{2+} abundances when only S^{+} is observed.

The 'average' abundances by number for non-Type I PN are as follows:

$He/H = 0.112 \pm 0.015$, $O/H = (4.93 \pm 2.22) \times 10^{-4}$,

$N/H = (1.40 \pm 0.88) \times 10^{-4}$, $C/H = (6.48 \pm 5.35) \times 10^{-4}$,

$Ne/H = (1.25 \pm 0.63) \times 10^{-4}$, $Ar/H = (2.42 \pm 2.28) \times 10^{-6}$,

$S/H = (8.08 \pm 6.19) \times 10^{-6}$.

For Type I PN, the average helium abundance is increased by a factor of 1.2 over non-Type I PN, the average nitrogen abundance is increased by a factor of 3.8, the average carbon abundance is decreased by a factor of 2.2, and the average oxygen, neon, argon and sulphur abundances are the same within the errors as found for the non-Type I PN.

In our sample, we find that helium abundances in the non-Type I PN are consistent with the predictions of Becker & Iben (1980) for the first and third dredge-up phases. We find that the conversion of about one-third of the initial carbon into nitrogen following the first dredge-up phase is sufficient to account for the increase in nitrogen abundances of non-Type I PN over H II regions. For the Type I PN, no evidence for depletion of oxygen compared to non-Type I PN is found, and hence the ON cycle which operates during the second dredge-up does not significantly affect the surface abundances of the progenitor star. The high nitrogen abundances found in Type I PN require nitrogen production via the CN cycle during convective envelope burning following the third dredge-up phase, a process that is predicted to occur for sufficiently massive stars (Becker & Iben 1980). Total C+N+O abundances are found to correlate with C/H for the combined non-Type I and Type I sample; the carbon abundance is enhanced by He-burning processed material brought to the surface by the third dredge-up.

REFERENCES

Aaquist O. B., Kwok S., 1990, A&AS, 84, 229

Acker A., Chopinet M., Marcout J., Ochsenbein F., Roques J. M., 1982, Catalogue of the Central Stars of Planetary Nebulae. Publ. Speciale du C.D.S. No. 3

Acker A., Koppen J., Stenholm B., Jasniewicz G., 1989, A&AS, 80, 201

Acker A., Ochsenbein F., Stenholm B., Tylenda R., Marcout J., Schohn C., 1992, Strasbourg–ESO Catalogue of Galactic Planetary Nebulae. ESO, Munich

Aggarwal K. M., 1983, ApJS, 52, 387

Allen D., 1973, The Observatory, 93, 28

Aller L. H., Czyzak S. J., 1979, A&SS, 62, 397 (AC79)

Aller L. H., Czyzak S. J., 1983, ApJS, 51, 211 (AC83)

Aller L. H., Keyes C. D., 1987, ApJS, 65, 405, (AK87)

Aller L. H., Keyes C. D., Czyzak S. J., 1981, ApJ, 250, 595

Baldwin J. A., Ferland G. J., Martin P. G., Corbin M. R., Cota S. A., Peterson B. M., Slettebak A., 1991, ApJ, 374, 580

Barker T., 1978, ApJ, 219, 914 (Ba78)

Barker T., 1980, ApJ, 240, 99

Barker T., 1983, ApJ, 267, 630

Barlow M. J., 1991, in Haynes R., Milne D., eds, IAU Symp., The Magellanic Clouds. Kluwer, Dordrecht, p. 291

Becker S. A., Iben I., 1980, ApJ, 237, 111

Bohlin R. C., Grillmair C. J., 1988, ApJS, 66, 209

Borkowski K. J., Harrington J. P., Tsvetanov Z., Clegg R. E. S., 1993, ApJ, 415, L47

Brocklehurst M., 1971, MNRAS, 153, 471

Butler K., Zeippen C. J., 1989, A&A, 208, 337

Burstein D., Heiles C., 1982, AJ, 87, 1165

Carrasco L., Serrano A., Costero R., 1983, Rev. Mex. Astron. Astrofis., 8, 187

Caswell J. L., Haynes R. F., 1987, A&A, 171, 261

Chu Y. H., Jacoby G. H., Arendt R., 1987, ApJS, 64, 529

Clavel J., Gilmozzi R., Preito A., 1986, *IUE* ESA Newsletter No. 26, p. 65

Clegg R. E. S., 1987, MNRAS, 221, 31P

Clegg R. E. S., 1989, in Torres-Peimbert S., ed., IAU Symp. 131, Planetary Nebulae. Kluwer, Dordrecht, p. 139

Clegg R. E. S., Harrington J. P., Barlow M. J., Walsh J. R., 1987, ApJ, 314, 551

Cohen M., Barlow M. J., 1980, ApJ, 238, 585

Cohen M., Hudson H. S., O'Dell S. L., Stein W. A., 1977, MNRAS, 181, 233

de Freitas Pacheco J. A., Maciel W. J., Costa R. D. D., Barbuy B., 1991, A&A, 250, 159

de Freitas Pacheco J. A., Maciel W. J., Costa R. D. D., 1992, A&A, 261, 579

Dufour R. J., 1984, in van der Bergh S., de Boer K. S., eds, IAU Symp. 108, Structure and Evolution of the Magellanic clouds. Kluwer, Dordrecht, p. 353

Dufour R. J., 1991, PASP, 103, 857

Dufton P. L., Berrington K. A., Burke P. G., Kingston A. E., 1978, A&A, 62, 111

Gau J. N., Henry R. J. W., 1977, Phys. Rev. A, 16, 986

Giles K., 1981, MNRAS, 195, 63P

Grevesse N., Anders E., 1989, in Waddington C. J., ed., AIP Conf. Proc. 183, Cosmic Abundances of Matter. Am. Inst. Phys., New York, p. 1

Grevesse N., Lambert D. L., Sauval A. J., van Dishoeck E. F., Farmer C. B., Norton R. H., 1990, A&A, 232, 225

Grevesse N., Lambert D. L., Sauval A. J., van Dishoeck E. F., Farmer C. B., Norton R. H., 1991, A&A, 242, 488

Gutiérrez-Moreno A., Moreno H., Cortés G., 1985, PASP, 97, 397

Gutiérrez-Moreno A., Moreno H., Cortés G., 1987, Rev. Mex. Astron. Astrofis., 14, 344

Harrington J. P., Feibelman W. A., 1984, ApJ, 277, 716

Harrington J. P., Seaton M. J., Adams S. A., Lutz J. H., 1982, MNRAS, 199, 517

Harrington J. P., Borkowski K. J., Blair W. P., Bregman J., 1993, in Weinberger R., Acker A., eds, Proc. IAU Symp. 155, Planetary Nebulae. Kluwer, Dordrecht, p. 386

Hayes M. A., Nussbaumer H., 1984, A&A, 134, 194

Heap S. R., 1993, in Weinberger R., Acker A., eds, IAU Symp. 155, Planetary Nebulae. Kluwer, Dordrecht, p. 23

Henry R. B. C., 1989, MNRAS, 241, 453

Henry R. B. C., 1990, ApJ, 356, 229

Henry R. B. C., Liebert J., Boroson T. A., 1989, ApJ, 339, 872

Howarth I. D., 1983, MNRAS, 203, 301
Howarth I. D., Murray J., 1988, SERC Starlink User Note No. 50
Hummer D. G., Storey P. J., 1987, MNRAS, 224, 801
Iben I., Jr, Renzini A., 1983, ARA&A, 21, 271
Jacoby G. H., 1979, PASP, 91, 754
Jacoby G. H., Ford H. C., 1983, ApJ, 266, 298
Johnson C. T., Kingston A. E., 1990, J. Phys. B, 23, 3393
Jourdain de Muizon M., Preite Martinez A., Heydari-Malayeri M., 1987, in Preite Martinez A., ed., Planetary and Proto-Planetary Nebulae: from IRAS to ISO. Reidel, Dordrecht, p. 185
Jourdain de Muizon M., Cox P., Lequeux J., 1990, A&AS, 83, 337
Kaler J. B., 1978a, ApJ, 220, 807
Kaler J. B., 1978b, ApJ, 226, 947
Kaler J. B., 1983, ApJ, 271, 188
Kaler J. B., 1986a, ApJ, 308, 322
Kaler J. B., 1986b, ApJ, 308, 337
Kaler J. B., Shaw R., Feibelman W. A., Lutz J. H., 1989, ApJS, 70, 213
Kaler J. B., Shaw R., Kwitter K., 1990, ApJ, 359, 392
Kaler J. B., Shaw R., Feibelman W. A., Imhoff C. L., 1991, PASP, 103, 67
Kingsburgh R. L., Barlow M. J., 1992, MNRAS, 257, 317
Kingsburgh R. L., English J., 1992, MNRAS, 259, 635
Kohoutek L., 1987, Ap&SS, 131, 781
Köppen J., Acker A., Stenholm B., 1991, A&A, 248, 197
Lennon D. J., Burke V. M., 1991, MNRAS, 251, 628
Liebert J., Green R., Bond H. E., Holberg J. B., Wesemael F., Fleming T. A., Kidder K., 1989, ApJ, 346, 251
Liu X. W., Danziger J., 1993, MNRAS, 263, 256
Longmore A. J., 1977, MNRAS, 178, 251
López J. A., Falcón L. H., Ruiz M. T., Roth M., 1991, A&A, 241, 526
López J. A., Meaburn J., Palmer J. W., 1993a, ApJ, 415, L135
López J. A., Roth M., Tapia M., 1993b, A&A, 267, 194
Louise R., Macron A., Pascoli G., Maurice E., 1987, A&AS, 70, 201
Lutz J. H., 1984, ApJ, 279, 714
Meaburn J., Walsh J. R., 1989, A&A, 223, 277
Méndez R. H., 1991, in Michaud G., Tutukov A., eds, IAU Symp. 145, Evolution of Stars: The Photospheric Abundance Connection. Reidel, Dordrecht, p. 375
Mendoza C., 1983, in Flower D. R., ed., IAU Symp. 103, Planetary Nebulae. Reidel, Dordrecht, p. 143
Mendoza C., Zeippen C. J., 1982a, MNRAS, 198, 127
Mendoza C., Zeippen C. J., 1982b, MNRAS, 199, 1025
Mendoza C., Zeippen C. J., 1983, MNRAS, 202, 981
Milne D. K., 1982, MNRAS, 200, 51P
Milne D. K., Aller L. H., 1975, A&A, 38, 183
Milne D. K., Aller L. H., 1982, A&AS, 50, 209
Monk D. J., Barlow M. J., Clegg R. E. S., 1988, MNRAS, 234, 583
Nussbaumer H., Rusca C., 1979, A&A, 72, 129
Nussbaumer H., Storey P. J., 1978, A&A, 64, 139
Nussbaumer H., Storey P. J., 1979a, A&A, 71, L5
Nussbaumer H., Storey P. J., 1979b, A&A, 74, 244
Nussbaumer H., Storey P. J., 1981a, A&A, 96, 91
Nussbaumer H., Storey P. J., 1981b, A&A, 99, 177
Nussbaumer H., Storey P. J., 1982a, A&A, 109, 271
Nussbaumer H., Storey P. J., 1982b, A&A, 115, 205
O'Dell C. R., 1963, ApJ, 138, 293
O'Dell C. R., Miller C. O., 1992, ApJ, 390, 219
Oke J. B., 1974, ApJS, 27, 21
Osterbrock D. E., Wallace R. K., 1977, Astrophys. Lett., 19, 11
Peimbert M., 1967, ApJ, 150, 825
Peimbert M., 1985, Rev. Mex. Astron. Astrofis., 10, 125
Peimbert M., Serrano A., 1980, Rev. Mex. Astron. Astrofis., 5, 9
Peimbert M., Torres-Peimbert S., 1983, in Flower D. R., ed., IAU Symp. 103, Planetary Nebulae. Reidel, Dordrecht, p. 233
Peimbert M., Storey P. J., Torres-Peimbert S., 1993, ApJ, 414, 626
Perek L., Kohoutek L., 1967, Catalogue of Galactic Planetary Nebulae. Academia Publ. House of the Czechoslovak Academy of Sciences
Plez B., Smith V. V., Lambert D. L., 1993, ApJ, 418, 812
Pottasch S. R., Dennefeld M., Jing-er Mo, 1986, A&A, 155, 397
Pradhan A. K., 1976, MNRAS, 177, 31
Robinson L. B., Wampler E. J., 1972, PASP, 84, 161
Rola C., Stasińska G., 1994, A&A, 282, 199
Rubin R. H., Simpson J. P., Haas M. R., Erickson E. F., 1991, ApJ, 374, 564
Saraph H. E., Seton M. J., 1980, MNRAS, 193, 617
Schneider S. E., Terzian Y., Purgathofer A., Perinotto M., 1983, ApJS, 52, 399
Seaton M. J., 1978, MNRAS, 185, 5P
Seaton M. J., 1979, MNRAS, 187, 73P
Shaw R., Kaler J. B., 1989, ApJS, 69, 495
Shields G. A., Aller L. H., Keyes C. D., Czyzak S. J., 1981, ApJ, 248, 569 (SAKC)
Shortridge K., 1989, SERC Starlink User Note No. 86
Smith V. V., Lambert D. L., 1989, ApJ, 345, L75
Stanghellini L., Kaler J. B., 1989, ApJ, 343, 811
Stasinska G., 1978, A&A, 66, 257
Straede J., 1980, AAO Preprint No. 135
Talavera A., 1988, *IUE* ESA Newsletter No. 30
Tamura S., Shaw R. A., 1987, PASP, 99, 1264 (TS87)
Teays T. J., Garhart M. P., 1990, *IUE* NASA Newsletter No. 41, p. 94
Torres-Peimbert S., Peimbert M., 1977, Rev. Mex. Astron. Astrofis., 2, 181 (TPP77)
Torres-Peimbert S., 1984, in Chiosi C., Renzini A., eds, Stellar Nucleosynthesis. Reidel, Dordrecht, p. 3
Tylenda R., Acker A., Gleizes F., Stenholm B., 1989, A&A, 213, 520
Viadana L., de Freitas Pacheco J. A., 1985, Rev. Bras. Fis., 15, 70
Walton N. A., Barlow M. J., Monk D. J., Clegg R. E. S., 1991, in Haynes R., Milne D., eds, IAU Symp. 148, The Magellanic Clouds. Kluwer, Dordrecht, p. 34
Walton N. A., Barlow M. J., Clegg R. E. S., 1993, in Weinberger R., Acker A., eds, IAU Symp. 155, Planetary Nebulae. Kluwer, Dordrecht, p. 581
Webster B. L., 1969, MNRAS, 143, 79
Webster B. L., 1978, MNRAS, 158, 45P
Webster B. L., 1983, PASP, 95, 610
Weinberger R., 1977, A&AS, 30, 335
Werner K., Hamann W. R., Heber U., Napiwotzki R., Rauch T., Wessolowski U., 1992, A&A, 259, L69
Westerlund B., Henize K. G., 1967, ApJS, 14, 154
Wiese W. L., Smith M. W., Glennon B. M., 1966, Atomic Transition Probabilities, Vol. 1 (NSRDS-NBS4) National Bureau of Standards, Washington, D.C.
Zeippen C. J., 1982, MNRAS, 198, 111
Zeippen C. J., Butler K., le Bourlot J., 1987, A&A, 188, 251
Zijlstra A. A., Pottasch S. R., Bignell C., 1989, A&AS, 79, 329
Zuckerman B., Aller L. H., 1986, ApJ, 301, 772 (ZA86)

APPENDIX A: IONIZATION CORRECTION FACTORS

The ionization correction factors (ICFs) adopted in this work are summarized below. They were developed based on 10 detailed photoionization models of PN by Walton, Barlow, Monk & Clegg (1994, in preparation; WBCM), and will be more fully discussed in a future paper by these authors.

In the following discussion, $ICF(X)$ is the ionization correction factor for element X and $A(X)$ is the total abundance by number of element X relative to hydrogen. All ionic

abundances (X^{m+}) are relative to H^+. $f(X^{m+})$ is the fraction of the total abundance of element X present in the ionic stage $m+$.

A1 Nitrogen

If UV spectra are available for a PN and all ionization stages of nitrogen are seen, then N/H is straightforwardly the sum of all ionization stages. If, however, in the UV spectrum N^{2+} is not seen, due to poor S/N of the N III] 1750-Å feature, the N^{2+} abundance is assumed to be halfway between N^+ and N^{3+}. If only optical spectra are available, N^+ is the only observed stage of ionization and

$$ICF(\mathrm{N}) = \mathrm{O}/\mathrm{O}^+, \tag{A1}$$

$$A(\mathrm{N}) = ICF(\mathrm{N})\mathrm{N}^+/\mathrm{H}^+. \tag{A2}$$

A2 Oxygen

If the O^+, O^{2+} and O^{3+} ions are seen, and N^{4+} is also present, then O^{4+} needs to be corrected for as follows:

$$f(\mathrm{O}^{4+}) = 0.95\, f(\mathrm{N}^{4+}), \tag{A3}$$

$$f(\mathrm{N}^{4+}) = \frac{\mathrm{N}^{4+}}{\mathrm{N}^+ + \mathrm{N}^{2+} + \mathrm{N}^{3+} + \mathrm{N}^{4+}}, \tag{A4}$$

$$ICF(\mathrm{O}) = \frac{1}{1 - 0.95\, f(\mathrm{N}^{4+})}, \tag{A5}$$

$$A(\mathrm{O}) = ICF(\mathrm{O})(\mathrm{O}^+ + \mathrm{O}^{2+} + \mathrm{O}^{3+})/\mathrm{H}^+. \tag{A6}$$

Equation (10) has been empirically derived by WBCM, using the results from the 10 photoionization models. If the O^+, O^{2+} and O^{3+} ions are seen, but N^{4+} is not, then the total oxygen abundance is the sum of the three observed stages of ionization. If O^{3+} is not seen, but N^{4+} is seen, then both O^{3+} and O^{4+} need to be corrected for. In this case

$$ICF(\mathrm{O}) = \frac{\mathrm{N}^+ + \mathrm{N}^{2+} + \mathrm{N}^{3+} + \mathrm{N}^{4+}}{\mathrm{N}^+ + \mathrm{N}^{2+}}, \tag{A7}$$

$$A(\mathrm{O}) = ICF(\mathrm{O})(\mathrm{O}^+ + \mathrm{O}^{2+})/\mathrm{H}^+. \tag{A8}$$

For cases when only lines of O^+ and O^{2+} are seen (for example when optical spectra only are available), higher stages of ionization are corrected via

$$ICF(\mathrm{O}) = \left(\frac{\mathrm{He}^+ + \mathrm{He}^{2+}}{\mathrm{He}^+}\right)^{2/3}, \tag{A9}$$

$$A(\mathrm{O}) = ICF(\mathrm{O})(\mathrm{O}^+ + \mathrm{O}^{2+})/\mathrm{H}^+. \tag{A10}$$

The $ICF(O)$ suggested by TPP77 is $(He^+ + He^{2+})/He^+$, and is based on the similarities between the ionization potentials of He^+ and O^{2+}. However, the photoionization model of Harrington et al. (1982) for NGC 7662 and the models listed by WBCM show that the fraction of He^{2+} is greater than the fraction of the $O^{3+} + O^{4+} + \ldots$, because of the large charge exchange rate for the $O^{3+} + H^0 \rightarrow O^{2+} + H^+$ reaction. The old $ICF(O)$ thus overestimates O/H as He^{2+}/H^+ increases. The power of 2/3 introduced in equation (15) was found as a best fit for the 10 ionization structure models of WBCM.

A3 Carbon

The carbon ICF scheme has many cases. If no C^{4+} is present (indicated by the lack of He^{2+}), and all other ionic stages are seen, the total abundance is just the sum of all seen species. If no C II lines are seen, the C^+ abundance needs to be corrected for using

$$ICF(\mathrm{O}) = \frac{\mathrm{O}^+ + \mathrm{O}^{2+}}{\mathrm{O}^{2+}}, \tag{A11}$$

$$A(\mathrm{C}) = ICF(\mathrm{C})(\mathrm{C}^{2+} + \mathrm{C}^{3+})/\mathrm{H}^+. \tag{A12}$$

Again for the case of no C^{4+}, if only C^{2+} is observed and O^{2+} is also seen, then C^{3+} needs to be corrected for using

$$ICF(\mathrm{C}) = \frac{A(\mathrm{O})}{\mathrm{O}^{2+}/\mathrm{H}^+}, \tag{A13}$$

$$A(\mathrm{C}) = ICF(\mathrm{C})\mathrm{C}^{2+}/\mathrm{H}^+. \tag{A14}$$

In high-excitation PN, where both N^{4+} and He^{2+} are seen, C^{4+} is present and needs to be corrected for. Two cases for $ICF(C)$ are found, depending on the excitation of the PN.

$$f(\mathrm{N}^{4+}) = \frac{\mathrm{N}^{4+}}{\mathrm{N}^+ + \mathrm{N}^{2+} + \mathrm{N}^{3+} + \mathrm{N}^{4+}}, \tag{A15}$$

$$ICF(\mathrm{C}) = \frac{1}{1 - 2.7\, f(\mathrm{N}^{4+})}, \quad \text{when } ICF(\mathrm{C}) < 5. \tag{A16}$$

For very high-excitation PN, $ICF(C) > 5$, and a significant amount of carbon is in C^{4+}; hence equation (A16) breaks down. So, for $ICF(C) > 5$,

$$f(\mathrm{N}^{4+}) = f(\mathrm{C}^{4+}), \tag{A17}$$

$$ICF(\mathrm{C}) = \frac{\mathrm{N}^+ + \mathrm{N}^{2+} + \mathrm{N}^{3+} + \mathrm{N}^{4+}}{\mathrm{N}^+ + \mathrm{N}^{2+} + \mathrm{N}^{3+}}, \tag{A18}$$

$$A(\mathrm{C}) = ICF(\mathrm{C})(\mathrm{C}^+ + \mathrm{C}^{2+} + \mathrm{C}^{3+})/\mathrm{H}^+. \tag{A19}$$

For nebulae that are hot enough to contain He^{2+}, but not N^{4+}, the following is used in order to correct for C^{4+}:

$$ICF(\mathrm{C}) = \left(\frac{\mathrm{He}^+ + \mathrm{He}^{2+}}{\mathrm{He}^+}\right)^{1/3}, \tag{A20}$$

$$A(\mathrm{C}) = ICF(\mathrm{C})(\mathrm{C}^+ + \mathrm{C}^{2+} + \mathrm{C}^{3+})/\mathrm{H}^+. \tag{A21}$$

To correct for the presence of C^{4+} in the cases where C^+ is not seen (for example if no *IUE* long-wavelength spectrum is available), it is assumed that $C^+/C = N^+/N$, and hence

$$ICF(\mathrm{C}) = \frac{1}{1 - f(\mathrm{N}^+) - 2.7\, f(\mathrm{N}^{4+})}, \quad \text{when } ICF(\mathrm{C}) < 5, \tag{A22}$$

$$ICF(\mathrm{C}) = \frac{\mathrm{N}^+ + \mathrm{N}^{2+} + \mathrm{N}^{3+} + \mathrm{N}^{4+}}{\mathrm{N}^{2+} + \mathrm{N}^{3+}}, \quad \text{when } ICF(\mathrm{C}) > 5, \tag{A23}$$

$$A(\mathrm{C}) = ICF(\mathrm{C})(\mathrm{C}^2 + \mathrm{C}^{3+})/\mathrm{H}^+. \tag{A24}$$

Finally, if N^{3+} or N^{4+} is not seen, the $ICF(C)$ is based on optical fluxes only:

$$ICF(C)=\left(\frac{O^{+}+O^{2+}}{O^{2+}}\right)\left(\frac{He^{+}+He^{2+}}{He^{+}}\right)^{1/3}, \quad \text{(A25)}$$

$$A(C)=ICF(C)(C^{+}+C^{2+}+C^{3+})/H^{+}. \quad \text{(A26)}$$

A4 Neon

If all stages of ionization are seen, the total abundance is the sum of all stages of ionization. The Ne^{+} contribution is assumed to be negligible in all cases. When lines of Ne IV are not seen (they are very weak in the optical),

$$A(Ne)=1.5(Ne^{2+}+Ne^{4+})/H^{+}. \quad \text{(A27)}$$

If only Ne^{2+} is seen,

$$ICF(Ne)=\frac{A(O)}{O^{2+}}, \quad \text{(A28)}$$

$$A(Ne)=ICF(Ne)Ne^{2+}/H^{+}. \quad \text{(A29)}$$

A5 Argon

Lines of Ar II are never observed in the optical or UV, thus Ar^{+} needs to be corrected for. It is assumed that $f(Ar^{+})=f(N^{+})$, so

$$ICF(Ar)=\frac{1}{1-f(N^{+})}, \quad \text{(A30)}$$

$$A(Ar)=ICF(Ar)(Ar^{2+}+Ar^{3+}+Ar^{4+})/H^{+}. \quad \text{(A31)}$$

For the cases where only Ar^{2+} is observed, the $ICF(Ar)$ was derived using the average Ar^{2+}/Ar ratio derived for 28 PN using the above equations (A30) and (A31), where $Ar^{2+}/Ar=1.873\pm0.41$. Hence

$$ICF(Ar)=1.87, \quad \text{(A32)}$$

$$A(Ar)=ICF(Ar)Ar^{2+}. \quad \text{(A33)}$$

For rare cases when Ar^{3+} is the only observed stage of ionization, to correct for the other stages, the $ICF(Ar)$ is based on the similarity of ionization potentials for Ar^{3+} and Ne^{2+}:

$$ICF(Ar)=\frac{Ne}{Ne^{2+}}, \quad \text{(A34)}$$

$$A(Ar)=ICF(Ar)Ar^{3+}/H^{+}. \quad \text{(A35)}$$

A6 Sulphur

The total sulphur abundance is generally quite uncertain, as usually only trace stages of ionization are observed. [S III] 6312 Å arises from an auroral transition, hence it is particularly temperature sensitive. When only S II lines are observed, the total abundance is particularly uncertain.

$$ICF(S)=\left[1-\left(1-\frac{O^{+}}{O}\right)^{3}\right]^{-1/3}, \quad \text{(A36)}$$

$$A(S)=ICF(S)(S^{+}+S^{2+})/H^{+}. \quad \text{(A37)}$$

Equation (A28) is from Barker (1980), who adopted it from ionization models of H II regions by Stasinska (1978). Equation (A37) is valid when both S^{+} and S^{2+} are observed. For cases when S^{+} but not S^{2+} is observed, the fraction of S in S^{2+} was estimated as follows: S^{2+}/S^{+} versus O^{2+}/O^{+} was plotted for all PN with all measurements available in Fig. 15. A least-squares fit to the 22 points in Fig. 15 yielded

$$\frac{S^{2+}}{S^{+}}=4.677+\left(\frac{O^{2+}}{O^{+}}\right)^{0.433} \quad \text{(A38)}$$

and was used to estimate S^{2+} when only S^{+} was available (or vice versa, in a few rare cases). Hence for PN, where S^{+} is the only observed stage of ionization, the S/H ratio is particularly uncertain. (Note: the ICF scheme for sulphur adopted here differs from that in WBCM, who assume an S^{2+}/S^{+} ratio based on excitation class, for predicting the S^{2+} abundance when only S^{+} is observed. The relation used by WBCM was not found to be valid for the galactic sample.)

A7 Abundances for very high-excitation PN

For PN of very high excitation, where all He is found in its doubly ionized state, the previously mentioned ICF schemes for oxygen and carbon break down. For these rare cases, an ICF based on neon is adopted for both oxygen and carbon:

$$ICF(O)=ICF(C)=\frac{A(Ne)}{Ne^{2+}/H^{+}}, \quad \text{(A39)}$$

$$A(O)=ICF(O)(O^{+}+O^{2+}+O^{3+})/H^{+}, \quad \text{(A40)}$$

$$A(C)=ICF(C)(C^{2+}+C^{3+})/H^{+}. \quad \text{(A41)}$$